Deanship of Graduate Studies

Al-Quds University

The Geochemical Characteristics of Wadi Al-Ghar Stream Sediments as Indicators of their Source and Paleo-Weathering

Adli Mohammad Ahmad Khalayleh

M.Sc. Thesis

Jerusalem – Palestine

1440 – 2018

The Geochemical Characteristics of Wadi Al-Ghar Stream Sediments as Indicators of their Source and Paleo-Weathering

Prepared By:

Adli Mohammad Ahmad Khalayleh

B.Sc. in Computer Engineering, An-Najah National University, Nablus, Palestine

Supervisor: **Prof. Dr. Mutaz Ali Qutob**

A thesis submitted in partial fulfillment of requirements for the degree of Master of Science in Environmental Studies

Department of Earth and Environmental Studies, Deanship of Graduate Studies, Al-Quds University

1440 - 2018

Al-Quds University

Deanship of Graduate Studies

Environmental Studies Program

Thesis Approval

The Geochemical Characteristics of Wadi Al-Ghar Stream Sediments as Indicators of their Source and Paleo-Weathering

Student Name: Adli Mohammad Ahmad Khalayleh

Registration No.: 21410226

Supervisor: Prof. Dr. Mutaz Ali Qutob

Master Thesis submitted and accepted, Date 24/11/2018

The names and signatures of the examining committee are as follows:

1- Head of Committee: Prof. Dr. Mutaz Qutob Signature ……

2- Internal Examiner: Dr. Mahmoud Al-Khateeb Signature ……

3- External Examiner: Dr. Ayman Mohsen Signature ……

Jerusalem – Palestine

1440 – 2018

Declaration

I certify that this thesis submitted for the degree of Master, is the result of my own research, except where otherwise acknowledged, and that this study (or any part of the same) has not been submitted for a higher degree to any other university or institute.

Signed 

Name: Adli Mohammad Ahmad Khalayleh

Date: 24/11/2018

Acknowledgement

First of all, I am grateful to Almighty Allah, the creator of the whole world, the Merciful, because without His will nothing can be done, and so He guided me through the path to complete this research project successfully, which would otherwise have not been possible.

Secondly, I would like to thank my thesis advisor Professor Mutaz Qutob of the Science and Technology Faculty at Al-Quds University. Professor Qutob was always welcoming whenever I ran into a trouble or had a question about my research. He consistently allowed this paper to be my own work, but steered me in the right direction whenever he thought I needed it.

I would also like to thank the expert who was involved in the sample collection for this research project: Mr. Mahmoud Zaid, in addition to his assistance and guidance in the laboratory work. Gratitude is also due to Mr. Husam Utair, Mr. Husam Malassa and Mr. Sameh Nusseibeh. Without their passionate participation and input, the laboratory analysis and work could not have been successfully conducted.

I would also like to acknowledge my great indebtedness to the respected Professors of the Science and Technology Faculty at Al-Quds University for their highly valuable enrichment of my academic knowledge that led me to write this thesis.

Finally, I must express my very profound gratitude to my parents, siblings; especially Cana'an (M.Eng.), and to my friend Dr. Rand A.Sh. for providing me with unfailing support and continuous encouragement throughout my years of study and through the process of researching and writing this thesis. This accomplishment would not have been possible without them. Thank you.

Table of Contents

List of Tables

List of Figures

List of Abbreviations

ICP-MS	Inductive Coupled Plasma Mass Spectroscopy
MARS 5	Digestion Microwave
mg/kg	Milligram Per Kilogram
cm	Centimeter
mm	Millimeter
ml	Milliliter
°C	Degree Celsius
n.d.	Not Detectable
SEM	Standard Error of Measurement
cal yr BP	Calibrated Years Before the Present
REE	Rare Earth Element
TREE	Total Rare Earth Elements
LREE	Light Rare Earth Elements

HREE	Heavy Rare Earth Elements
TC%	Total Carbon Percentage
TOC%	Total Organic Carbon Percentage
TN%	Total Nitrogen Percentage
C/N	Carbon Nitrogen Ratio
IOC%	Inorganic Carbon Percentage
$CaCO_3$%	Calcium Carbonate Percentage
δ^{13}Corg‰	Delta Organic Carbon-13 per mille (‰, parts per thousand)
δ^{13}Ccarb‰	Delta Carbonate Carbon-13 per mille (‰, parts per thousand)
δ^{18}Ocarb‰	Delta Carbonate Oxygen-18 per mille (‰, parts per thousand)

Abstract

Bani Na'im heights, to the east of Hebron, is the drainage heading east towards the Dead Sea composing a number of dry valleys and streams, and they have a steep slope at their upper reaches and discharge into the Dead Sea. It is deeply affected by the economic development of the nearby quarries. The runoff transports a large amount of metals and considerable portions of them deposit and accumulate at the sediment basin. In this study, surface and profile sediment samples from two streams and their merge at the catchment area of Bani Na'im were collected and analyzed by inductive coupled plasma mass spectroscopy (ICP-MS). Statistical analysis using the "GRANISTAT" software for the data obtained by sieving indicates a sand textural group of the catchment area and a muddy sand textural group of the quarries, manifesting terrestrial clastic sediment formed from an altered regolith derived by climatic and tectonic controls of pristine bedrock and a calcite source of mineral grains for alluvial fans, where the Dead Sea Rift is the major tectonic control of the region. Statistical analyses of the trace elements indicate that both streams; Wadi Al-Ma'zzeh and Wadi Masyadeh contribute to Wadi Al-Ghar with an evident greater contribution from Wadi Al-Ma'zzeh; the trace element concentrations were correlated with the inorganic carbon concentration revealing that quarries have a substantial impact on Wadi Masyadeh sediments distribution as an upland sediment source. Trace and major elements distribution and analyses indicate that stream sediments form by the physical and chemical weathering of bedrock within the catchment area. The sediment geochemistry reflects that stream sediments are a combination of geomorphic elements and human uses. The spatial variations of REEs and the minor anomalies of Ce/Ce* and Eu/Eu*, in addition to the Chondrite-normalized plot of the REEs revealed a possible environment of erosivity, terrestrial stream sediment sources and lithologically controlled distribution

from crystalline basement source rock. This is supported by the Ce/Ce* negative anomaly that is indicative of a development in corestones during spheroidal weathering. The Eu/Eu* anomaly revealed the contribution of weathering. The La/Yb ratios indicate high erosional rates, suggesting that La was removed from crustal source via weathering process. The high C/N ratio reflects influence from terrestrial organic matter to the sediment. The calcium carbonate and the isotopic analysis of δ^{13}Ccarb‰, δ^{18}Ocarb‰ and their horizontal and vertical distributions indicate a pedogenic carbonate of biotic and abiotic processes and tectonic controls on sedimentation; pedogenic carbonate is classically referred to a semiarid paleo-climate. Al-Ma'zzeh and Masyadeh profiles are not homogeneous; they show considerable variations in leachable and residual fractions in vertical stream cross sections with higher depletion at Al-Ma'zzeh profile. Information obtained from continental sediments should be combined with other proxies (precipitation, seasonality and temperature) whenever possible for improved resolution of the paleo-environmental record. Consequentially, further seasonal sampling and analyses of sediment, hydrology and atmosphere are highly recommended, in addition to bedrock sampling for radioactive isotopes analysis.

As there are no regional background values and sediment guidelines, this study could be considered a baseline geochemical study of the area, and as a datum for monitoring future change in the geochemical stream sediment, whether natural or human-induced.

الخصائص الجيوكيميائية لرواسب وادي الغار كمؤشر لمصدرها وحالة المناخ

إعداد: عدلي محمد أحمد خلايلة

إشراف: الأستاذ الدكتور معتز علي قطب

الملخص

تقع مرتفعات بني نعيم إلى الشرق من مدينة الخليل، وهي مجرى تصريف المياه الذي يتجه شرقاً نحو البحر الميت، وهو يتألف من عدد من الأودية والجداول الجافة، ولها منحدرات حادة عند الروافد العليا وترفد إلى البحر الميت. تأثرت منطقة بني نعيم بشدة بالتنمية الاقتصادية للمقالع القريبة. جريان المياه ينقل كميات كبيرة من المعادن ويودع جزء كبير منها في حوض الترسبات. في هذه الدراسة؛ تم جمع عينات الرواسب السطحية والجانبية من واديين اثنين في منطقة مستجمع بني نعيم وتم تحليلها بواسطة مطيافية الكتلة البلازمية المقترنة الحثية (ICP-MS). التحليل الإحصائي باستخدام برنامج "GRANISTAT" للبيانات التي تم الحصول عليها عن طريق الغربلة يشير إلى مجموعة تركيب رملية في منطقة مستجمعات المياه ومجموعة تركيب رملية موحلة في المحاجر، تظهر الرواسب التفكيكية الأرضية (terrestrial clastic sediment) المتكونة من ريجوليت متغير (altered regolith) تم استنباطه من خلال التحكم المناخي والتكتوني للصخر الأساس والأصلي ومصدر الكالسيت من الحبيبات المعدنية للغرين ذي الشكل المروحي (alluvial fans)، حيث يعتبر صدع البحر الميت هو السيطرة التكتونية الرئيسية في المنطقة. تشير التحليلات الإحصائية للعناصر الزهيدة إلى أن كلا الواديين؛ وادي المعزّة ووادي مصيدة يساهمان في وادي الغار بمساهمة أكبر من وادي المعزّة، ارتبطت تركيزات العناصر الزهيدة بتركيز الكربون غير العضوي مما يدل على أن المحاجر لها تأثير كبير على توزيع رواسب وادي مصيدة كمصدر للرواسب المرتفعة. تشير عملية التتبع والتوزيع للعناصر الزهيدة والرئيسية والتحليلات إلى أن رواسب الوادي تتشكل بسبب التجوية الفيزيائية والكيميائية للصخور الأساسية داخل منطقة مستجمعات المياه. وتعكس جيوكيميائية الرواسب أن رواسب الوادي هي مزيج من العناصر الجيومورفولوجية والاستخدامات البشرية. الاختلافات المكانية للعناصر الأرضية النادرة والشذوذ البسيط في Ce/Ce* وEu/Eu*، بالإضافة إلى مخطط chondrite المطبع للعناصر الأرضية النادرة أظهرت بيئة محتملة للتعرية ومصادر أرضية لرواسب الوادي وتوزيع مسيطر عليه من مصدر صخور بلورية من الجزء السفلى. ويدعم هذا؛ الشذوذ السلبي لِـ Ce/Ce* الذي يشير إلى تطور في الحجر الأساسي أثناء التجوية

الكروية. كشف شذوذ *Eu/Eu مساهمة عوامل التجوية. تشير نسب La/Yb إلى معدلات تآكل عالية، مما يشير إلى أن La تمت إزالته من مصدر القشرة عبر عملية التجوية. تعكس نسبة C/N العالية تأثير من المواد العضوية الأرضية إلى الرواسب. تشير تحليلات كربونات الكالسيوم والنظائر δ^{13}Ccarb‰ وδ^{18}Ocarb‰ والتوزيعات الأفقية والعمودية إلى كربونات من أصول أرضية (pedogenic) لعمليات حيوية وغير حيوية والضوابط التكتونية على الترسيب؛ الكربونات الأرضية في الأصل تحول إلى المناخ شبه القاحل السائد. لا يعتبر القطع الجانبي للمعزّة والمصيدة متجانس؛ تظهر اختلافات كبيرة في الكسور القابلة للارتشاح والمتبقية في المقاطع العرضية العمودية للوديان مع نفاذية أعلى في القطع الجانبي للمعزّة. المعلومات التي يتم الحصول عليها من الرواسب القارية ينبغي أن تُجمع مع بيانات أخرى (هطول الأمطار، الموسمية ودرجة الحرارة) كلما أمكن ذلك لتحسين دقة السجل البيئي القديم. ونتيجة لذلك، يُوصى بشدة بأخذ عينات وتحاليل موسمية أخرى للرواسب والهيدرولوجيا والغلاف الجوي، بالإضافة إلى أخذ عينات من صخور الأساس من أجل تحليل النظائر المشعة.

نظراً لعدم وجود قيم خلفية إقليمية ومبادئ توجيهية للرواسب، يمكن اعتبار هذه الدراسة بمثابة دراسة جيوكيميائية أساسية للمنطقة، وكمرجع لرصد التغير المستقبلي في جيوكيميائية رواسب الوادي، سواء كان ذلك ناتجاً عن الطبيعة أو الإنسان.

Chapter One

Introduction

Chapter One

1. Introduction

1.1 Background

Sediment is conglomerate solid material that is transported and deposited in a new location. A sediment can consist of rocks and minerals (inorganic), as well as the remains of plants and animals (organic). It can be smaller than a grain of sand or as large as a boulder. Sediments move from one place to another (by wind, water, or ice) through erosion, a process by which rock or soil gets transported or removed (Dunn, 1989-1993).

Water can wash sediments, such as gravel or pebbles, down a stream into a water body. The sides and bottom of a stream are common areas for sediments to accumulate. Sediment accumulation is important because it often enriches the soil with nutrients, and results in higher biodiversity. Sedimentary soil is usually better for farming. Regions where much sediment is deposited are often the most fertile agricultural areas (Dunn, 1989-1993), (Leeder, 2011).

Sediments transported by a stream will commonly represent a mixture of sediments derived from different locations and different types of sediment sources within the contributing drainage basin. Knowledge of sediment provenance is an important requirement in the examination of sediment routing and delivery and in the construction of catchment sediment budgets (Walling, et al., 1999).

Sediment accumulations may be grandly viewed as the great stratal archive of past surface environments, or more basically as ‘dirt’. There has been sediment on the

surface of the Earth since the Archaean, with the oldest known sediment grains dating from at least 4.4 Ga (Leeder, 2011).

Sediment is best divided into three end-members: clastic – originating from pre-existing rock outside a depositional area as transported grains, the commonest being mineral silicate grains, known widely as siliciclastic sediment; and chemical – being the result of inorganic or organically mediated chemical precipitation within the depositional area (Leeder, 2011).

Terrestrial clastic sedimentary rocks are usually quite different in their composition from the igneous and metamorphic rocks that sourced them. This is because they are derived from an altered regolith with a soil profile produced by chemical weathering of pristine bedrock and a calcite source of mineral grains for such sediment (Leeder, 2011).

Deposited sediment accumulates as successive layers, termed strata, and such deposits as a whole are said to be stratified. The succession of strata in any given deposit is controlled by environmental factors and their correct interpretation involves a deep understanding of how present and past environments have evolved over time. Sediment simply fell out of the rock cycle in which primary rock is chemically and physically altered (Leeder, 2011).

It is traditional to divide rock weathering into physical and chemical components, but in reality the two are inextricably interlinked. Water is the chief reactant and plays a dual role since it also transports away both dissolved and solid weathering products (Leeder, 2011).

Chemical weathering involves aqueous reactions with a strong biochemical component since dissolved atmospheric gases are aided by soil-generated gases, dilute acids and organic ligands. The result is a regolith and soil profile whose characteristics depend upon climate and rock type (Leeder, 2011).

Physical weathering involves the application of differential stresses to rock and mineral discontinuities in the unsaturated zone. The combined effects of biochemical and physical weathering produce a weathered regolith profile in bedrock (Leeder, 2011).

1.2 Chemical Characteristics

The chemical composition of sediments is closely related to the mineral composition of sources, post-depositional weathering and transportation of sediments from the source region to the deposition center. The bulk chemistry of these sediments preserves the near-original signature of the provenance; consequently, sediments differ in chemical composition from one region to another and even from one stratigraphic unit to another. The sediments subjected to various degrees of chemical weathering and leaching, these sediments also reveal paleo-weathering conditions (Leeder, 2011).

1.2.1 Trace Elements

Trace elements are elements that occur in very small amounts (usually less than 1 to 10 parts per million in composition). The typical trace elements that were analyzed are Na, Mg, Al, P, V, Cr, Mn, Fe, Co, Ni, Zn, Sr and Pb. Trace elements are usually described in terms of their total content and availability. Trace elements include heavy metals, which is a term that refers to any metallic chemical element that has a relatively high density and is toxic or poisonous at low concentrations. Examples of heavy metals include Cr, and Pb (Albright, 2004). Major trace elements are usually greater than 1% in

composition and refer to the primary rock-forming elements, while minor trace elements are usually between 0.1 - 1% in composition (Gill & Ramsey, 2014)

Trace elements withhold in sediments depending on several sediment characteristics that include pH, Cation Exchange Capacity (CEC), particle size distribution, organic matter content, and oxide content. These characteristics cause trace elements to either accumulate in the sediment, or leave for other components in the environment. When parent materials have high trace element concentrations, the sediments that develop over them have the same or even higher trace element concentrations. Concentrations of trace elements in sediments are important not only for environmental purposes, such as quantifying contamination, but also to help solve problems associated with human and plant toxicity (Albright, 2004).

1.2.2 Rare Earth Elements (REEs)

REEs are members of the group IIIB in the periodic table (La, Ce, Pr, Nd, Sm, Eu, Gd, Tb, Dy, Ho, Er, Tm, Yb and Lu) and are defined as the 15 naturally-occurring elements of the lanthanide series. They are progressively used as proxies to trace origin and processes in lithology. REEs occur in more than 200 minerals distributed in a wide variety of mineral classes, and therefore in most minerals present in sediments (Walters & Lusty, 2011).

The large variations of Total-REE contents in sediments are highly dependent on the source types of sediments and their special origin. Some REE sources in sediments are atmospheric depositions (atmospheric particles, rainwater and snow) and others are anthropogenic (waste samples, irrigation and sewage waters, and fertilizers) (Walters & Lusty, 2011).

1.2.3 Total Organic Carbon and Total Nitrogen

Total organic carbon ‘TOC’ and total nitrogen ‘TN’ contents are an important parameter for the environmental status estimation to distinguish marine and terrestrial sources of organic matter in soils and sediments. The sediments organic carbon and nitrogen are mainly derived by decomposition of the plants and animals or plankton or anthropogenic sources such as chemical contaminants, fertilizers or organic rich waste (Avramidisa, et al., 2015).

Moreover, organic matter and nitrogen content ratios have been used widely as biomarkers for the reconstruction of sedimentological depositional environments and the environmental changes of the past. The presence of the organic matter is an important constitute as it consists an index for the sediments depositional environments (Avramidisa, et al., 2015).

1.2.4 Isotope Tracers

Isotopes are atoms of the same element having the same numbers of protons (atomic number), but different numbers of neutrons. Most stable elements occur naturally on Earth in multiple stable isotopes. They have same chemical properties due to the same electronic configuration but different physical properties. A common use of stable isotopes is as tracers based on the natural variations in the relative abundances of isotopes of various elements which reveal information about the ages and origins of Earth (Anderson, 2007). The stable isotopes that were analyzed are carbonated carbon-13 and oxygen-18 and organic carbon-13.

1.2.5 Grain Size

Particle-size is an important character that influences the properties of the sediment. The particle-size distribution is also an important property of sediment deposits; it is important in predicting the behavior of sediment. The particles have various shapes and it is defined numerically by sphericity and roundness. The size, shape and arrangement of particles composing a sediment deposit determine its texture as shown in Appendix D – Table 15. Textures can be clastic or crystalline; clastic textures are composed of grains from pre-existing rocks, while crystals grew from a fluid producing an interlocking mosaic of crystals. The unconsolidated sediment texture is important in controlling sediment element concentrations because sediment tends to collect, concentrate and retain trace elements by adsorption (United States Department of Agriculture, n.d.).

1.3 Objectives of the Study

1.3.1 Project Background

This research paper aims to determine the elemental background of sediments in Wadi Al-Ghar at the catchment area of Bani Na'im by studying the geochemical characteristics of two streams located within the area; Wadi Al-Ma'zzeh and Wadi Masyadeh as a study case. After which, they can be used as references to addresses the provenance, paleo-weathering, sediment development, and possible contamination along the streams until the Dead Sea.

1.3.2 Main Objectives

This study is based on collecting and analyzing sediment samples for a range of diagnostic properties; measuring trace element and REE concentrations using spectrophotometer. This is followed by conducting quantitative calculations and qualitative interpretation of the results to determine the source type, special origin and paleo-weathering of sediments, and to identify any contamination along the catchment area.

The objectives of this study are:

- Determine the source of sediments in Wadi Al-Ghar and the Dead Sea according to their REEs and trace elements
- Study the origin, paleo-weathering and formation processes of sediments
- Compare Wadi Al-Ghar and the Dead Sea sediments, and the contribution of Wadi Al-Ghar into the Dead Sea sediments
- Study the differences in the sediment profiles
- Understand the impact of quarries on the sediments

1.3.3 Significance of the Study

This study has significant importance since it can give a general idea about the sediment characteristics of the chosen streams. As there are no regional background values and sediment guidelines, it is expected that the outcome of this research can be considered a baseline geochemical study of the area, and as a datum for monitoring future changes in the geochemical stream sediment, whether natural or human-induced.

Chapter Two

Literature Review

Chapter Two

2. Literature Review

Several studies about fluvial and marine sediments have been conducted at various places worldwide to inspect sediment provenance and paleo-environmental records, whereas studies about continental sediments have been conducted at a lower pace. Below are some scientific papers that could be highly recommended to be reviewed in order to get abroad understanding of my research.

Collins, et al. had reviewed and presented recent developments for several key aspects of fingerprinting, namely: sediment source classification, catchment source and target sediment sampling, tracer selection, grain size issues, tracer conservatism, source apportionment modelling, and assessment of source predictions using artificial mixtures. Source estimates are difficult to obtain using traditional monitoring techniques, but sediment source fingerprinting or tracing procedures, have emerged as a potentially valuable alternative. Reliable information on the principal sources is needed for the growing awareness of the environmental significance of fine-grained sediment fluxes through catchment systems, several key challenges and uncertainties continue to hamper consensus among the scientific community on key components of the existing methodological procedures. Accordingly, a decision-tree representing the current state of knowledge had been presented, to guide end-users in applying the fingerprinting approach (Collins, et al., 2017).

Albright had established background concentrations for 16 trace elements in surface soils, subsoils, and parent materials of the Georgia Piedmont, for the importance from both a regulatory and environmental impact standpoint. Soils (A, B, and C horizons)

and parent materials were sampled from remote areas, based on observed and mapped parent material (rock) type (grouped as felsic, mafic, and intermediate), and analyzed for selected major and minor elements. Trace metal content varied little between soil horizons, and mafic soils were clearly higher in a suite of elements (including Cr, Mn, Ni, and V), while felsic rocks were higher in certain heavier elements (Pb and U). Implications were that regulatory levels of trace elements should be referenced to parent rock for a given site (Albright, 2004).

Chahi, et al. had determined the REE contents and distribution patterns of the deposits of the Ganntour Basin (Morocco), detrital smectite in a sandy claystone and a phosphorite, and authigenic palygorskite in a dolomitic marl and a porcellanite from Cretaceous-Tertiary phosphorite were purified using cation exchange resin, leached with dilute acid, and analysed before and after acid treatment. The normalized patterns confirm a detrital origin for the smectite in the sandy claystone, whereas the origin of the smectite from the phosphorite is obscured by the addition of REE from the phosphogenic environment. The normalized REE patterns of the palygorskite suggested formation in non-oxidizing restricted environments. The $Al_2O_3/\sum REE$ ratio of the two clay types suggests formation of diagenetic palygorskite (and mixed-layer illite-smectite) from Al-bearing detrital smectite by a dissolution-crystallization process (Chahi, et al., 1999).

Heikkilä, et al. had analyzed isotopic multi-component of a sediment core from Lake Saarikko, Finland, it had given insight into Holocene climate changes in northern Europe. Oxygen isotopic records from aquatic cellulose and authigenic carbonate reflected consistent, similar trends in hydrological balance, and were employed jointly to infer relative changes in lake water temperature. Other geochemical and isotopic

tracers shed light on fluctuations in lake level and nutrient cycling, facilitating the interpretation of the oxygen isotopic archives. In the early Holocene (~10,000 – 9000 calibrated years before the present), the lake level was low and dry conditions prevailed despite low temperatures. Higher lake levels and depleted oxygen isotopic values ~9000 – 7500 cal yr BP were probably caused by several factors: higher effective humidity, an isotopically depleted precipitation source, a cold event around 8300 cal yr BP, and increased spring snowmelt. In contrast, higher summer temperatures, lower effective humidity, lower lake levels and enriched oxygen isotopic values were experienced during the mid-Holocene ~7500 – 3300 cal yr BP. The occurrence of the warmest inferred lake water and the most enriched cellulose oxygen-isotope values ~6000 – 5000 cal yr BP is consistent with a summer temperature maximum inferred from other proxy sources from the region. The late Holocene was characterized by higher effective humidity and higher lake levels. Increase in spring snowmelt and colder temperatures, most likely related to the Little Ice Age, induced a drastic change in the lake hydrology and probably caused the formation of its present outlet ~800 cal yr BP. Changes in the lake hydrological balance and climate variables inferred from oxygen isotopic records can be related to atmospheric circulation, most clearly to changes in the dominance and strength of westerly air-flow as well as summertime anticyclonic circulation (Heikkilä, et al., 2010).

Alien, et al. had indicated that a significant base-metal association occurred in three areas within the Jabal Habashi quadrangle, sheet 26F, Kingdom of Saudi Arabia. Panned-concentrate samples from wadi sediments were collected over terranes of Precambrian age intrusive, volcanic, sedimentary, and metamorphic rocks, within the quadrangle. The chemical data was multivariate analyzed; an association of strontium, barium, and calcium possibly indicated areas of hydrothermal alteration. Three other

associations that were found defined the major rock lithologies: niobium-yttrium-lanthanum outlines granitic terranes; magnesium-nickel indicated mafic rocks; and cobalt-vanadium-chromium had an indefinite relation with units mapped as graywacke in the central part of the quadrangle (Alleh, et al., 1985).

Walling, et al. had established the main sources of the suspended sediment transported through the lower, non-tidal reaches of the River Ouse and one of its main tributaries, the River Wharfe, during the period 1994 – 1997. The suspended sediment samples were collected from the River Ouse, statistically verified composite fingerprints and a multivariate mixing model had been employed. The load-weighted mean contributions from uncultivated topsoil, cultivated topsoil and channel bank sources were estimated. Suspended sediment samples collected during higher flows evidenced a greater contribution from channel banks than samples collected during lower flows. Source materials were also differentiated according to the three main geological source areas (Carboniferous, Permian and Triassic, and Jurassic) and their load-weighted mean contributions were estimated for the River Ouse and the River Wharfe. Suspended sediment samples from tributary streams were used to characterize each geological source area. Considering the three main tributaries that contribute to the River Ouse, the load-weighted mean contributions from the rivers Swale, Ure and Nidd were estimated. The values had been compared with estimates of the relative magnitude of the annual suspended sediment loads of these three rivers for the years 1995 and 1996 derived from continuous monitoring of discharge and turbidity. Differences between the two sets of results were ascribed to the different periods of record involved and to the timing of suspended sediment sampling relative to the overall storm hydrograph, and thus the degree to which the available samples were representative of the overall suspended sediment flux. The fingerprinting approach to source ascription was seen as providing

valuable information regarding suspended sediment sources in the study catchments, although a number of limitations must been recognized (Walling, et al., 1999).

The fact of the matter is that no similar studies have been conducted in Palestine concerning the geochemical characteristics of stream sediments to indicate their source and paleo-weathering. However, there have been few studies concerning metals content, occurrence and distribution in soil in Palestine.

Chapter Three

Methodology

Chapter Three

3. Methodology

3.1 Study area

This study is about the Bani Na'im catchment area, shown in Figure 1. Hebron hills with the heights of Bani Na'im and Halhul constitute a watershed (water line divider) between the drainage that is heading west towards the Mediterranean Sea and the drainage that is heading east towards the Dead Sea, which permeates the territory of Bani Na'im, composing a number of dry valleys and streams that form integrated alluvial basins from upstream to downstream (ARIJ, 1995).

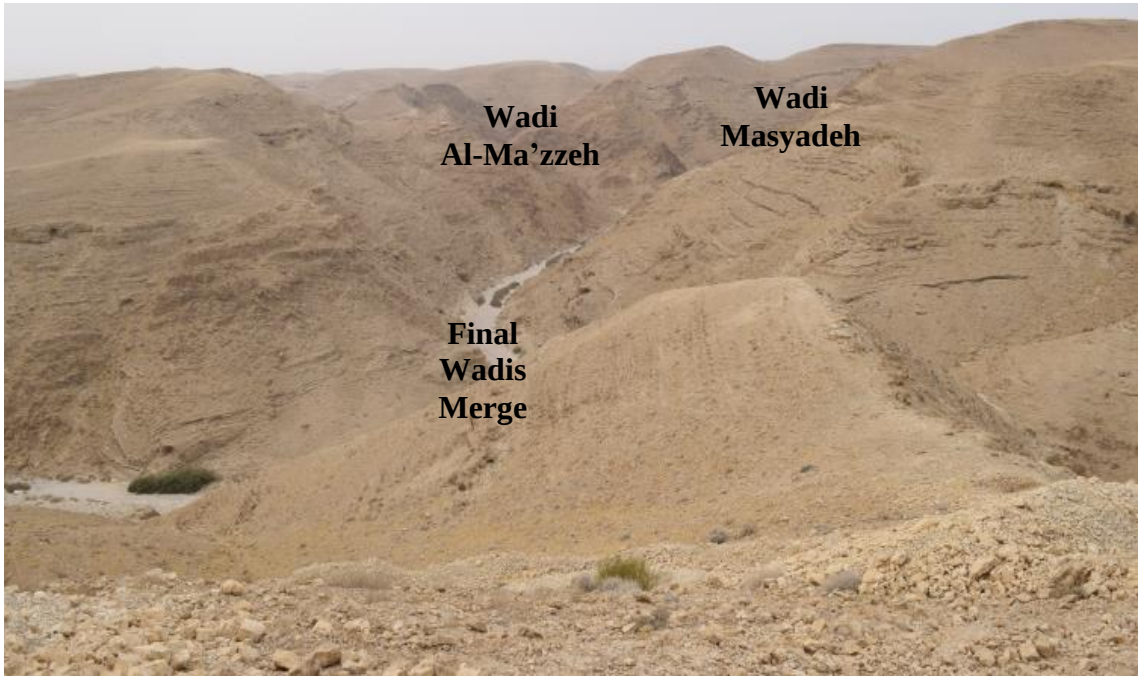

Figure 1: Wadi Al-Ghar (Al-Ma'zzeh and Masyadeh Wadis) (Khalayleh, 2017)

The streams along are about 23 km, and that is the horizontal distance between the town of Bani Na'im and the Dead Sea as shown in Figure 2, and they have a steep slope at

their upper reaches and discharge into the Dead Sea. These streams (wadis: ephemeral rivers) are: Wadi Al-Ghar, Wadi Seif, Wadi Jerfan, Wadi Al-Mentar, Wadi A'mreh, Wadi Al-Wa'reh, Wadi Al-Ma'zzeh and Wadi Masyadeh (ARIJ, 2009).

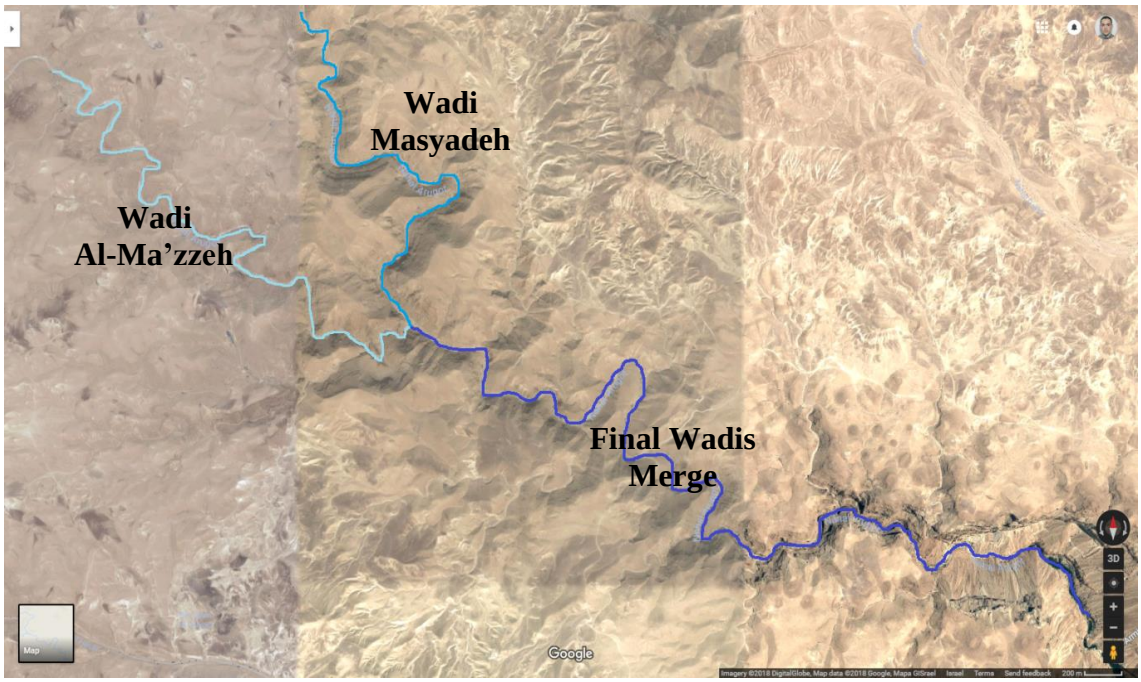

Figure 2: Al-Ma'zzeh and Masyadeh Wadis – Catchment Area (Google Maps, Adli, 2017)

Case study samples from stream sediments were collected within Al-Ma'zzeh and Masyadeh wadis. Analysis of the chemical composition data for the trace elements and RREs was conducted to follow the changes of the sediments along the streams. Spectrographic analysis of samples was performed at the laboratory. The results were then interpreted using multivariate statistical procedures.

3.1.1 Location

Bani Na'im town is located approximately 8 km east of Hebron in Palestine, as shown in Figure 3, latitude of 31° 30' 57.3" N and longitude of 35° 9' 51" E, with an average

elevation of 968 meters above sea level. The Israeli settlement of Kiryat Arba is situated northwest of Bani Na'im. South of Bani Na'im are the village of Hureiz and the city of Yatta, north of it are Sa'ir and Al-Shuyukh, west of it are Halhul and the forest of Hebron, while Bani Na'im's lands extend east to the mountains that overlook the Dead Sea (Siraj Center, Human Interest, Visit Palestine, 2015).

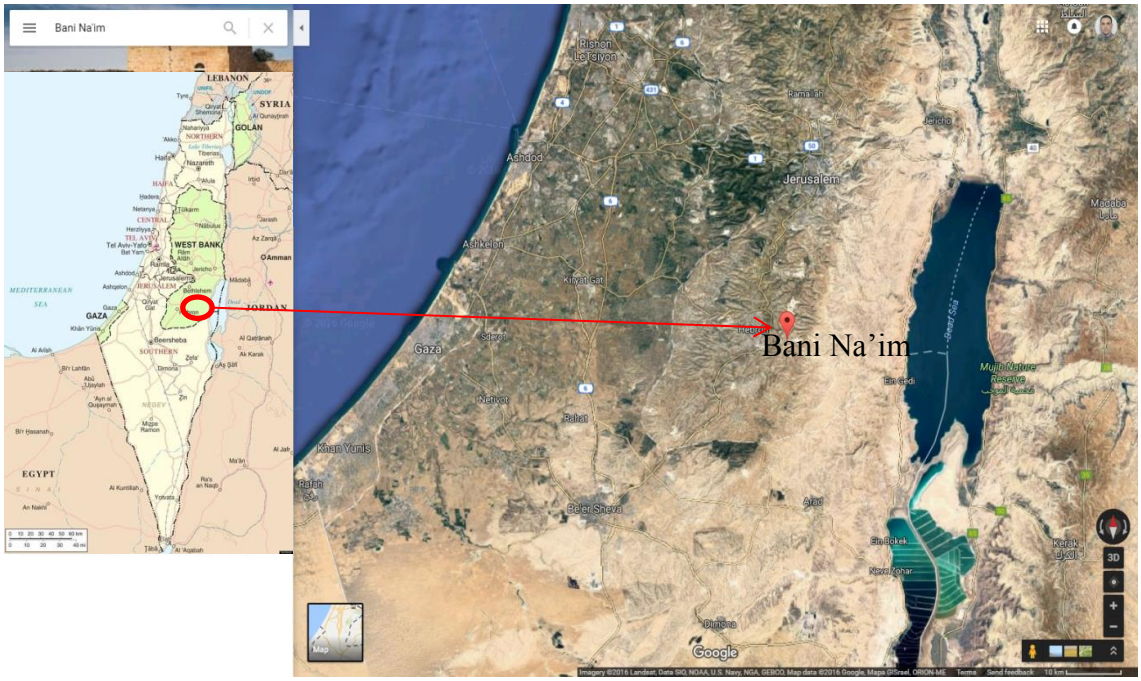

Figure 3: Bani Na'im Town, Palestine (Google Maps, Adli, 2017)

The rainwater at Bani Na'im catchment begging area starts flowing from the upstream at the west where the land's surface is flat and the runoff quantity is less. As the amount of the runoff increases and the area slopes towards the east – downstream as seen in Figure 4, cracks and fissures are formed along the sides of the streams (wadis) of variant heights, as Figure 5 shows, in addition to the change in the width of the streams. Sediment deposited from flows accumulates to form alluvial fans.

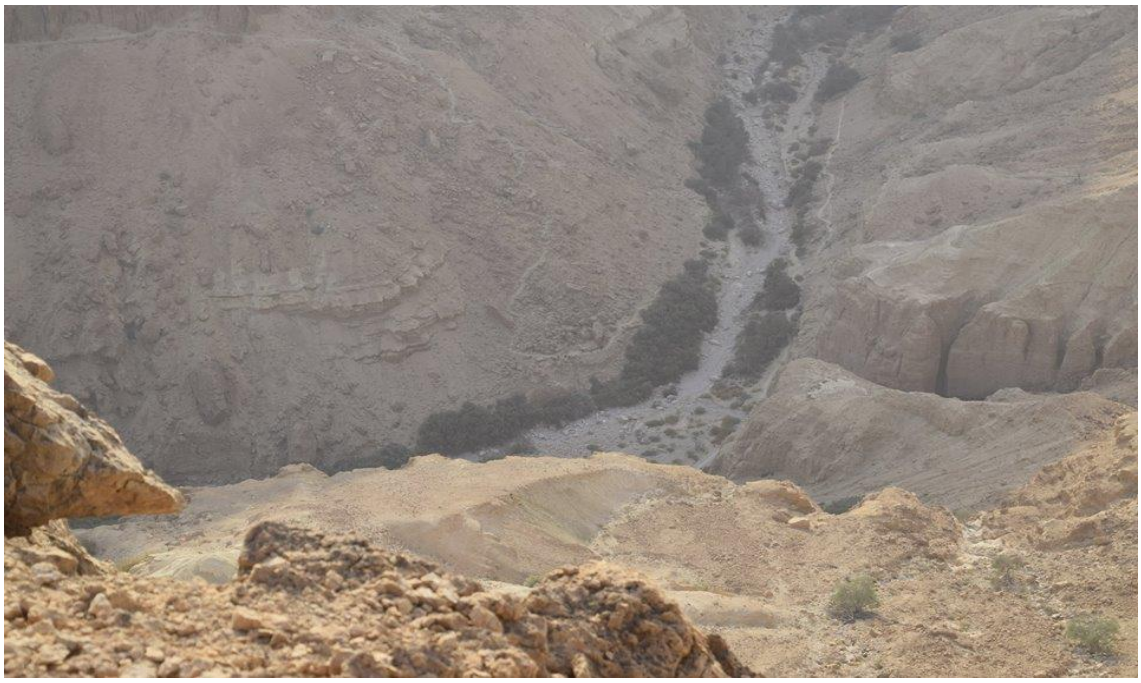

Figure 4: Wadi Al-Ghar Crack – Downstream (Khalayleh, 2017)

Figure 5: Wadi Masyadeh Fissure (Khalayleh, 2017)

3.1.2 Topography

Bani Na'im is a mountainous area with the heights of Hebron and Halhul to the west, which declines clearly east towards the Dead Sea, as observed in Figure 6. This decline led to the emergence of valleys and streams (wadis) by sculpture and erosion, but the erosion process has been slow due to the drought that characterizes the climate of the area. These streams which form sedimentary basins from upstream to downstream start at 970 meters above sea level and go down to 392 meters below sea level as illustrated in Figure 7, which translates into a difference of 1362 meters between the upstream and the downstream (ARIJ, 2009).

Figure 6: Downstream, Ein Gedi - Dead Sea (Khalayleh, 2017)

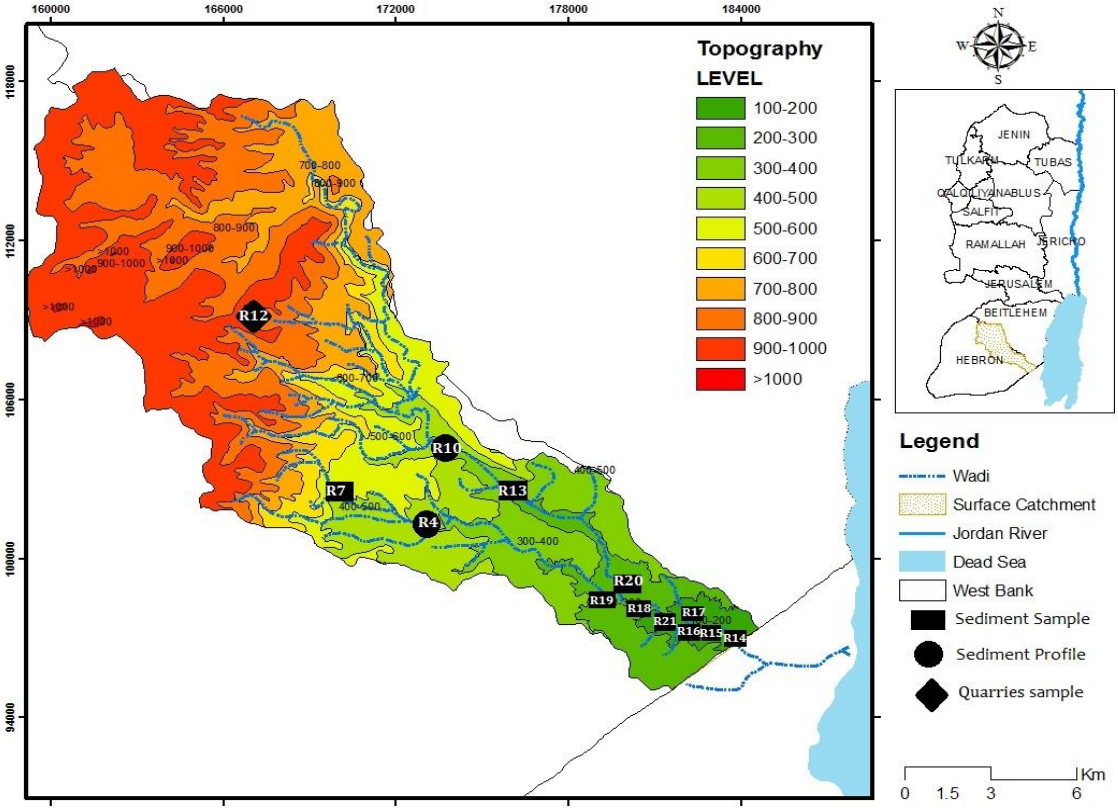

Figure 7: Topography of Bani Na'im Catchment Area (Department of Earth & Environmental Sciences, 2017)

3.1.3 Geology

The catchment area is underlain mainly by Abu-Dis Formation of the Senonian age at the east consisting of chalk and chert, and Jerusalem Formation of the Turonian age at the middle consisting of limestone, stilolithes and dolomites as shown in Figure 8, as well as Hebron – Bethlehem Formation of the Cenomanian age consisting of dolomite, chalky limestone, chalk, and marl, and Beit Kahel Formation of the Albian age consisting of dolomite, limestone, and marl, with the latter two formations located at the west, as Figure 9 and Appendix A - Table 2 show (Department of Earth & Environmental Sciences, 2017).

Figure 8: Wadi Masyadeh (Khalayleh, 2017)

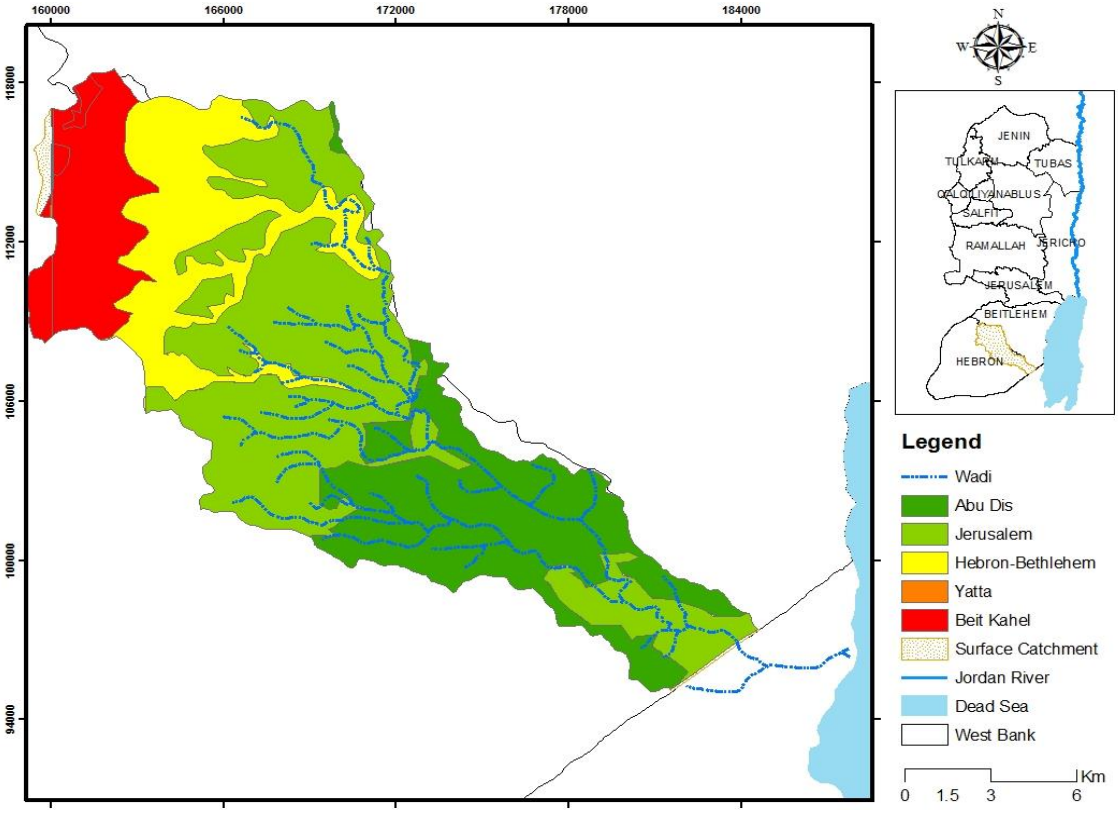

Figure 9: Geology of Bani Na'im Catchment Area (Department of Earth & Environmental Sciences, 2017)

3.1.4 Climate

Bani Na’im’s location makes it among the sun-rich regions in Palestine, as illustrated in Figure 10. The average annual rainfall in Bani Na'im is 369 millimeters, the average temperature is 16 °C, and the average annual humidity is 61%. It is characterized by descending unsaturated air masses, generally light winds, hot dry summers and cool wetter winters (ARIJ, 2009).

Low-latitude Trade Wind belts over continents are arid with little vegetation, so chemical weathering is negligible, and physical breakdown predominates, and semiarid climates with scrub vegetation have low water tables but sufficient summer convective or weak monsoonal precipitation to develop characteristic calcisols, vertisols and in situ oxidative weathering of shallow buried sediment to produce “red beds” (Leeder, 2011).

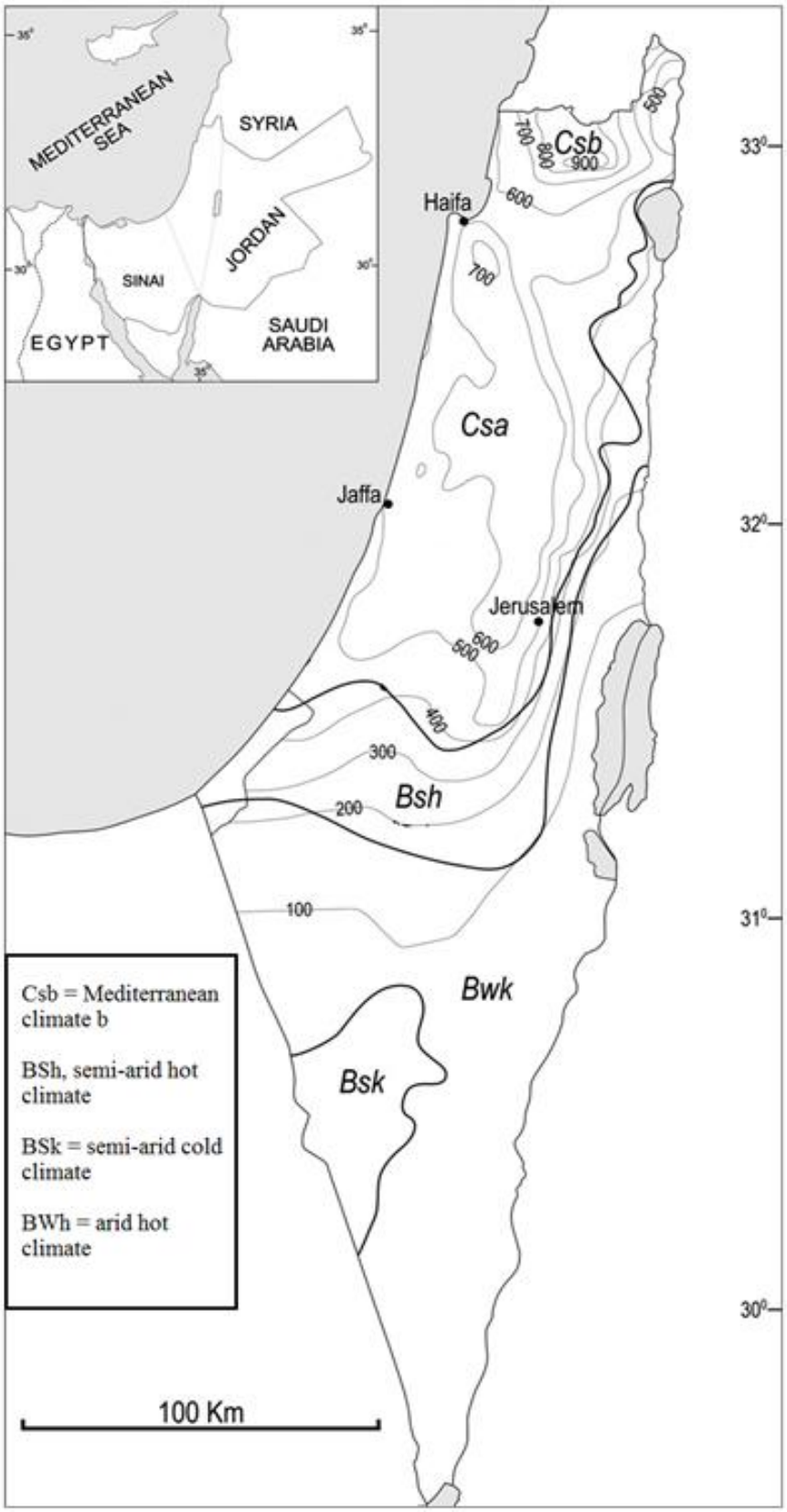

Figure 10: Climate of Palestine (CATENA, 2013)

3.1.5 Population

Bani Na’im has a growing population of approximately 26,000 people with an area of about 157,000 dunums. The gender makeup of Bani Na'im's population is about 50.2% male and 49.8% female. It is also observed that there are several Bedouin communities in the region (PCBS, 2009).

3.1.6 Economy

There are various factories and industrial sites mainly for stone-cutting (quarries), bricks, textiles, olive press, metal and carpentry workshops, and merchandizing. Figure 11 and Figure 12 show examples of such areas in Bani Na’im. The most cultivated crops are grains, especially barley, followed by lentils and chick peas. There is also a sizable segment of livestock. In addition, there are quite a few historical and touristic sites, and a military zone (CIA, 2017).

Figure 11: Quarries near Masyadeh Stream (Khalayleh, 2017)

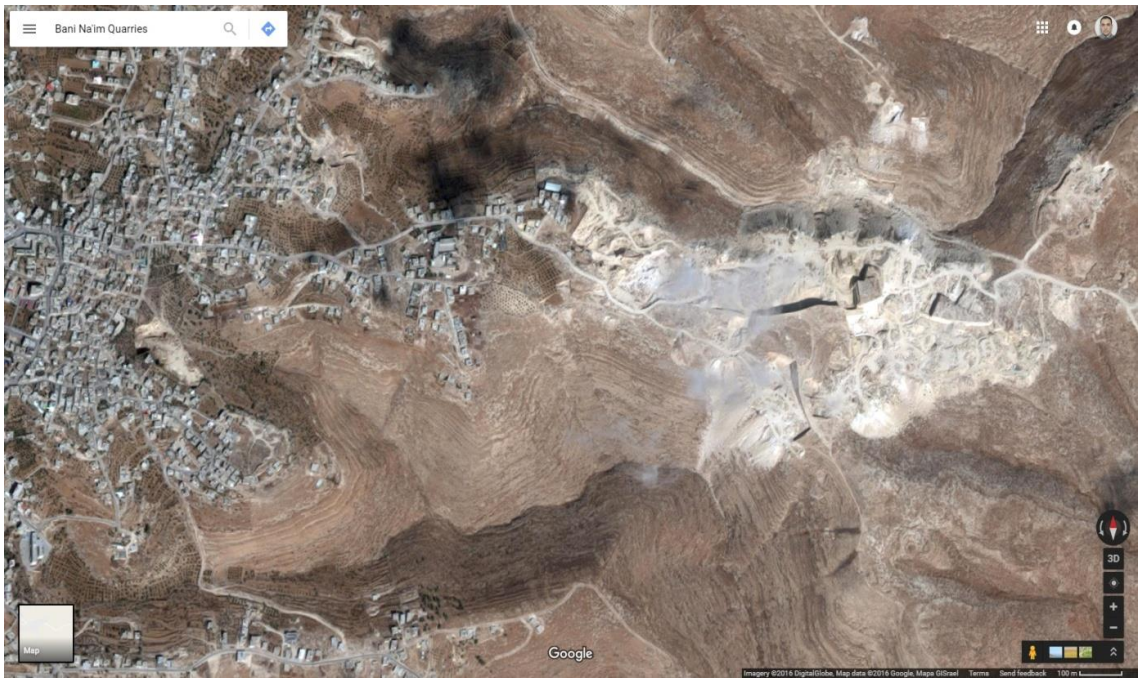

Figure 12: Quarries in Bani Na'im Catchment Area (Google Maps, Adli, 2017)

Quarries are places from which stones are extracted; they provide raw materials and stones classified by quality and color. Usually quarries are located at hills and mountains where rough and large stones are cut then they are manufactured and refined in near stone factories (Makhool & Abu Al-Rob, 1999).

Stone industry in Palestine is considered one of the conventional industries in which raw materials for construction stone is available at quantities and distinguished for its type, quality (hardness), size, and multicolor. It contributes approximately 25% to the national overall industry revenue (Hussain, 2014).

Serious environmental damage is created by these industries, including solid and liquid waste, dust and noise. These have a detrimental impact on the human population as well as on plants and natural resources. These problems are mainly related to inadequate infrastructure services and other economic and administrative factors (Makhool & Abu Al-Rob, 1999).

3.2 Collecting Samples

Sampling was conducted in October and November. Weather during this period was warm and no precipitation events occurred. Stream sediment samples were collected from different lithology in Bani Na'im catchment area along the two streams Al-Ma'zzeh and Masyadeh, and along the stream Al-Ghar (the merge of the two streams). Generally, twelve sample sites distributed along the streams were chosen and one sample from the near quarries, as shown in Figure 13 and Table 1; starting from upstream and going towards downstream.

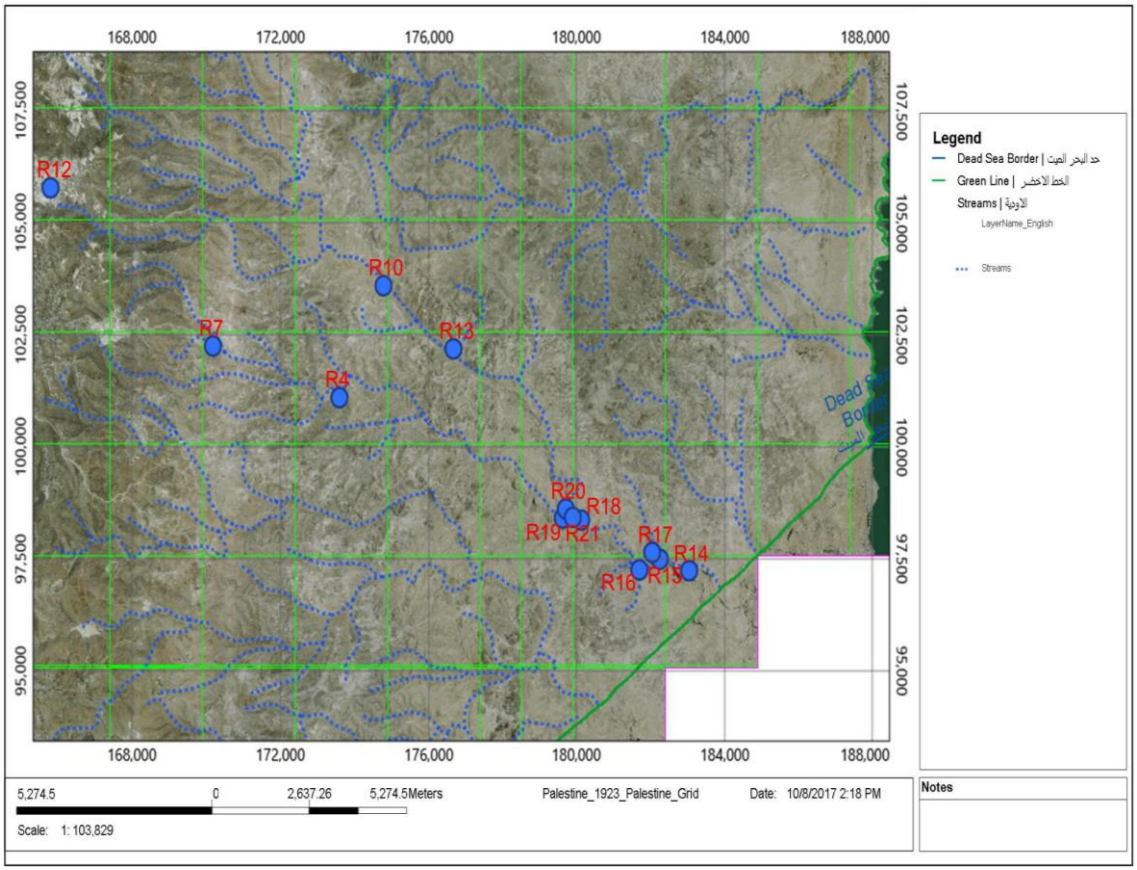

Figure 13: Location of Samples (Khalayleh, 2017)

Table 1: Location and Coordinates of Samples

Location (surface samples – 0 cm)	**Sample**	**Coordinates** **Palestine Grid**			**Sample**	**Depth** (above and below surface - cm)
		East-X	**North-Y**			
Upper Al-Ma'zzeh	**R7**	170177	102249			
Middle of Al-Ma'zzeh	**R4**	173592	101097		**Al-Ma’zzeh Profile**	
Lower Al-Ma'zzeh (before merge)	**R19**	179627	98410		**R6**	345
Upper Masyadeh	**R10**	176880	102038		**R2**	225
Middle of Masyadeh	**R13**	176673	102185		**R1**	120
Lower Masyadeh (before merge)	**R20**	179711	98613		**R3**	35
Middle 1 of Al-Ghar (after merge)	**R18**	180125	98365		**R4**	-12.5
Middle 2 of Al-Ghar (after merge)	**R16**	181695	97253		**R5**	-47.5
Middle 3 of Al-Ghar (after merge)	**R14**	183041	97234		**Masyadeh Profile**	
Quarries	**R12**	165788	105778		**R9**	265
Middle of Al-Ghar (after merge)	**R15**	182246	97491		**R8**	115
Branch Al-Ghar (after merge)	**R17**	182043	97643		**R10**	10
Upper Al-Ghar (after merge)	**R21**	179899	98425		**R11**	-20

Ten other samples were collected from two fissures (rift) sites; one represents Wadi Al-Ma’zzeh profile (Figure 14) and the second represents Wadi Masyadeh profile (Figure 15), and they were collected from different elevations, including above and below the surface.

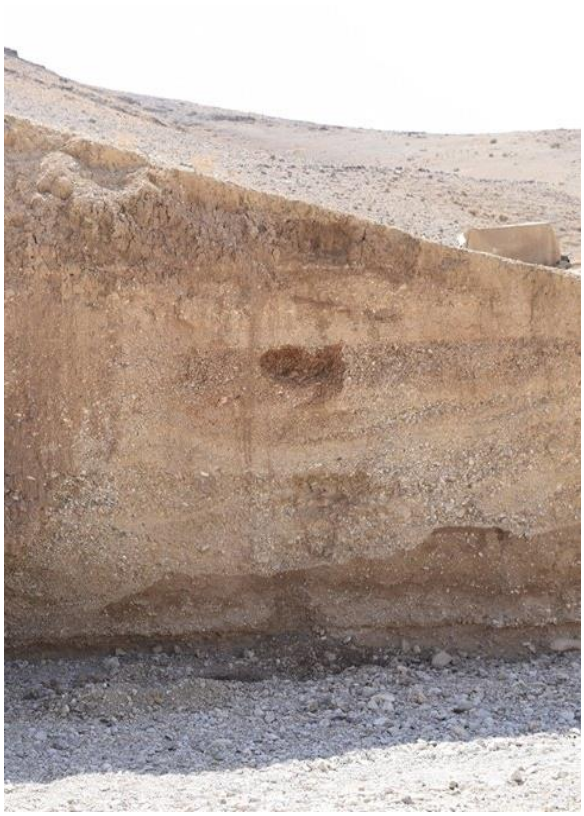

Figure 14: Wadi Al-Ma'zzeh Profile (Khalayleh, 2017)

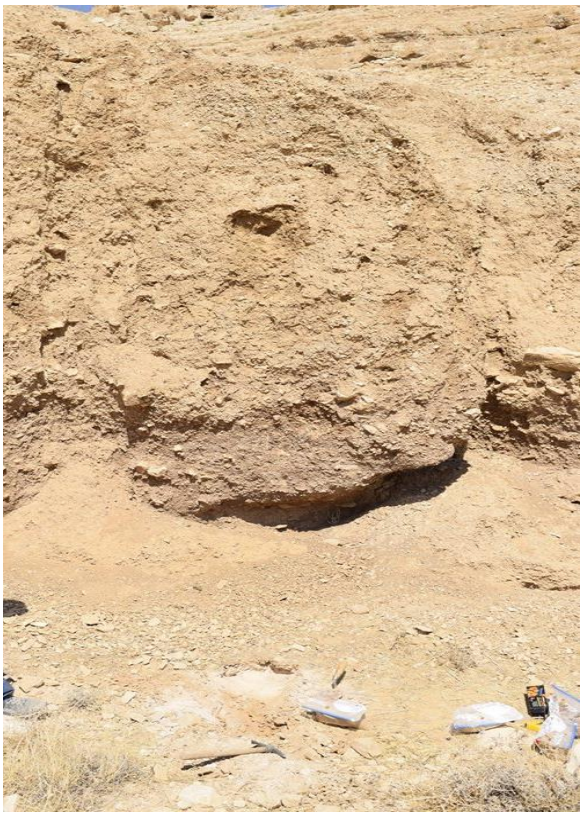

Figure 15: Wadi Masyadeh Profile (Khalayleh, 2017)

3.3 Laboratory Analysis

Samples were obtained by panning about one kilogram of sediment at different elevations from each site. Samples were dried in the oven at 50 °C for 48 hours, all sediment samples were screened through a 2 mm sieve prior to analysis in order to provide a more direct comparison as the finer grain sizes can contain the majority of the trace elements associated with sediments (Horowitz, 1991), about 0.5 gram from each sample was then mixed with 3 ml HF (Hydrofluoric acid), 3 ml HCl (Hydrochloric acid), and 5 ml HNO_3 (Nitric acid) in a digestion vessel, and digested for 50 minutes using microwave (CEM MARS 5), in accordance to the pre-programmed U.S. EPA

method of Microwave Assisted Acid Digestion of Sludges, Soils and Sediments, and sample material and the reagents standards.

The samples were then transferred and diluted into a 50 ml vessel for analysis, in accordance to the method of U.S. EPA Elemental Analysis of Solution Samples with ICP-MS. The samples were chemically analyzed by Inductive Coupled Plasma Mass Spectrometer (ICP-MS) for REE and trace element concentrations.

For total carbon, total organic carbon and total nitrogen, the laboratory analysis took place in Germany at the "Geo-Forschungs Zentrum". The mass spectrometer "Delta plus XL Thermo Fisher" was used, for TC and TN sample preparation; 10 mg in Sn-capsules were used in accordance to EUROVECTOR Elemental Analyzer method. And for TOC sample preparation; 1 mg in Ag-capsules with 20% HCl were used at 75°C in accordance to Carlo-Erba NC2500 Elemental Analyzer method.

For stable isotopes of carbonated carbon-13, oxygen-18 and organic carbon-13, the laboratory analysis took place in Germany at the "Geo-Forschungs Zentrum". The mass spectrometer "MAT253 Thermo" and the carbonate device "KIEL IV" were used, for δ^{13}Corg‰ sample preparation; 1 mg in Ag-capsules with 20% HCl were used at 75°C, and for δ^{13}Ccarb‰ and δ^{18}Ocarb‰ sample preparation; 0.40-0.200 mg with 103% H_3PO_4 were used at 70°C in accordance to Carlo-Erba NC2500 Elemental Analyzer methods.

Grain size analysis by Sieving is used to characterize the sediment samples in different textures in the range of gravel, sand, silt and clay forms; using sieves of different mesh size that are mechanically shaken. The amount trapped in each sieve is weighed and taken as an estimate of the particle size range in the sample.

3.3.1 Inductive Coupled Plasma Mass Spectrometer "ICP-MS"

ICP-MS is a technique to determine low concentrations and ultra-low concentrations of elements. The ICP source converts the elements' atoms in the sample to ions, as illustrated in Figure 16; these ions are then separated and detected by the mass spectrometer. The ICP source has argon gas that flows inside the concentric channel, and there is a radio frequency generator connected to RF load coil, thus oscillating electric and magnetic fields are established. Electrons are striped off the argon atoms when a spark is applied to the argon, forming argon ions. The oscillating fields then catch these ions where they collide with other argon atoms, forming an argon discharge or plasma (Wolf & USGS/CR/CICT, March, 2005).

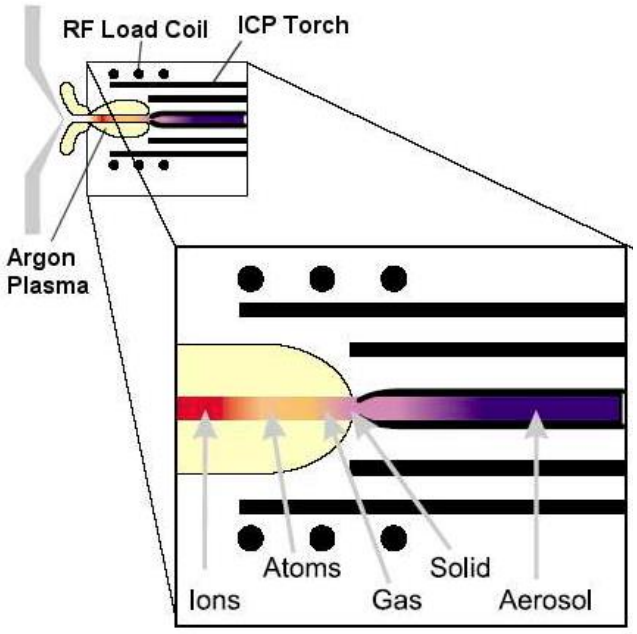

Figure 16: Schematic representation of an ICP source in an ICP-MS (Wolf & USGS/CR/CICT, March, 2005)

The sample is introduced into the ICP plasma as an aerosol, which is formed either by a laser that directly converts solid samples into an aerosol, or by aspirating dissolved solid

or liquid samples into a nebulizer. The sample aerosol is completely desolvated after it is introduced into the ICP torch, and the elements in the aerosol are then ionized towards the end of the plasma, after being converted into gaseous atoms (Wolf & USGS/CR/CICT, March, 2005).

Once the elements are converted into ions, they are transmitted into the mass spectrometer by the interface cones; the two interface cones create an intermediate vacuum region. The ions are brought into the mass spectrometer at low pressure ($<1*10^{-5}$ torr) from an atmospheric pressure region (1-2 torr) of the argon sample stream; this is done through the intermediate vacuum region, as shown in Figure 17 (Wolf & USGS/CR/CICT, March, 2005).

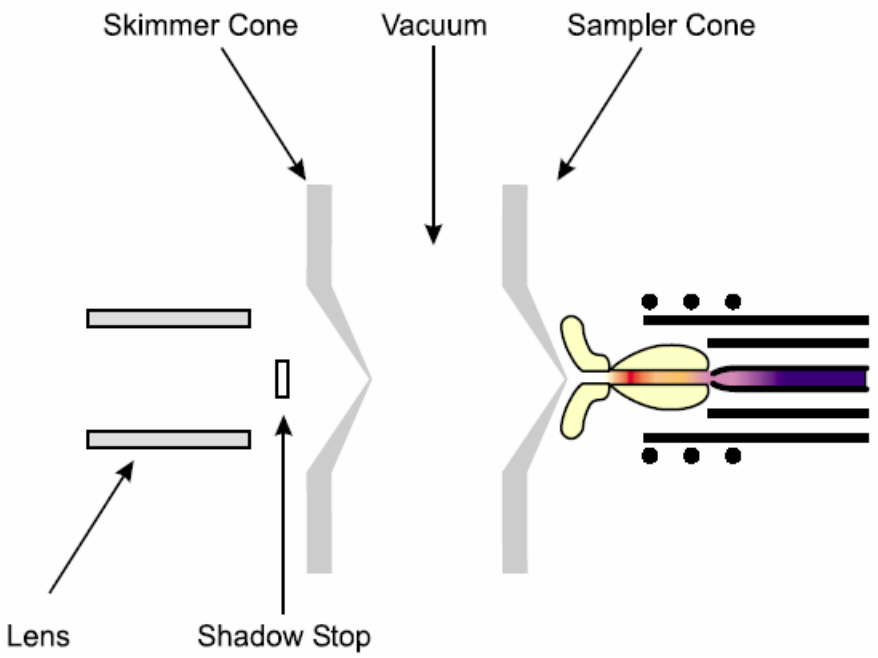

Figure 17: Interface region of an ICP-MS (Wolf & USGS/CR/CICT, March, 2005)

The ions from the ICP source are positively charged, and the system has positively charged electrostatic lenses that serve to collimate the ion beam and focus it into the entrance of the mass spectrometer. Once the ions enter the mass spectrometer, a mass

filter separates them by their mass-to-charge-ratio. A suitable detector either detects or counts these ions by translating the number of ions into an electrical signal; and through the use of calibration standards, the electrical signal can be measured and related to the number of atoms of that element in the sample (Wolf & USGS/CR/CICT, March, 2005).

The advantages of ICP-MS analysis include: extremely low detection limits, a large linear range, and possibility to detect isotope composition of elements. Therefore, it is a good analytical technique by which the nature of the samples can be discussed.

3.3.2 CEM MARS 5

The MARS 5 is a microwave acid digestion system that produces clear digestate from samples for elemental analysis by ICP, ICP-MS, or AA. Rocks, plants, soil, foods, pharmaceuticals, plastics, metals, and more can be digested easily, using preloaded methods. Microwave acid digestion is a technique to dissolve metals, bound within a sample matrix, into liquid. This is achieved by exposing a sample to a strong acid, in a closed vessel and raising the temperature and pressure through microwave irradiation. Both the speed of thermal decomposition of the sample and the solubility of heavy metals in solution are increased. Once these heavy metals are in solution, they can be quantified through elemental techniques (CEM MARS5, 2007).

Chapter Four

Results and Discussion

Chapter Four

4. Results and Discussion

Trace elements and REEs share certain physio-chemical properties which make them useful for near surface geochemical studies. It has been established that REEs in sediments are exceptionally unreactive, making them very useful for provenance studies. Sediments are sources of transportation and sinks for REEs and trace elements, and the fractionation of trace elements and REEs takes place in solid state phase. Information from trace elements and REEs distribution is used to interpret the fundamental geo-chemical conditions and probable source rocks of the sediments of interest (Obaje, et al., 2015).

To achieve the main aims of this study; the laboratory analyses and results developed were interpreted to better understand Wadi Al-Ghar stream sediments as indicators of their source and paleo-weathering and to serve as an important input to the geo-chemical characteristics of this catchment area.

4.1 Grain Size

Grain size was measured by sieving as shown in Appendix C – Table 10 and the data was analyzed by the "GRANISTAT" software which uses the Method of Moments. Results show that most sediment samples belong to the textural group 'Sand'; moderately sorted very coarse sand, with grain size distribution of ~97% sand and ~3% mud. Meanwhile, the quarries' sample belongs to the textural group 'Muddy Sand'; medium silty fine sand, with grain size distribution of ~77% sand and ~23% mud, as shown in Appendix C - Figure 47. Hence, the alluvial fans formed the catchment

terrestrial clastic sediment were influenced by both climatic and tectonic controls on fan architecture. The major tectonic feature of the region which controls the stratigraphic and structural evolution is the Dead Sea Rift (Zain Eldeen, et al., 2002). The terrestrial clastic sediment is derived from an altered regolith with a soil profile produced by chemical weathering of pristine bedrock and a calcite source of mineral grains for such sediment. Calcite is usually predominant in clastic sediments and comprises the most abundant sand-sized grains (Leeder, 2011).

4.2 Trace Elements

Appendix C – Table 4 and Table 5 shows the trace element concentrations in the samples. Thirteen trace elements were analyzed in stream sediment at Bani Na'im catchment area. Trace elements were graphed against Al as a reference element since it is the third abundant element in the earth's crust (Osman, 2013) to facilitate the comparison between catchment area sites.

The correlation coefficient R-squared is a statistical measure of how close the data are to the fitted regression line, i.e. how strong of a linear relationship there is between variables. The matrices; Figure 18 and Figure 19 show that there is strong positive linear correlation between aluminum and trace elements supported by the high R^2 values, except for Sr which has a moderate positive linear correlation, and for Ni which has a weak positive linear correlation supported by the low R^2 values. R^2 revealed that no negative linear relations exist among the trace elements. The positive relations explain the similar distribution that these elements show throughout the wadis.

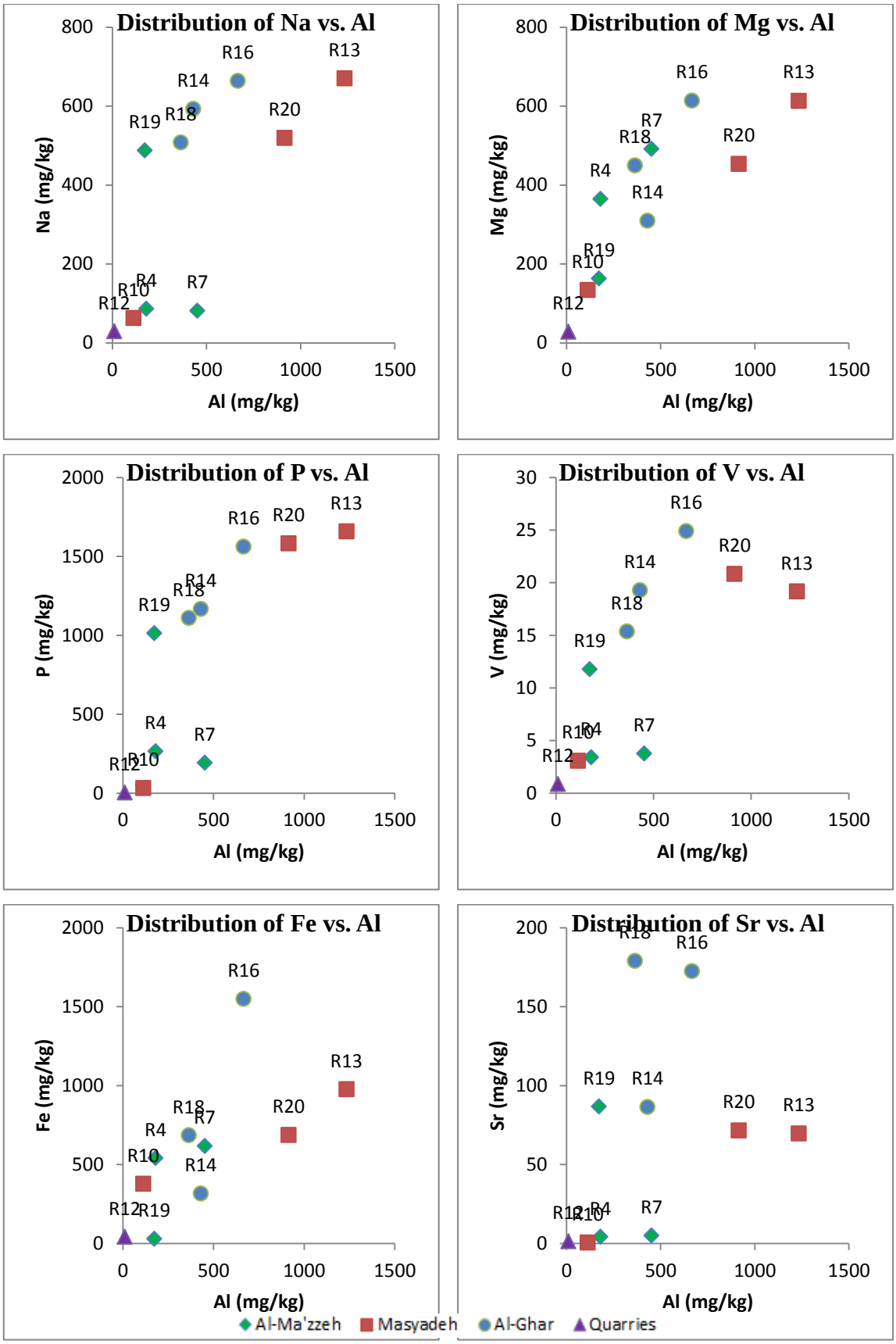

Figure 18: Distribution of Major - Trace Elements (Na, Mg, P, V, Fe, and Sr) vs. Al

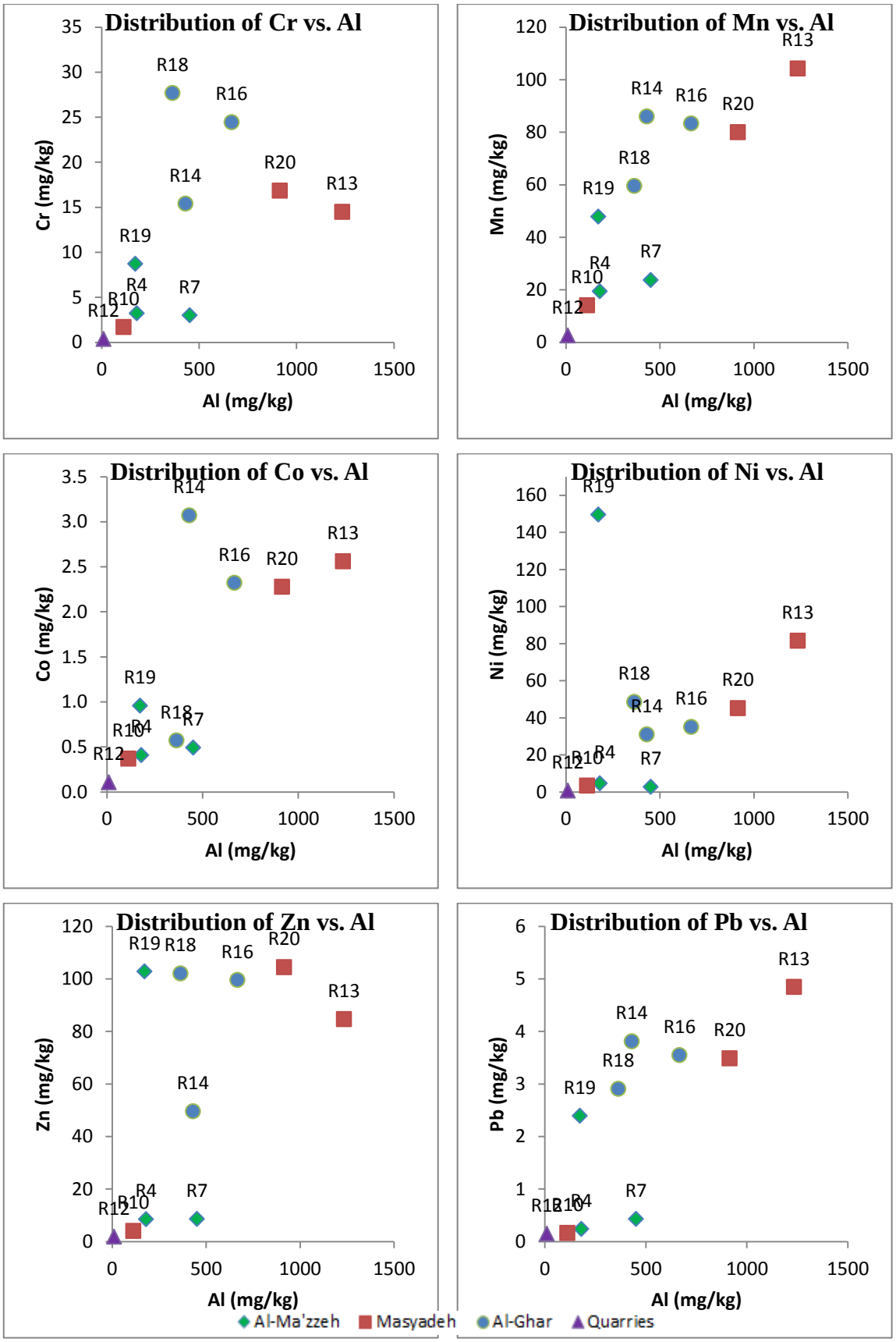

Figure 19: Distribution of Trace Elements (Pb, Zn, Ni, Co, Mn, and Cr) vs. Al

As for the possibility of measurement error, the SEM was found to be low in most cases, reflecting a relatively high accuracy of measurement for these trace elements, except for Fe and P, probably due to a couple of less accurate measurements that are spread farther away from the "true" measurement.

Concentrations of trace elements are mainly higher after the final merge of the wadis. Because of their elevated concentrations, it is concluded that both wadis – Al-Ma'zzeh and Masyadeh – contribute to Wadi Al-Ghar, with an evident greater contribution from Wadi Al-Ma'zzeh.

Figure 18 and Figure 19 show the distribution of trace elements versus Aluminum in stream sediments. It was observed in the scatterplots that Wadi Masyadeh's R10 sample was very close to the quarries sample of R12 in terms of trace elements distribution versus Aluminum. This shows that quarries probably have a substantial impact on the sediments distribution of Wadi Masyadeh.

Except for iron, the closely related R4 and R7 samples of Wadi Al-Ma'zzeh also showed a strong likelihood of quarries having effect on their trace elements distribution, as shown by their concentration closeness to R12 for the main part.

When comparing Wadi Al-Ma'zzeh and Wadi Masyadeh distribution, it was observed that Wadi Al-Ma'zzeh sample R19 seems to contribute more into Wadi Al-Ghar (the merge) than does Wadi Masyadeh sample R20; this can be seen by the proximity of R19 and R18 distribution in most cases. Moreover, it can be argued in some cases that these 3 samples are closely grouped to one another.

Figure 20 shows that the concentration of trace aluminum element in sediment increases after the merge of the two wadis and towards downstream.

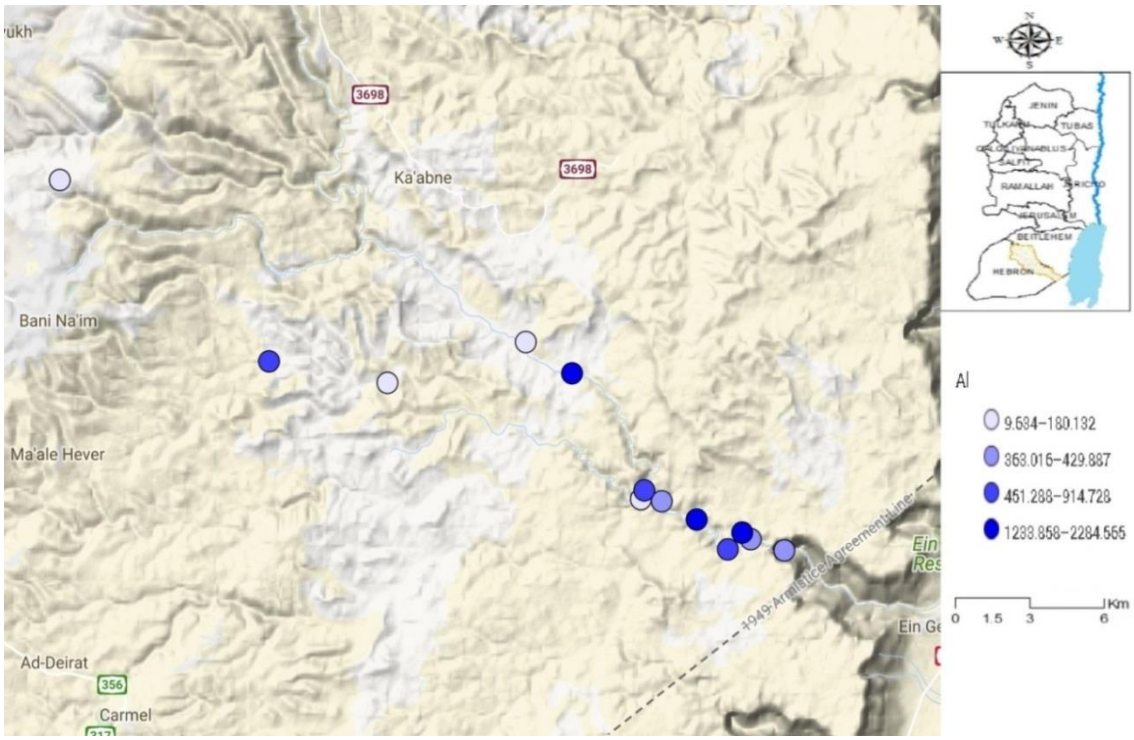

Figure 20: Territorial distribution of Aluminum (mg/kg)

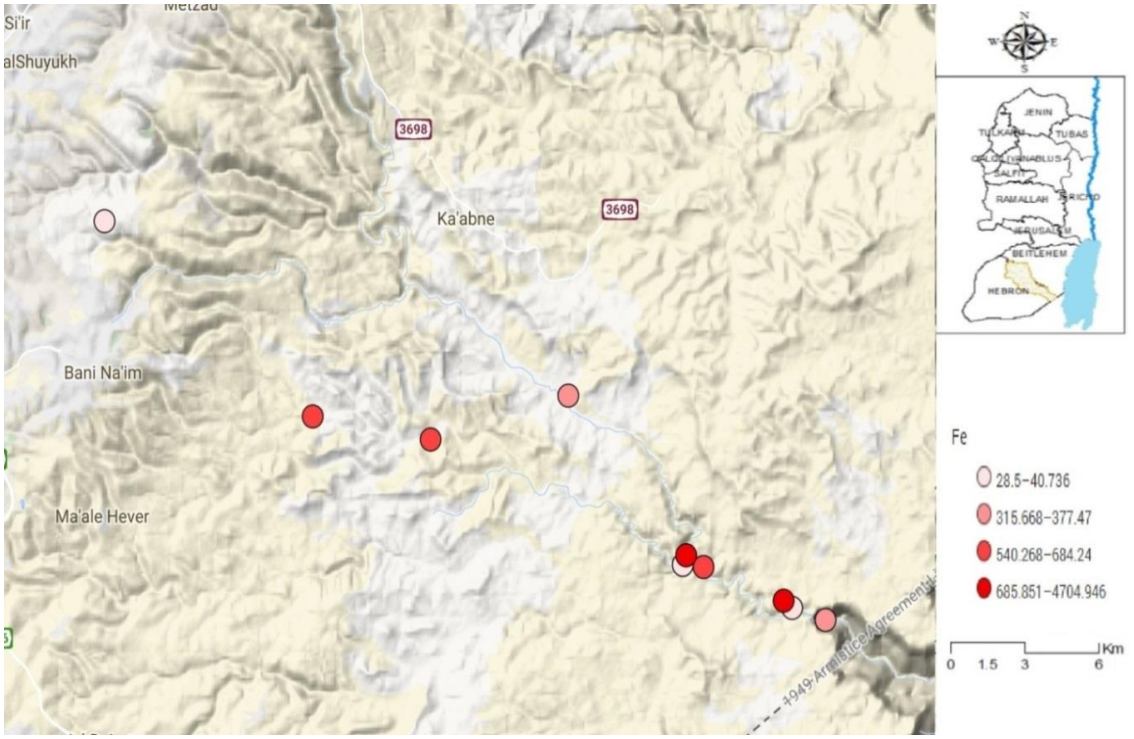

Figure 21: Territorial distribution of Iron (mg/kg)

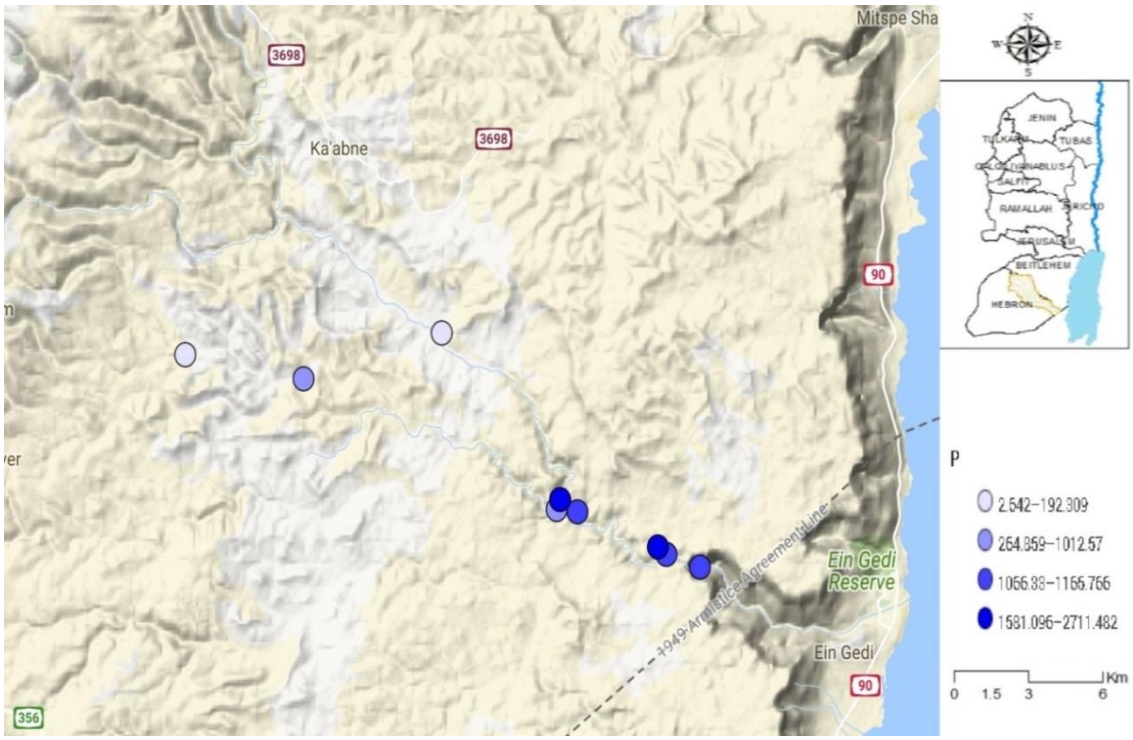

Figure 22: Territorial distribution of Phosphorus (mg/kg)

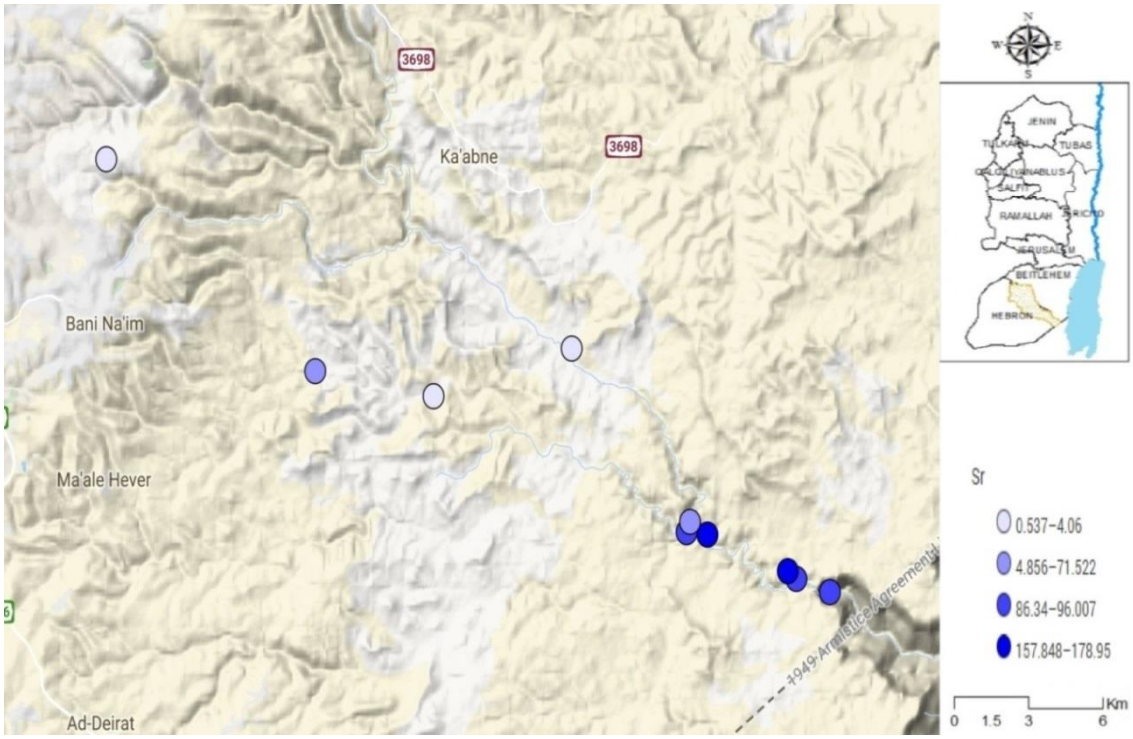

Figure 23: Territorial distribution of Strontium (mg/kg)

While Figure 21 shows an inconsistent pattern of trace iron element concentration in stream sediment.

Figure 22 shows that the concentration of trace phosphorus element in sediment increases after the merge of the two wadis and towards downstream.

Also Figure 23 shows that the concentration of trace strontium element in sediment increases after the merge of the two wadis and towards downstream.

The scatter plots and the territorial maps show the classification of sampling locations in the wadis. Generally, concentrations were highest at the site after the merge of the wadis.

The enrichment of Al, Fe, P, and Sr was mainly related to local deposition of sediments and associated to slope of the catchment area. The elements were enriched downstream, and this enrichment was linked to the merge of the wadis, further emphasizing the contribution of Wadi Al-Ma'zzeh and Wadi Masyadeh to Wadi Al-Ghar.

Stream sediments formed from parent material show high occurrence; chalk and limestone are the main sedimentary rocks and their major materials are mineral calcites. Concentrations of trace elements in the stream sediment probably originate from the levels of these elements in the rocks of the area. The above results emphasize the importance of parent material composition and stream sediment forming processes on background concentrations of trace and major elements in sediments.

It is clear that there are differences for trace and major element concentrations among the catchment area. These results show a strong indicator that both trace and major

elements data highly depend on local lithology representing small scale geochemical changes.

4.3 Rare Earth Elements

Appendix C – Table 6 shows the REE chondrite-normalized in the samples and Table 7 shows the REE concentrations (ppb). Fourteen REEs were analyzed in stream sediment at Bani Na'im catchment area. The elements were further grouped into light REEs (LREEs) from La to Gd and heavy REEs (HREEs) from Tb to Lu. The REE concentrations were normalized to their chondrites (ppm/chondrite) and displayed using a categorical graph as shown in Figure 24.

Figure 24 shows a moderate enrichment in LREE (average = 0.21), over the HREE (average = 0.07). The catchment area sediment is characterized by Ce and Eu anomalies; [Ce/Ce*] = [Ce/√(La*Pr)] ranges from 0.64 to 0.94 (average = 0.78) and [Eu/Eu*] = [Eu/√(Sm*Gd)] ranges from 0.70 to 1.27 (average = 0.98). It can also be observed that Cerium goes under some depletion, illustrated by its minor negative anomalies; this anomalous behavior is indicative of oxic environment and could be developed in corestones during spheroidal weathering (Seto & Akagi, 2008). On the other hand, Europium undergoes enrichment (ex. R18) and depletion (ex. R12) events reflecting a variety of anomalies with different sediment samples; a minor Eu anomaly indicates a preferential mobilization of Eu during weathering of host lithology (Bea, 2015). [La/Yb] ratios range from 5.711 to 7.37 (average = 6.61) and this indicates high erosional rates. The result suggests that La was removed from crustal source via weathering process, transported and deposited by the streams (Obaje, et al., 2015).

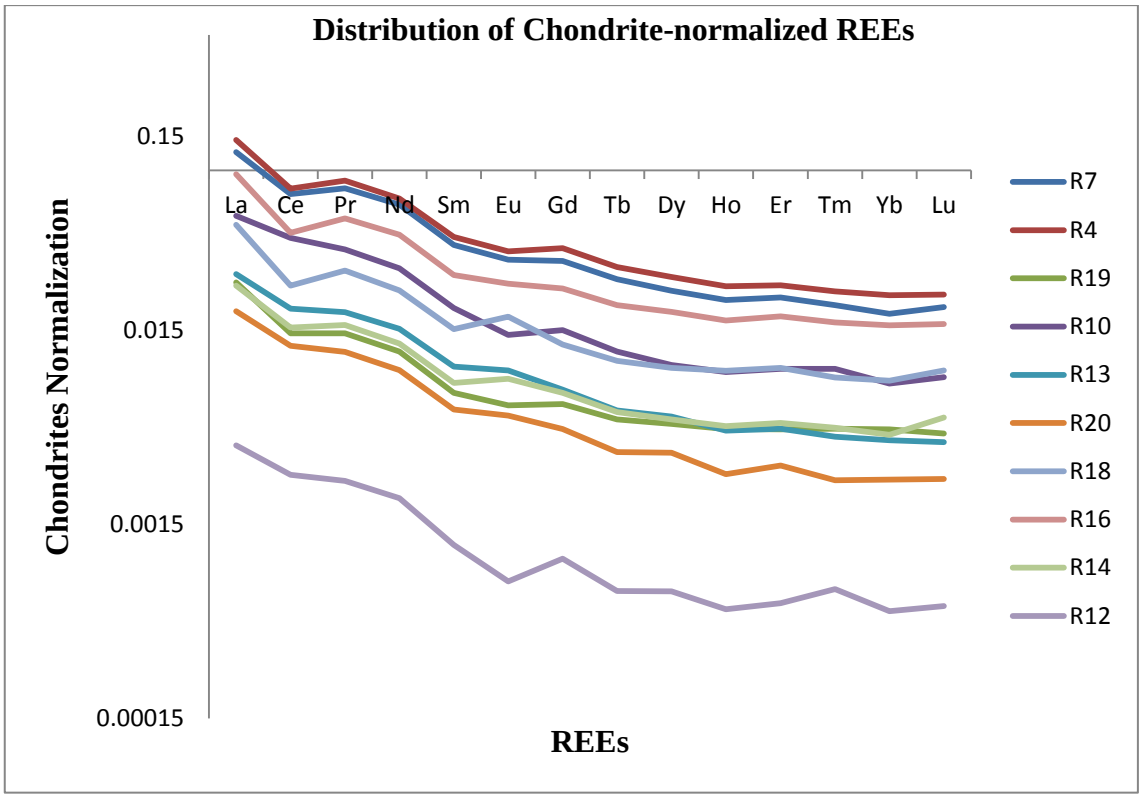

Figure 24: Distribution of Chondrite-normalized REE - Surface Samples

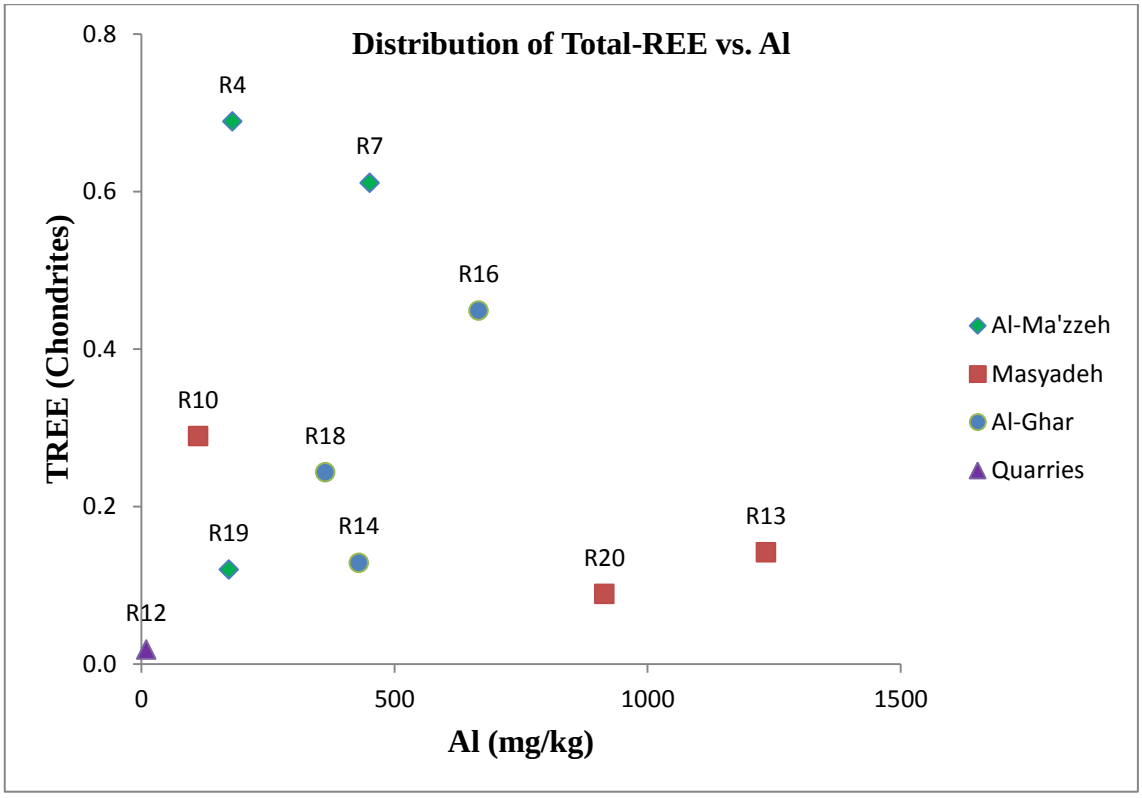

Figure 25: Distribution of Total-REE vs. Al

The distribution trend also revealed that REEs have high total concentration in the upstream areas when compared to the downstream area, and generally positive anomalies in the midstream areas. This indicates that some leaching took place while these REEs were travelling along the path.

In Figure 25 for Total-REE (TREE = ∑REE), it is evident that Wadi Al-Ma'zzeh – R19 and Wadi Masyadeh – R20 contribute to Wadi Al-Ghar – R18 (merge of the two wadis). It can also be seen that R4 and R7 samples of Wadi Al-Ma'zzeh have high concentrations of TREE, and this Wadi has greater contribution into Wadi Al-Ghar.

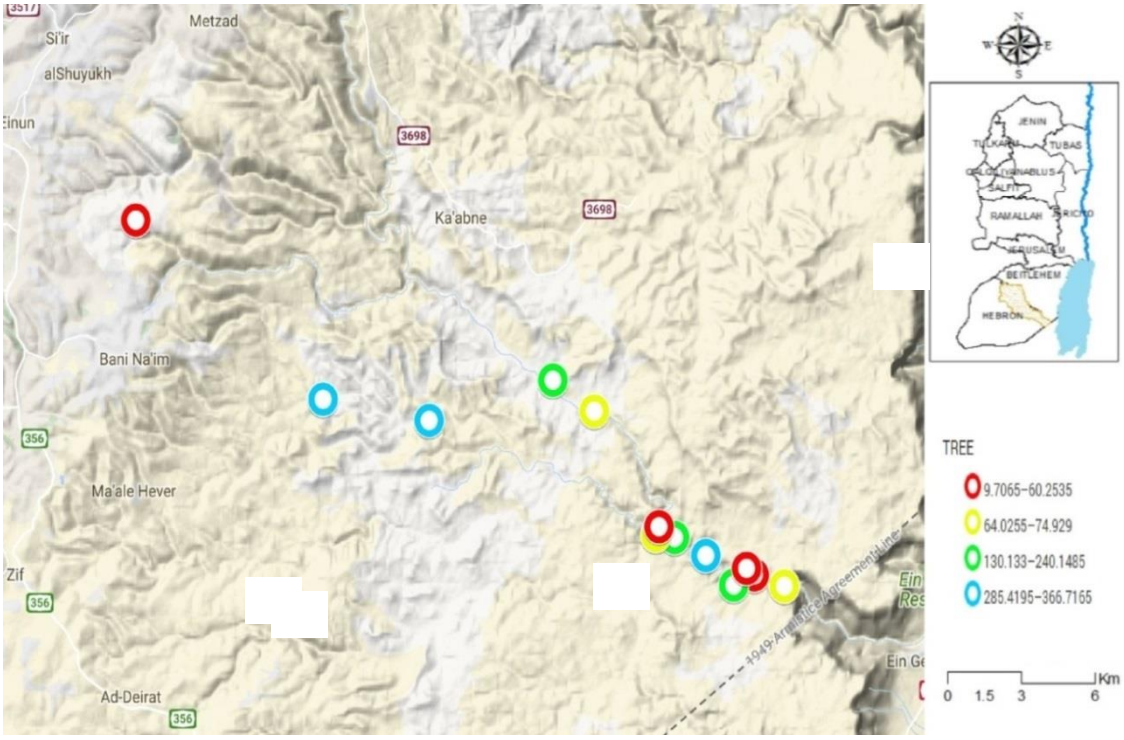

Figure 26: Territorial distribution of TREE (mg/kg)

Figure 26 shows that the midstream and the merge of Wadi Al-Ma'zzeh and Wadi Masyadeh have high TREE concentrations. The geochemistry of the stream sediments reflects the influence of quarries, while many features of their geochemistry are consistent with the element concentrations in the enclosing rocks. In these cases, local

mineralization or enrichment and depletion due to catchment morphology and differential weathering conditions may account for some changes.

The SEM for the overall REE (including all Wadis and the quarries) was low, hence reflecting a good level of accuracy for these measurements. When the SEM was calculated solely for the Al-Ma'zzeh profile, the resulting accuracy of measurements was high, with a somewhat lower accuracy level for Eu/Eu* (SEM = 0.635). A similar pattern is also seen for the SEM of the Masyadeh profile, but with the La/Yb having a relatively higher SEM value (0.487). The reason is probably due to one or two samples being seemingly different than the rest, thus probably not truly reflecting the "true" measurement.

4.4 Total Carbon and Total Nitrogen

Appendix C – Table 8 shows the total carbon, total organic carbon, total nitrogen, total inorganic and calcium carbonate percentages in the samples.

Generally, Wadi Masyadeh has higher component percentages of TC%, TN%, TOC%, and IOC% than does Wadi Al-Ma'zzeh, as shown in Figure 27. In addition, calcium carbonate is the largest source of inorganic carbon (IOC) as illustrated by their strong linear correlation. A clear direct relationship also exists between $CaCO_3$ and total carbon. It was also observed that the percentage of $CaCO_3$ decreases towards downstream revealing a possibility of leaching.

Abu Dis and Jerusalem formations are the main underlain of the catchment area consisting of chalk, chert and limestone, which form from minerals calcite; calcite is an ionic salt called calcium carbonate $CaCO_3$. Carbonates of all types are commonly associated with regions of tectonic stability. Terrestrial carbonates precipitate from

waters supersaturated with respect to calcium carbonate due to dissolution of carbonate bedrock. Figure 27 shows a pedogenic carbonate where the carbonate horizon has a sharp top and the carbonate content decreases downward (Tanner, 2010), this bares that quarries likely contribute largely to the abundance of calcium carbonate in the stream sediments.

Figure 28 shows the correlation of total carbon, and total nitrogen and Aluminum at each stream; the R^2 value of 0.14 shows that there is a somewhat weak positive relationship between Al and TOC%, as well as between Al and TN% where R^2 is -0.18 but negative relationship, while the other total component percentages do not necessarily show a clear linear relationship with Aluminum. This reveals that there is no similar distribution of total carbon and total nitrogen through the wadis.

Figure 29 shows a strong linear correlation existence between TN% and TOC% as supported by the high R^2 value of 0.95. Higher C/N ratios potentially reflect delivery of a greater proportion of terrestrial organic matter to the sediment (Heikkilä, et al., 2010). This high ratio observed in the stream sediment could be due to the contribution of plants in the region besides the human use of the land for livestock and grazing.

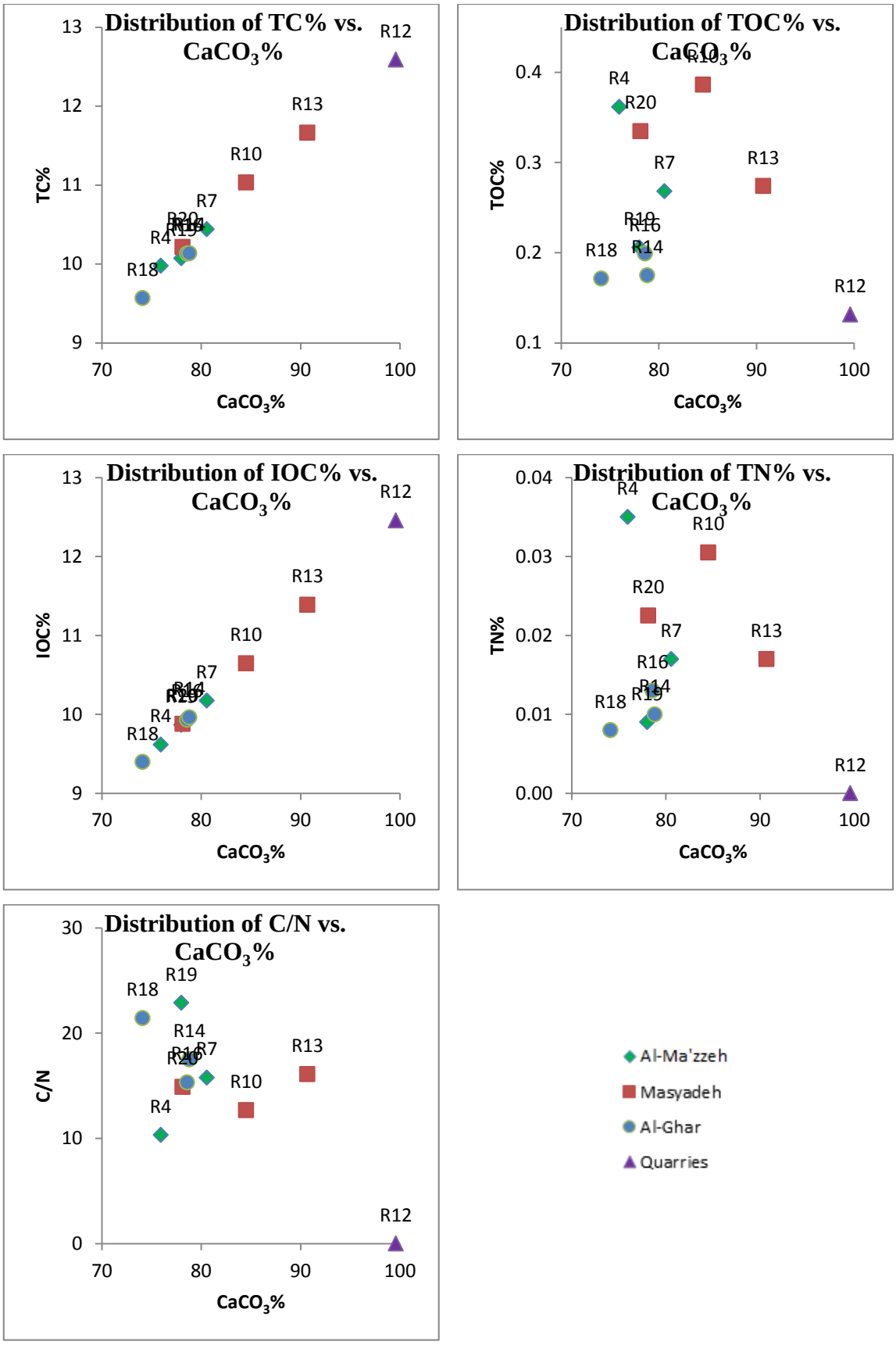

Figure 27: Distribution of TC%, TOC%, IOC%, TN%, and C/N vs. $CaCO_3$%

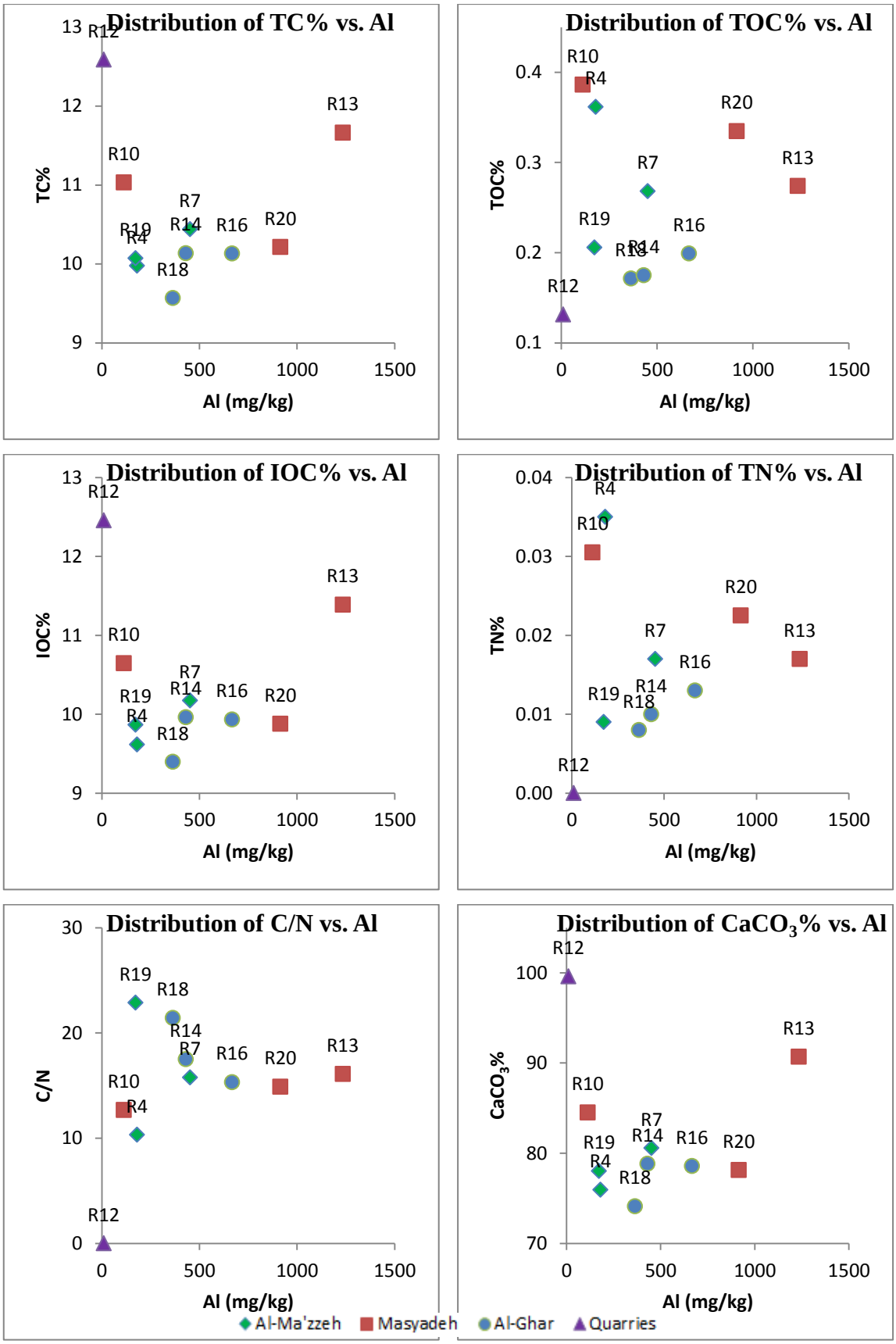

Figure 28: Distribution of TC%, TOC%, IOC%, TN%, C/N%, and $CaCO_3$% vs. Al

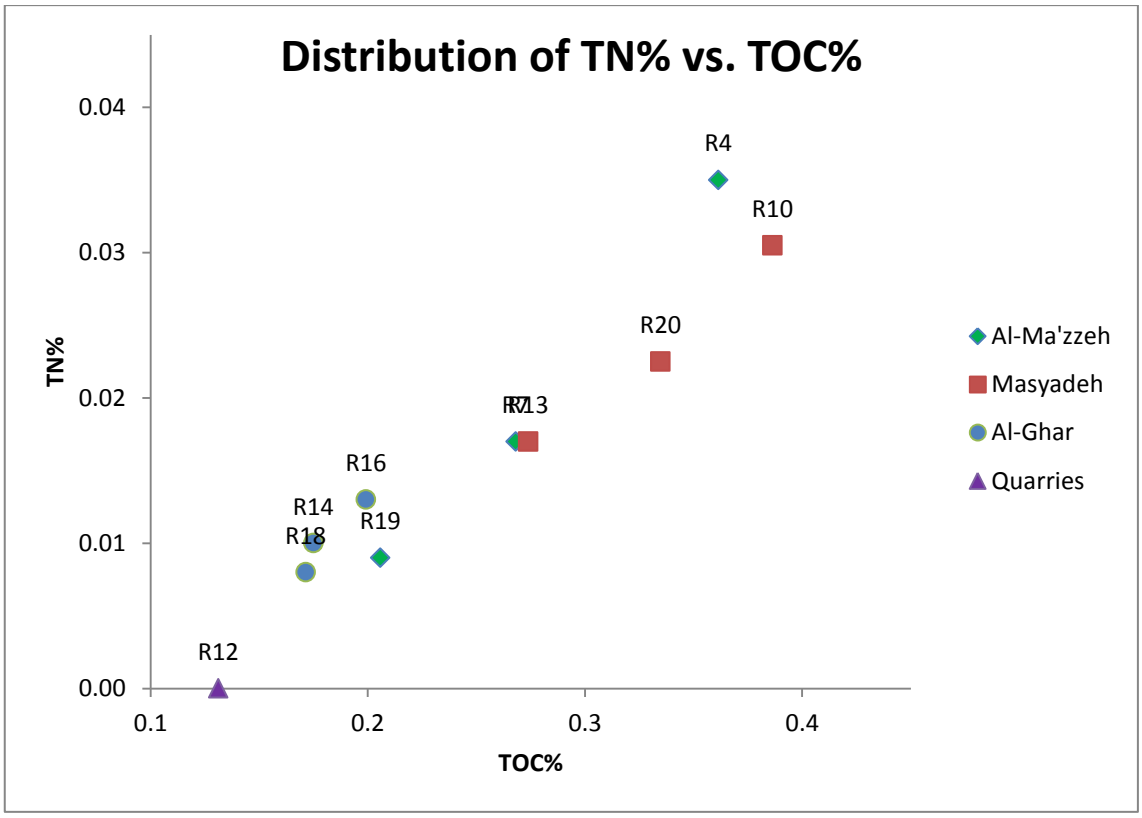

Figure 29: Distribution of TN% vs. TOC%

TC% and same trace elements; grouped each stream. Although not a clear trend is seen in Figure 30, the TC% does, to some extent, have a moderate negative relationship with Mg and Na with R^2 values of -0.38 and -0.35 respectively, a weak negative relationship with Fe with R^2 value of -0.24, and it can be argued that there is some weak negative correlation between the TC% and Al with R^2 value of -0.02. These negative relations indicate that total carbon and trace elements do not follow the same pattern and that trace elements distribution is not influenced by total carbon.

Generally, organic matter interacts strongly with trace metals; however, statistical analysis of selected trace elements indicated that the concentrations were not correlated with the organic carbon percentage in the wadis, but rather with their inorganic carbon percentage.

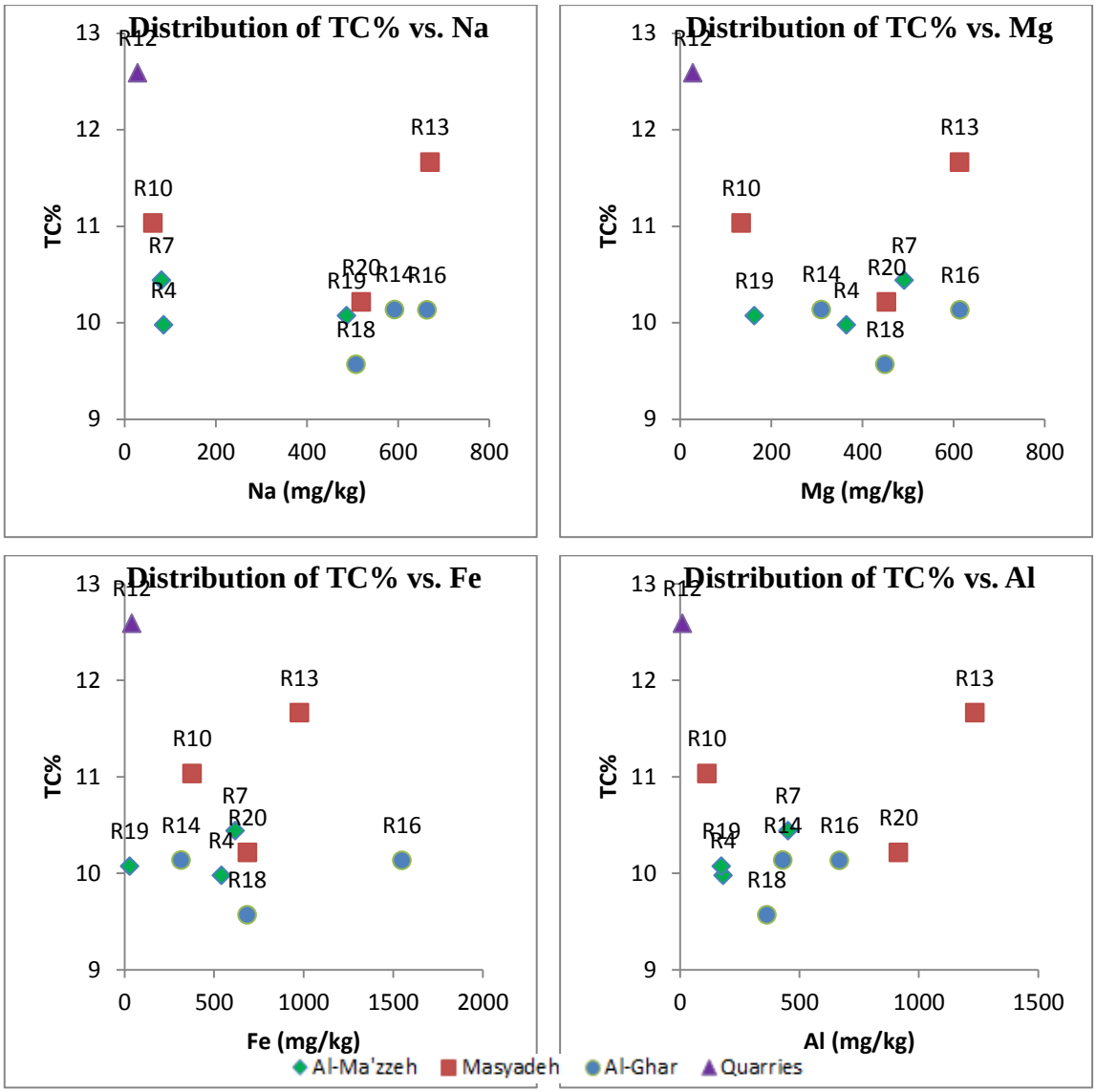

Figure 30: Distribution of TC% vs. Mg, Na, Fe, and Al

The SEM for the overall TC and TN (including all Wadis and the quarries) was generally on the low side, but the C/N vs. $CaCO_3$ distribution showed a bit more spreading around the "true" measurement. An example of that is the Quarries sample R12, which was a bit high than the rest of the measurements for C/N vs. $CaCO_3$.

Figure 31 shows the distribution of the total carbon concentration along the path of travel. It is evident that downstream has lower concentration of TC% than upstream, reflecting the fact that some leaching occurred on the way.

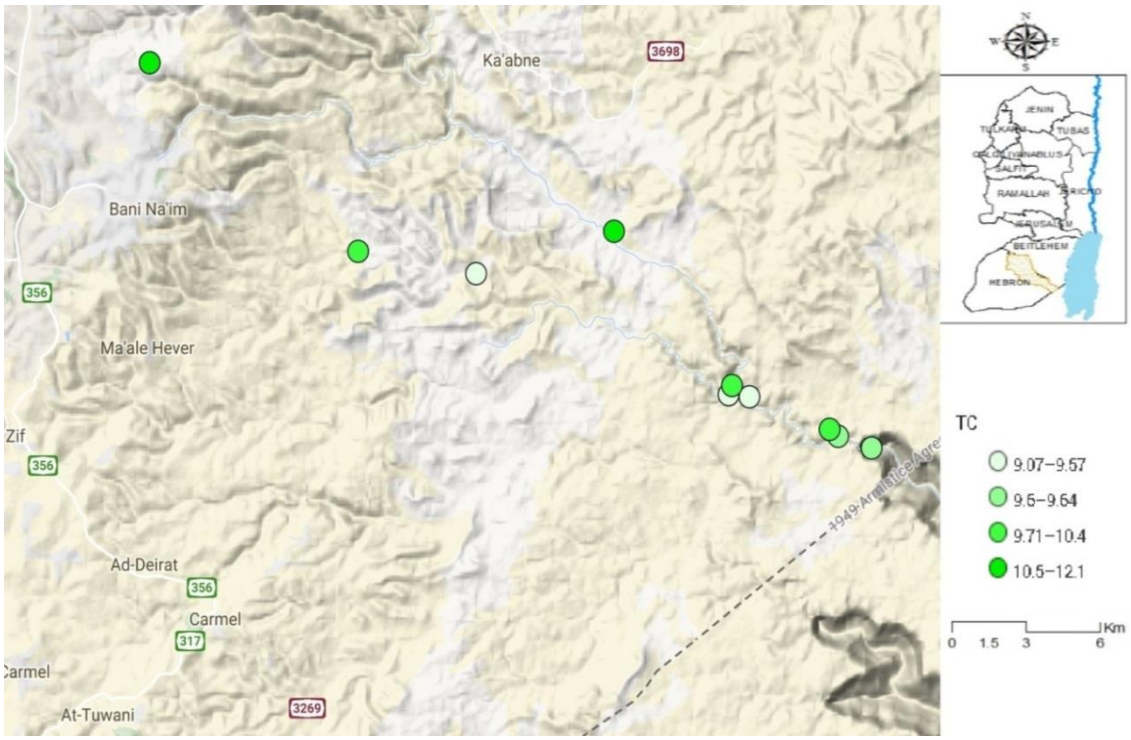

Figure 31: Territorial distribution of TC%

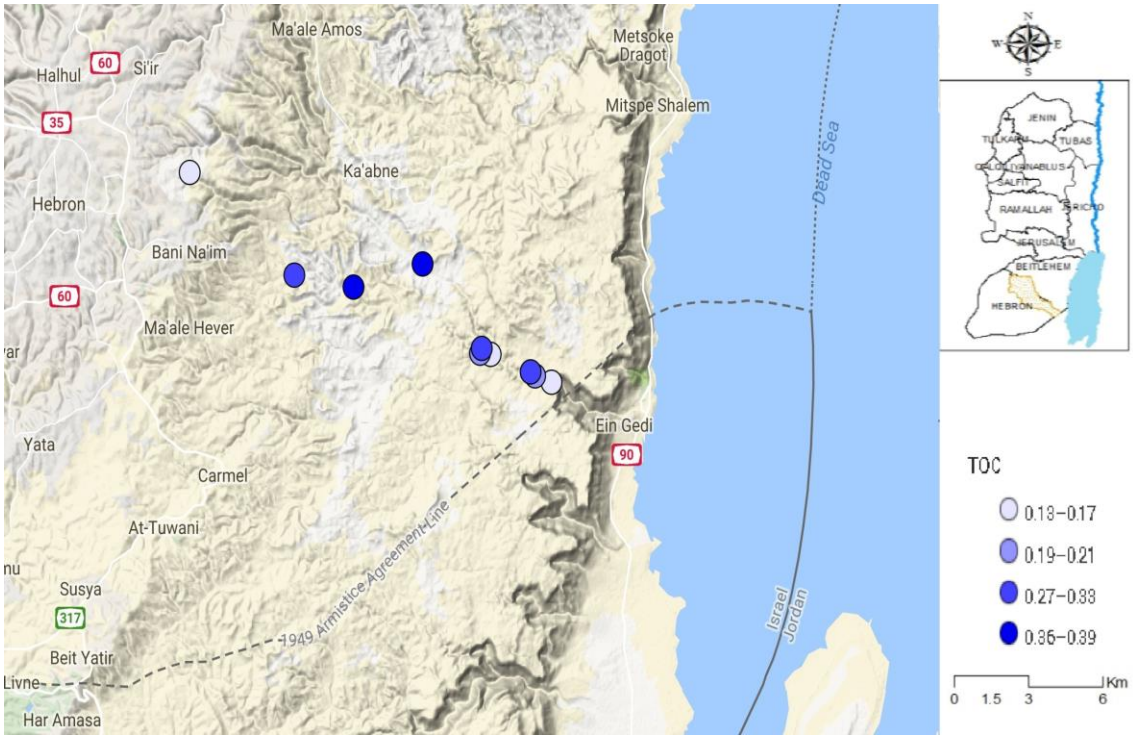

Figure 32: Territorial distribution of TOC%

Figure 32 shows the distribution of the total organic carbon concentration along the path of travel. It may be argued that upstream and midstream have higher concentrations of TOC% as compared to the downstream, indicative of a leaching possibility.

4.5 Isotopes

Appendix C – Table 9 shows the stable-isotopes of carbonated carbon-13, oxygen-18 and organic carbon-13 (‰, per mille) in the samples.

Figure 33 shows a moderate negative trend between δ^{13}Corg‰ and δ^{13}Ccarb‰ as supported by the R^2 value of -0.46. Both the δ^{13}Corg‰ and δ^{13}Ccarb‰ values have no significant covariance; the δ^{13}Corg‰ ranges from -26.76 to -23.17 (average = -24.57) and the δ^{13}Ccarb‰ ranges from -5.59 to -1.16 (average = -3.53). The carbon isotopic composition of carbonate (δ^{13}Ccarb‰) was typically heavier than organic carbon (δ^{13}Corg‰), therefore the source of sediment organic carbon is produced by vegetation which includes trees, shrubs and cool-season grasses and thus pedogenic carbonates are controlled by local vegetation; the organic δ^{13}C‰ under plant species has an average of −27‰ (Tanner, 2010).

Figure 34 shows a strong positive linear correlation between δ^{13}Corg‰ and δ^{18}Ocarb‰ as supported by the high R^2 value of 0.88, while the R^2 value of -0.76 indicates a strong negative linear correlation between δ^{13}Ccarb‰ and δ^{18}Ocarb‰. Statistically, there is no significant covariance between δ^{13}Ccarb‰ and δ^{18}Ocarb‰. Both the δ^{13}Ccarb‰ and δ^{18}Ocarb‰ show that samples R10 and R12 are associated, pointing out the impact of the quarries (R12) on Wadi Masyadeh (R10). The contribution of Wadi Al-Ma’zzeh and Wadi Masyadeh into Wadi Al-Ghar is indicated by the association of R20, R19 and R18.

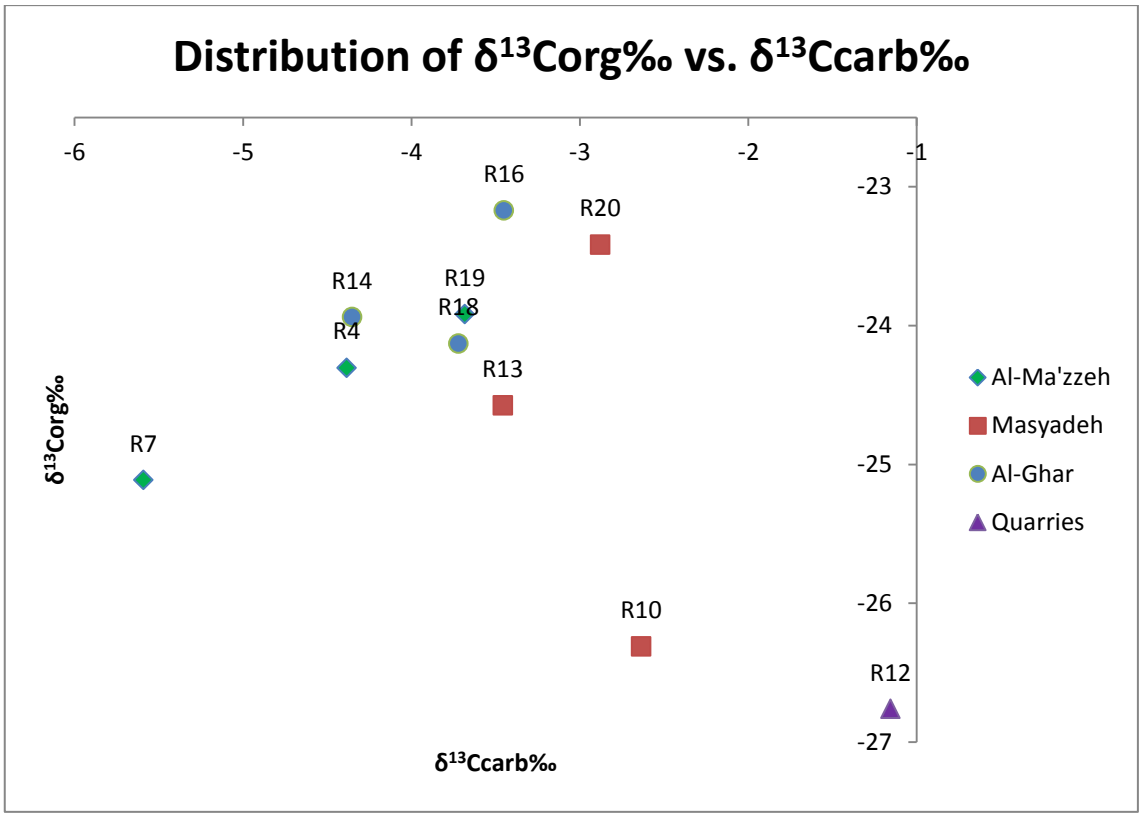

Figure 33: Distribution of δ^{13}Corg‰ vs. δ^{13}Ccarb‰

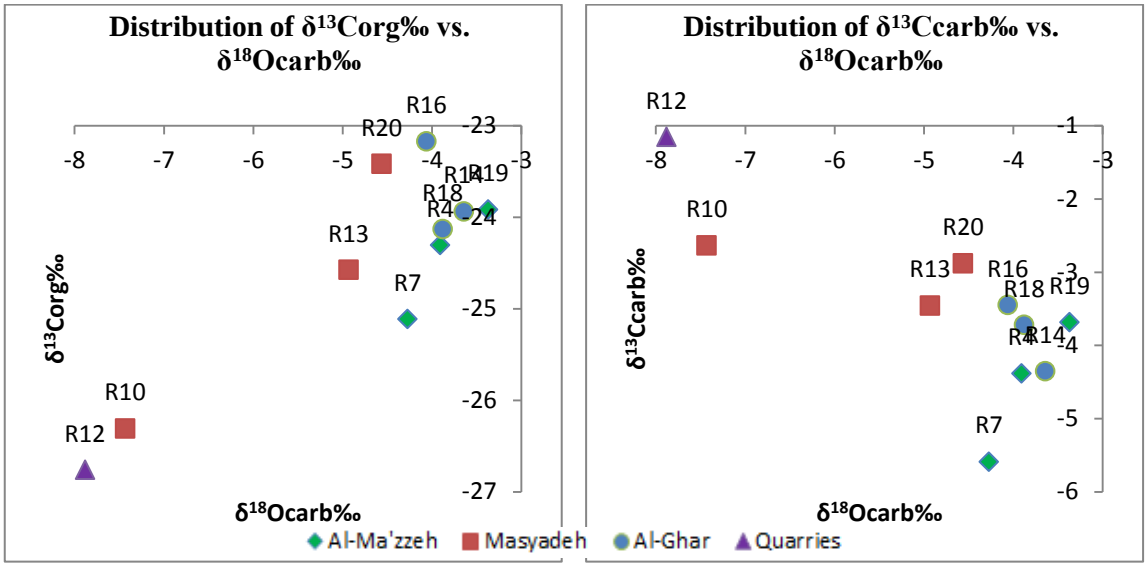

Figure 34: Distribution of δ^{13}Corg‰, and δ^{13}Ccarb‰ vs. δ^{18}Ocarb‰

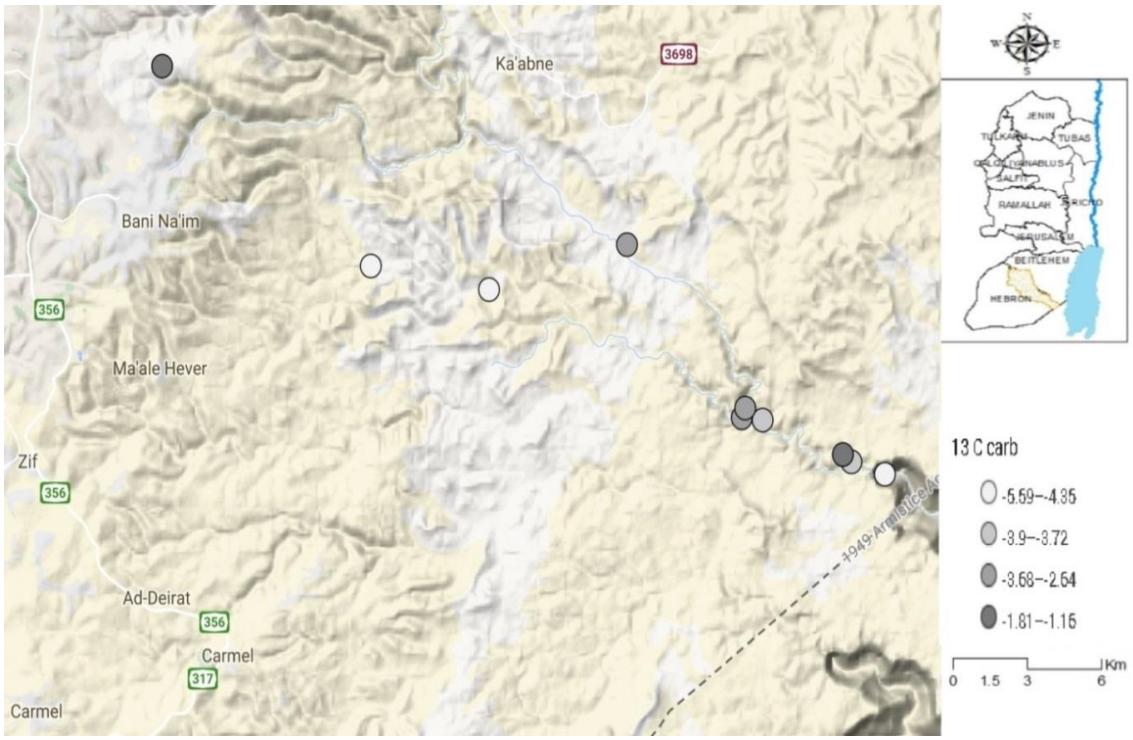

Figure 35: Territorial distribution of δ^{13}Ccarb‰

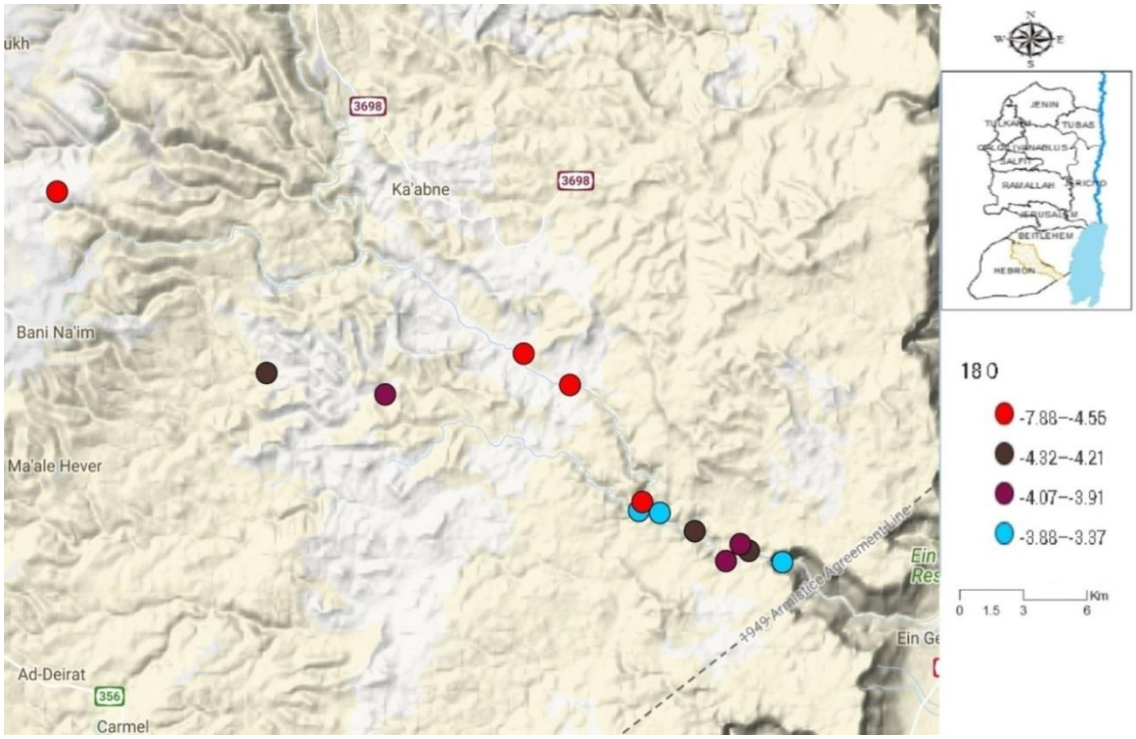

Figure 36: Territorial distribution of δ^{18}Ocarb‰

Figure 35 shows the distribution of the carbon-13 concentration along the path of travel which varies between -5.59‰ and -1.16‰. This enrichment of δ^{13}Ccarb‰ is a result of isotopic exchange with atmospheric carbon dioxide (Heikkilä, et al., 2010).

The δ^{18}Ocarb‰ has no large variation in its value that ranges from -7.88‰ to -3.37‰ (average = -4.80‰), and the oxygen-18 concentration distribution along the path of travel is shown in Figure 36.

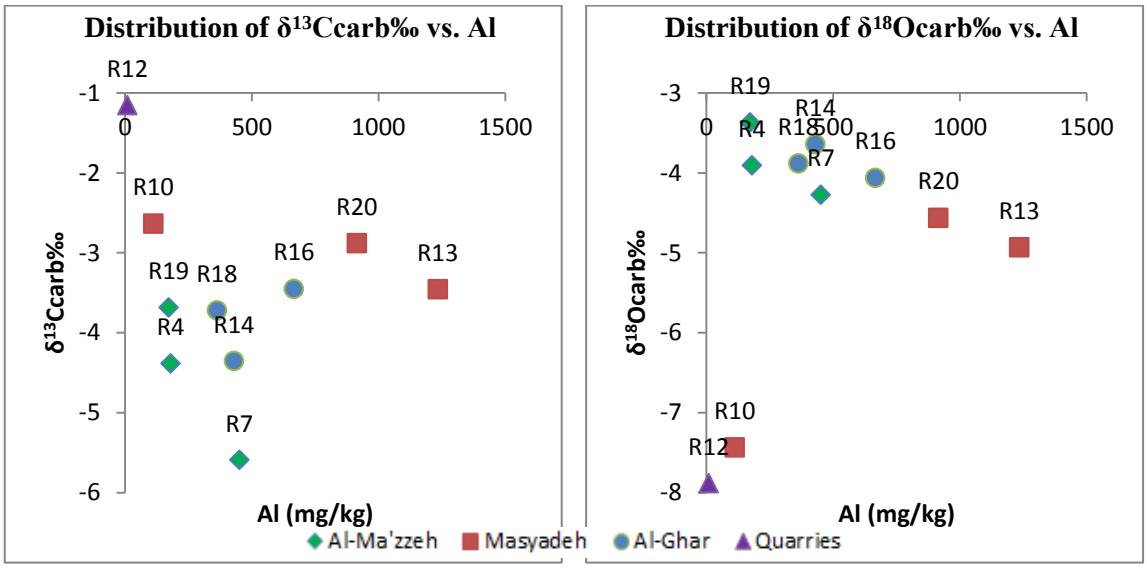

Figure 37: Distribution of δ^{18}Ocarb‰, and δ^{13}Ccarb‰ vs. Al

Figure 37 shows a moderate positive linear correlation between δ^{18}Ocarb‰ and Al with a low R^2 value of 0.31, and the low R^2 value of -0.16 indicates a weak negative linear correlation between δ^{13}Ccarb‰ and Al.

Figure 38 shows a strong negative linear correlation between δ^{18}Ocarb‰ and TC% as supported by the high R^2 value of -0.82, and shows a moderate positive linear correlation between δ^{13}Ccarb‰ and TC% with an R^2 value of 0.66.

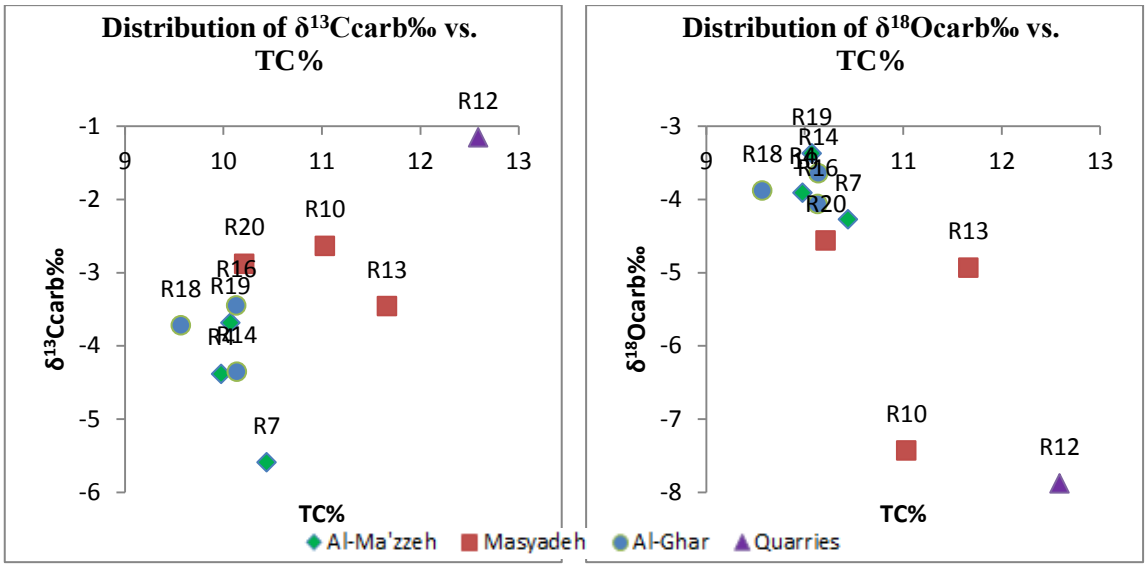

Figure 38: Distribution of δ^{18}Ocarb‰, and δ^{13}Ccarb‰ vs. TC%

The calculation of R^2 among stable isotopes, total carbon and trace elements reveals that no similar distributions exist among these elements and that they do not follow the same pattern as each other. The SEM values for isotopes distribution were low, representing close values to the "true" measurement. Particularly, all SEM values for the three stable isotope distributions were lower than 0.5.

4.6 Al-Ma'zzeh Profile

Figure 39 shows that the trace element contents are higher in upper layers than in deeper layers of Al-Ma'zzeh profile with some subsequent removal and regeneration, which indicates that the deeper layers may have undergone some degrees of depletion. The higher values in the upper layers point out the precipitation normal feature in the surface layers. The profile is homogeneous indicating steady state conditions.

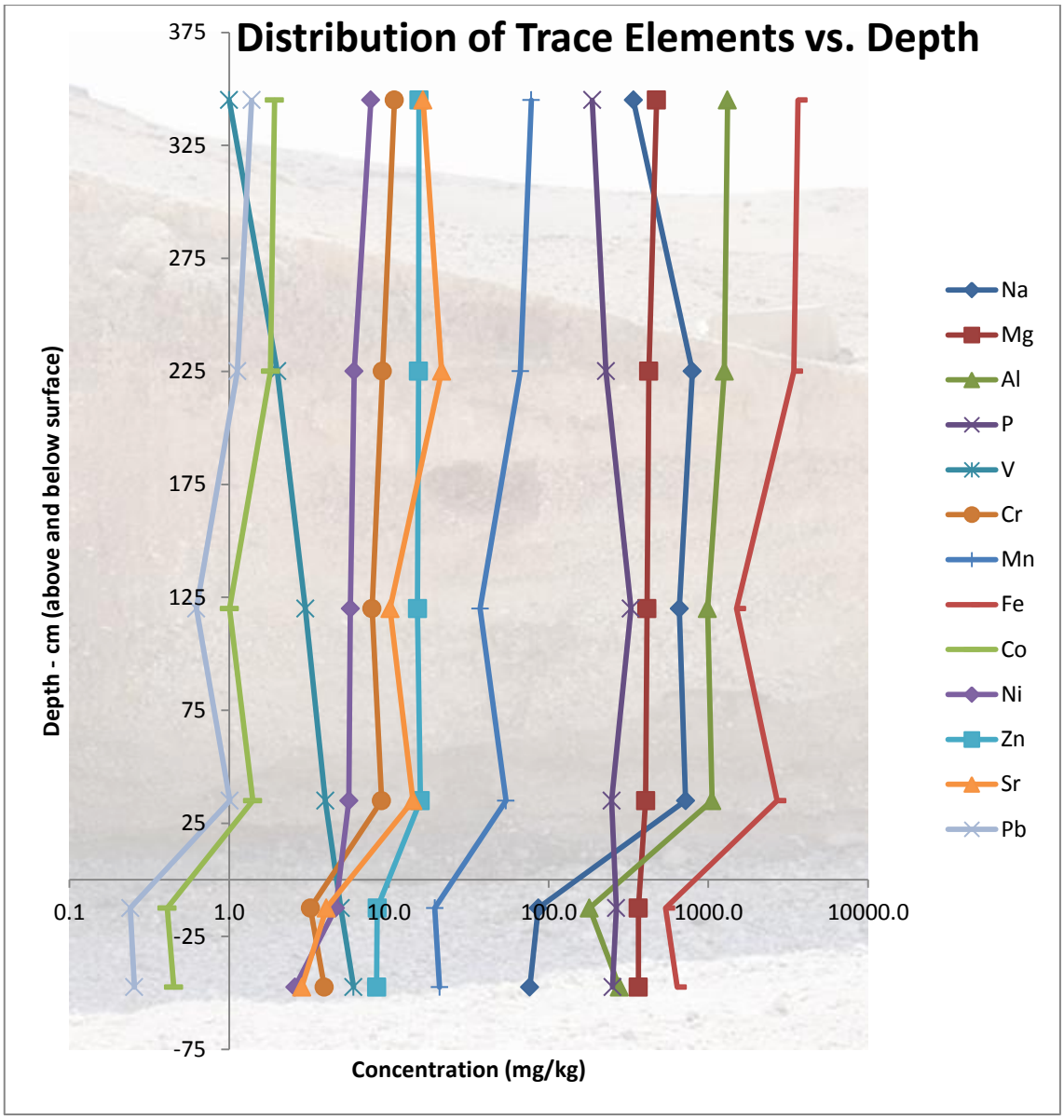

Figure 39: Distribution of Trace Elements vs. Depth

The distributions of TC%, TOC%, TN% and C/N ratios in the vertical profile of Al-Ma'zzeh are presented in Figure 40. A parallel behavior was observed for TOC% (average 0.3%) and TN% (average 0.03%) throughout the length of the profile. A large deviation is observed for TC% (average 6.7%) and C/N ratio (average 12.99%).

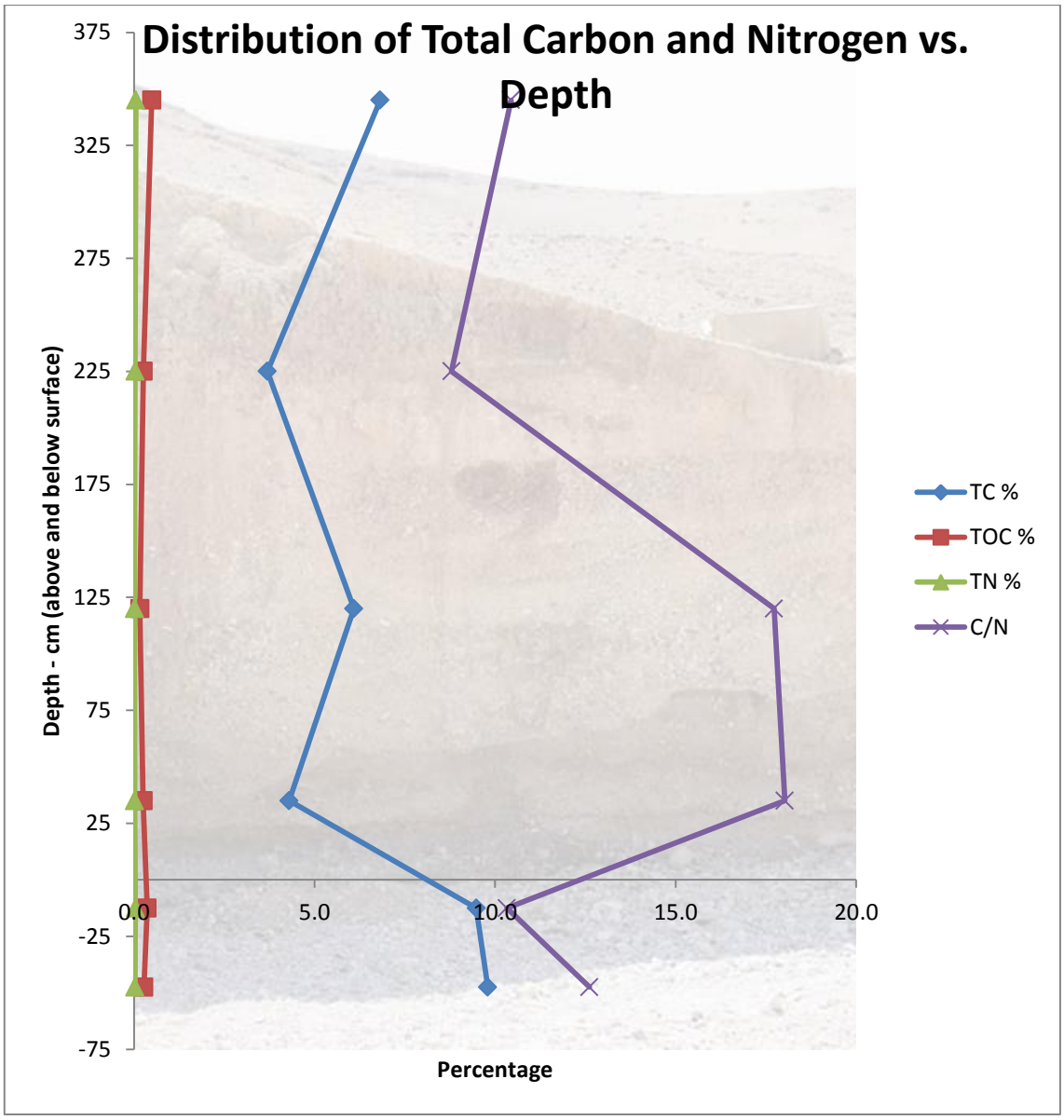

Figure 40: Distribution of TC%, TOC%, TN%, and C/N vs. Depth

From Figure 41 of Al-Ma'zzeh profile, distinct distribution patterns are observed of isotope tracers and depth. The total carbonate content of the upper layers is less than the carbonate content of the deeper layers; this is a method to form pedogenic carbonates, as a result of short-range carbonate dissolution and re-precipitation proximal to the depth of the upper contact with limestone, limestone is progressively transformed into pedogenic carbonate. Pedogenic carbonate involves the lithosphere that contributes calcium, the atmosphere that contributes carbon dioxide and calcium, the hydrosphere

that contributes water in which CO_2 and Ca dissolve and dissociate to form bicarbonate, and the biosphere that captures CO_2 via photosynthesis and emits it in soil via respiration. It is a result of co-evolution of biotic and abiotic processes (Curtis, 2002).

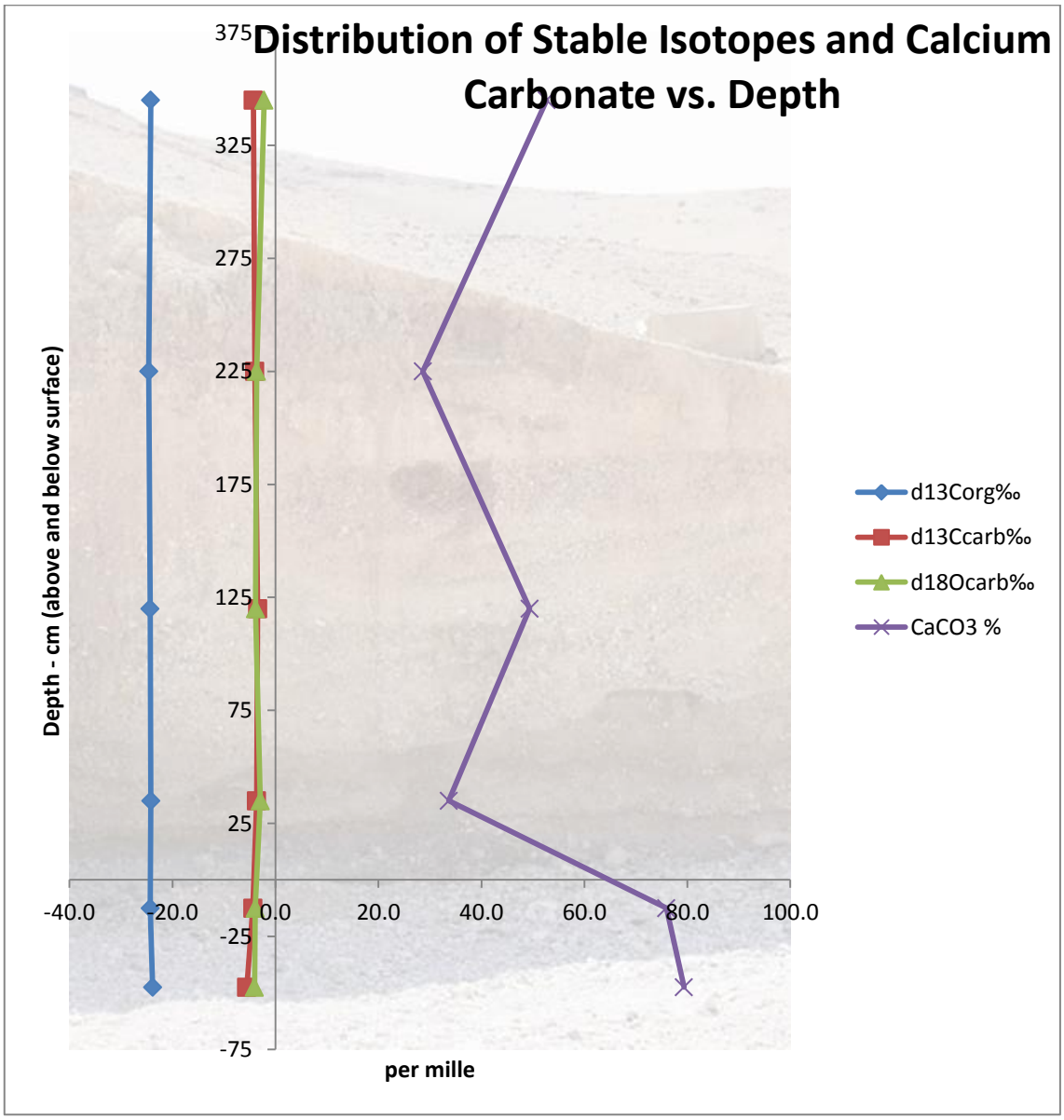

Figure 41: Distribution of δ^{13}Corg‰, δ^{13}Ccarb‰, δ^{18}Ocarb‰, and $CaCO_3$% vs. Depth

Figure 42 shows that the upper layer of Al-Ma'zzeh profile has lower chondrite-normalized REEs content than the deeper layer which has an apparent increase; this could reveal a high leaching and a mobilization of REEs of this profile.

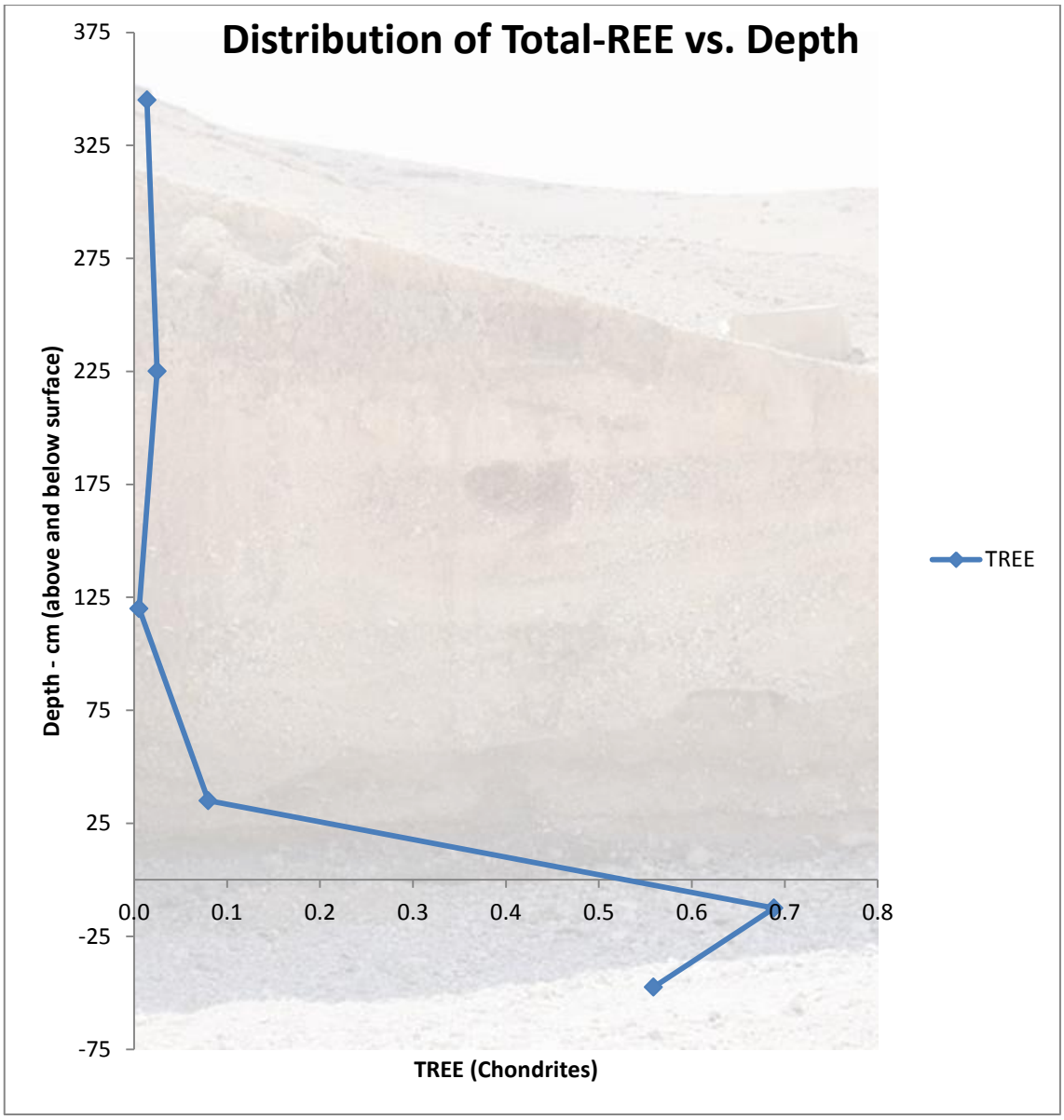

Figure 42: Distribution of Total-REE vs. Depth

With the exception of $CaCO_3$%, the SEM measurements for Al-Ma'zzeh profile distributions vs. depth were relatively low, and thus a decent level of accuracy is reflected. The SEM of 8.56 for $CaCO_3$% represented some variance in the spreading around the "true" measurement.

4.7 Masyadeh Profile

Figure 43 shows that the distributions are fairly homogeneous with depth indicating steady state conditions. The trace element content differences between the upper layer and the deeper layer were not very pronounced, while slightly higher than lower contents that were measured among the depth of Masyadeh profile. This indicates that most likely there is mobilization of trace elements for this profile.

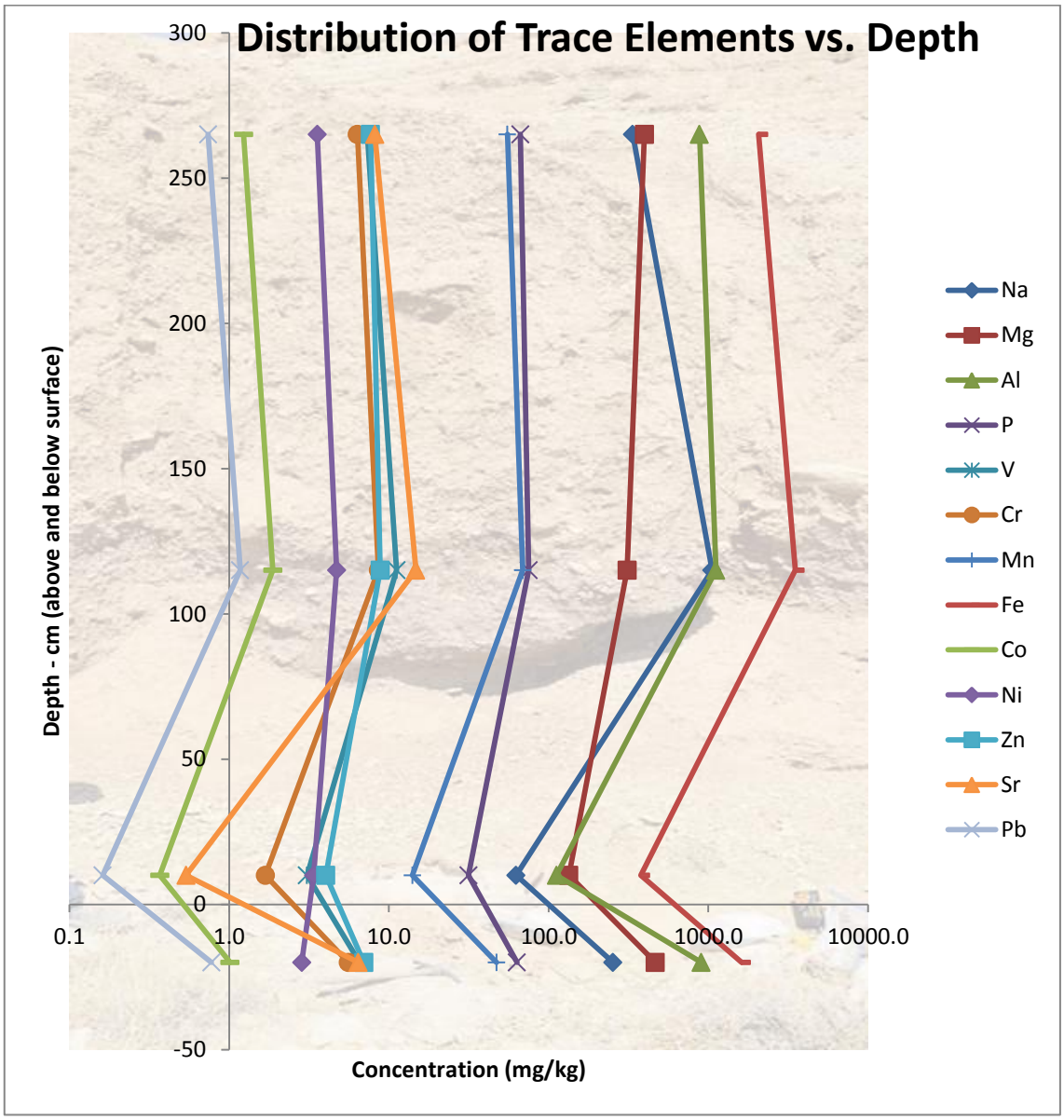

Figure 43: Distribution of Trace Elements vs. Depth

Figure 44 shows distinct enrichment in the profile sediment, where the enrichment of TC% seemed to be lower at the deeper layer, while it is observed that the carbon/nitrogen ratio was depleted.

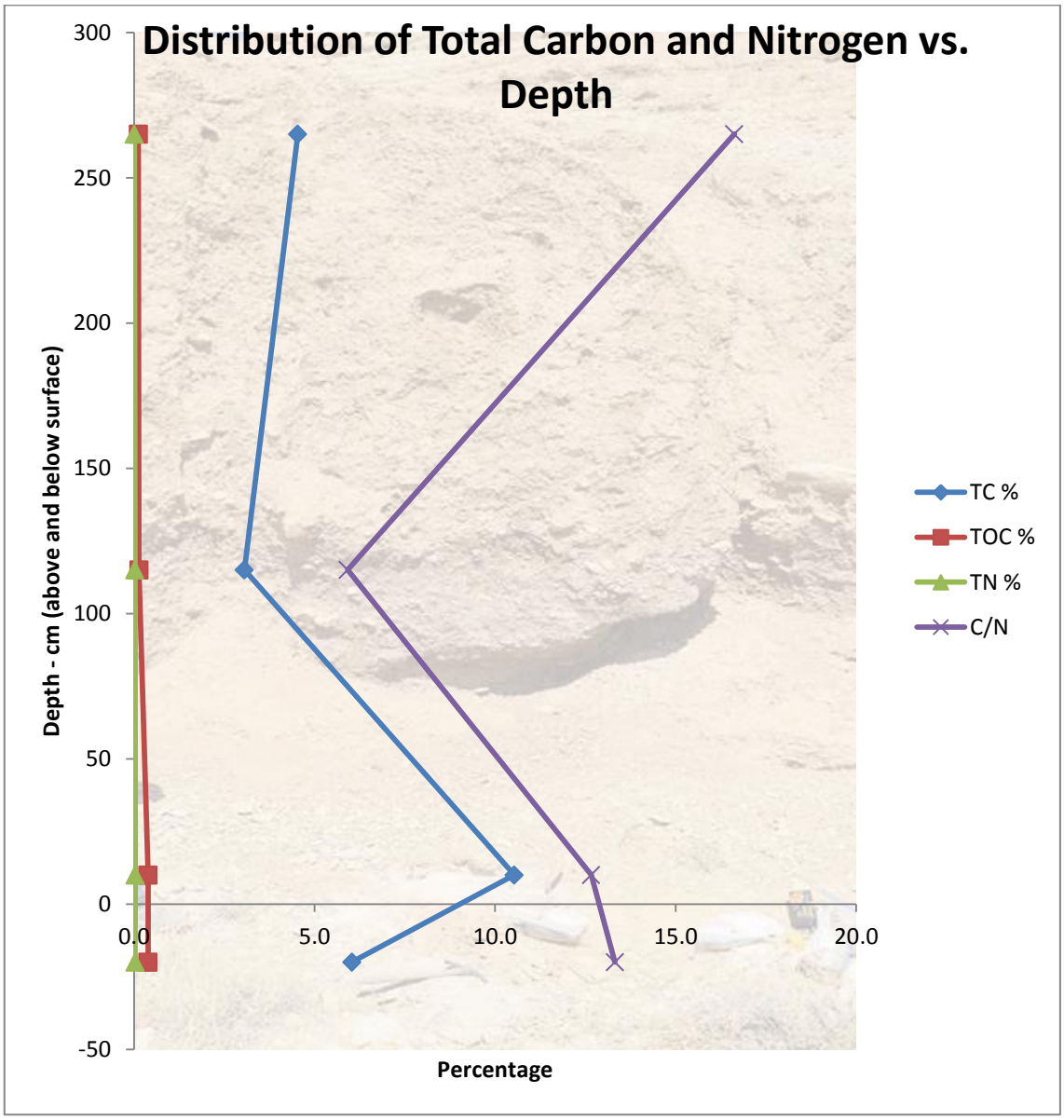

Figure 44: Distribution of TC%, TOC%, TN%, and C/N vs. Depth

In Figure 45 of Masyadeh profile, related distribution patterns are observed of isotope tracers and depth; a continued carbonate accumulation appears where most openings in the sediment become filled by carbonate of pedogenic origin and dominated by tectonic

controls, indicating that the oxidation of organic matter is relative to the weathering of carbonate rocks. Pedogenic carbonate accumulations are common in Holocene soils in regions where the climate is warm and seasonally to mostly dry (semiarid) (Tanner, 2010); Pedogenic carbonate is cited as evidence of a semiarid paleo-climate.

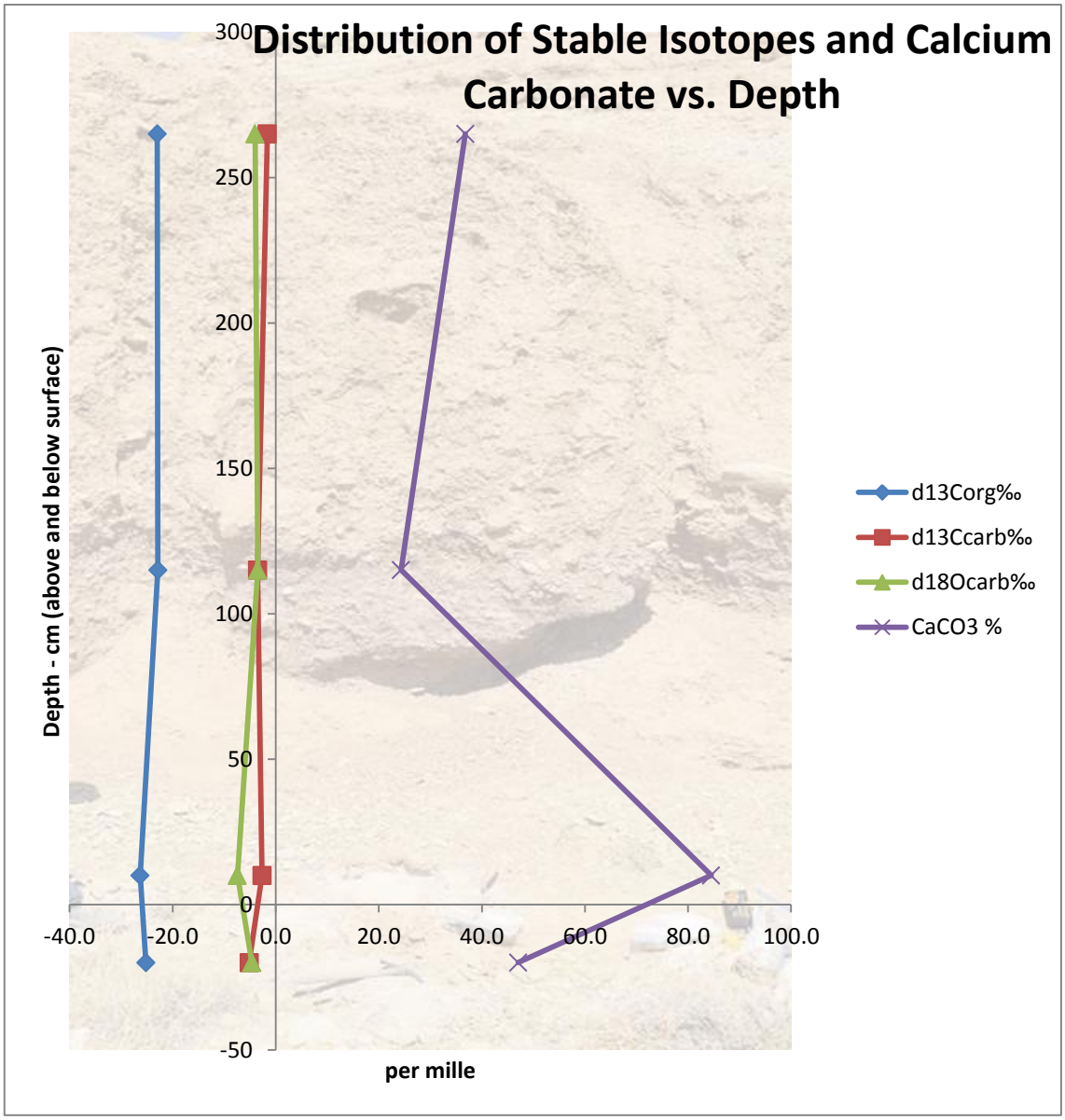

Figure 45: Distribution of δ^{13}Corg‰, δ^{13}Ccarb‰, δ^{18}Ocarb‰, and $CaCO_3$% vs. Depth

Figure 46 indicates substantial vertical spatial difference in chondrite-normalized TREE sediment with changes in depth; it shows that the upper layer of Masyadeh profile has

higher REEs than does the deeper layer, revealing that leaching was not clear in this profile.

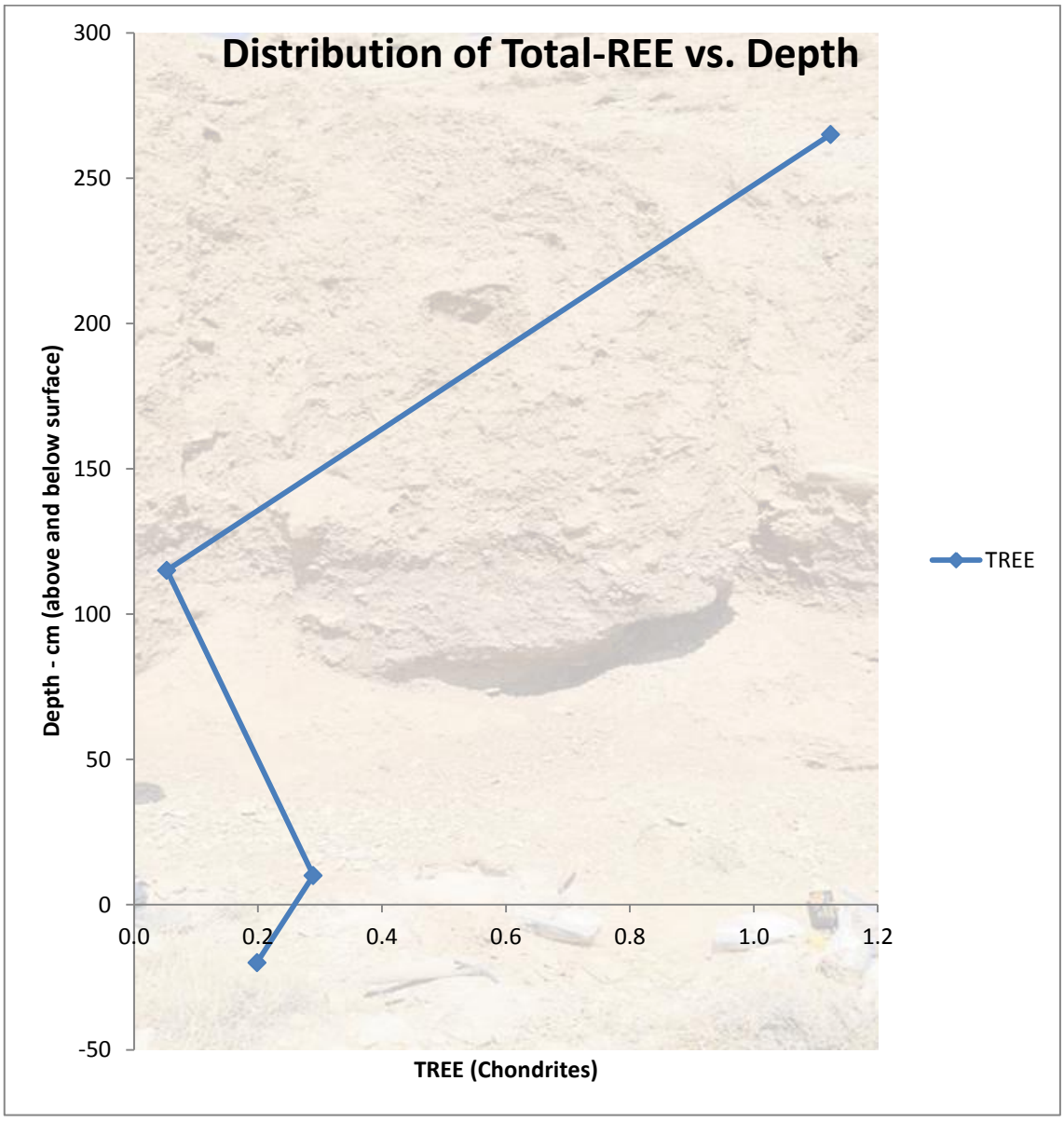

Figure 46: Distribution of Total-REE vs. Depth

Masyadeh profile distributions vs. depth showed relatively low SEM values. However, as was the case in Al-Ma'zzeh profile, the $CaCO_3$% showed more spreading around the "true" measurement, thus giving rise to higher SEM of 12.98.

Differences between Al-Ma’zzeh and Masyadeh profiles are clearly pronounced, this reinforces the conclusion that TREE may not be distributed homogeneously in vertical stream cross sections; the distributions of tracers show considerable variations in leachable and residual fractions. The depletion is higher at Al-Ma’zzeh profile.

Chapter Five

Conclusion and Recommendations

Chapter Five

5. Conclusion and Recommendations

5.1 Conclusion

Trace and rare earth elemental (REE) compositions of sediment samples collected from two streams and their merge at the catchment area in Bani Na'im, south-east Palestine and were analyzed; the grain size texture was found to reveal sand textural group of the catchment area and a muddy sand textural group of the quarries. The content of trace elements manifest terrestrial clastic sediment formed from an altered regolith derived by climatic and tectonic controls of pristine bedrock and a calcite source of mineral grains for alluvial fans. Analyses of the trace elements indicate that both streams Al-Ma'zzeh and Masyadeh contribute to the merge of the streams – Al-Ghar with an evident greater contribution from Al-Ma'zzeh stream, the concentrations of trace elements were correlated with the inorganic carbon concentration revealing that quarries have a substantial impact on Masyadeh stream sediments distribution as an upland sediment source. The distribution of trace elements with the increase of their concentrations towards downstream indicate that stream sediments form by the physical and chemical weathering of bedrock within the catchment area and reflects a combination of geomorphic elements and human uses. The REEs and their anomalies besides their Chondrite-normalized plot revealed a possible environment of erosivity, terrestrial stream sediment sources and lithologically controlled distribution from crystalline basement source rock, and indicative of a development in corestones during spheroidal weathering. The isotopic analysis reflected influence from terrestrial organic matter to the sediment, and its horizontal distributions indicate a pedogenic carbonate of biotic

and abiotic process and tectonic controls on sedimentation that is referred to a semiarid paleo-climate. There are differences between Al-Ma'zzeh and Masyadeh profiles revealing a heterogeneous distribution in vertical stream cross sections, which reinforces considerable variations in leachable and residual fractions, with higher depletion at Al-Ma'zzeh profile.

The study results can contribute to understanding the geochemical characteristics of Bani Na'im catchment area and can be used as a baseline measure for monitoring future changes.

5.2 Recommendations

Further seasonal sampling and analyses of sediment, precipitation, and temperature are highly recommended, in addition to radioactive isotopes analysis of bedrock samples in order to obtain more information about the continental sediments of Bani Na'im catchment area to improve the resolution of paleo-environmental record.

For further studies about the stream sediments of south-east of Palestine; it is highly recommended to:

- Collect samples from the Dead Sea core
- Collect samples near Ein Gedi
- Consider other streams/rivers like Jordan River which is the main tributary to the Dead Sea
- Take a look at Lake Tiberias and Lake Hula sediments, and
- Analyze minerals.

Bibliography

A. Chahi, N. Clauer, T. Toulkeridis, M. Bouabdelli, 1999. Rare-earth-elements as tracers of the genetic relationship between smectite and palygorskite in marine phosphorites. In: *Clay Minerals.* Strasbourg: Centre de Geochimie de la Surface (CNRS-ULP), pp. 419-427.

A.H. Kahn, R.F. Nolting, S.J. Vand Der G Aast, W. Van Raaphorst, 1992. Trace Element Geochemistry at the Sediment-Water Interface in the North Sea and the Western Wadden Sea. In: Texel: Netherland Institute for Sea Research.

A.L. Collins, S. Pulley, I.D.L. Foster, A. Gellis, P. Porto, A.J. Horowitz, 2017. Sediment source fingerprinting as an aid to catchment management: A review of the current state of knowledge and a methodological decision-tree for end-users. In: U.K., South Africa, U.S.A., Italy: Journal of Environmental Management, pp. 86-108.

Abigail Walters, Paul Lusty, 2011. Rare Earth Elements. In: Nottingham: British Geological Survey.

Albright, E. I., 2004. Background Concentrations of Trace Elements in Soils and Rocks of the Georgia Piedmont. In: Athens: The University of Georgia.

Anderson, D. L., 2007. The Other Isotopes. In: *New Theory of the Earth.* New York: Cambridge University Press, pp. 211-230.

Anon., n.d. *Let's Describe the Whole World.* [Online]
Available at:
http://wikimapia.org/#lang=en&lat=31.062640&lon=35.303879&z=14&tag=949
[Accessed 2017].

ARIJ, 1995. Environmental Profile for the West Bank. In: Jerusalem: Applies Research Institute - ARIJ.

ARIJ, 1997. The Status of the Environment in the West Bank. In: Jerusalem: Applied Research Institute - ARIJ.

ARIJ, 2009. Bani Na'im Town Profile. In: Jerusalem: Applies Research Institute - ARIJ.

Basim Makhool, Mahmoud Abu Al-Rob, 1999. Quarrying, Crushing and Stone Industries in Palestine. In: s.l.:Palestine Economic Policy Research Institute.

Bea, F., 2015. Geochemistry of the Lanthanide Elements. In: s.l.:University of Granada.

CATENA, 2013. Clay distribution over the landscape of Israel: From the hyper-arid to the Mediterranean climate regimes. In: Jerusalem: Amir Sandler, pp. 119-132.

CEM MARS5, 2007. Batch Microwave Acid Digestion System. In: s.l.:s.n.

CIA, 2017. [Online]
Available at: https://www.cia.gov/library/publications/the-world-factbook/geos/we.html [Accessed 2017].

Curtis, M. H., 2002. Pedogenic Carbonate: links between biotic and abiotic CaCO3. In: New Mexico: New Mexico State Univeristy.

Department of Earth & Environmental Sciences, 2017. *Maps,* Jerusalem: Al-Quds University.

Dunn, M. G., 1989-1993. *Exploring Your World: The Adventure of Geography.* [Online]

Available at: https://www.nationalgeographic.org/encyclopedia/sediment/ [Accessed 2017].

EPA, 1996. Acid Digestion of Sediments, Sludges and Soils - Method 3050B. In: Washington, DC.: U.S. Environmental Protection Agency - EPA.

Farkas, J., 2014. Environmental Isotope Geochemistry Radiogenic and Stable Isotopes. In: Prague: Czech Geological Survey (CGS).

Gill, R. & Ramsey, M. H., 2014. What a geochemical analysis means. In: *Modern Analytical Geochemistry: An Introduction to Quantitative Chemical Analysis Techniques for Earth, Environmental and Materials Scientists.* London: Routledge, pp. 2-11.

Harb, H., 2015. Metal Content, Occurence and Distribution in Soil of Al-Qilt Catchment. In: Nablus: An-Najah National University.

Horowitz, A. J., 1991. A Primer on Sediment-Trace Element Chemistry. In: Georgia: United States Geological Survey.

Hussain, N., 2014. Assessment of the Palestineian Stone and Marble Industry in Terms of Quality Management and Safety Management Systems. In: s.l.:An-Najah National University.

K. Pye, R. Johnson, 1988. Stratigraphy, geochemistry, and thermoluminescence ages of lower Mississippi Valley loess. In: Mississippi: Earth Surface Processes and Landforms, p. 103–124.

Khalayleh, A. M., 2017. *Google Maps.* Palestine.

Khalayleh, A. M., 2017. *Photographer.* Palestine.

Leeder, M., 2011. Sedimentology and Sedimentary Basins from Turbulence to Tectonics. In: 2nd ed. Norwich: Wiley Blackwell.

Maija Heikkilä, Thomas W.D. Edwards, Heikki Seppä, Eloni Sonninen, 2010. Sediment isotope tracers from Lake Saarikko, Finland, and implications for Holocene hydroclimatology. In: Helsinki, Ontario: Quaternary Science Reviews, pp. 2146-2160.

Mayumi Seto, Tasuku Akagi, 2008. Chemical condition for the appearance of a negative Ce anomaly in stream waters and groundwaters. In: Fukuoka, Japan: Kyushu University, pp. 371-380.

Michael D. Blum, Torbjörn E. Törnqvist, 2000. Fluvial Responses to Climate and Sea-Level Change: a review and look forward. In: Chicago: University of Illinois at Chicago, p. 2–48.

Michael S. Alleh, Ronald R. Tidball, Rashid M. Samater, Gary I. Selner, 1985. Interpretation of Geochemical Data from Panned Concentrates of Wadi Sediments Using R-Mode Analysis. In: Jiddeh: Ministry of Petroleum and Mineral Resources.

Osman, K. T., 2013. Soil as a Part of the Lithosphere. In: *Soil: Principles, Properties and Management.* s.l.:Springer Science+Business Media Dordrecht.

Pavlos Avramidisa, Konstantinos Nikolaoua, Vlasoula Bekiarib, 2015. Total Organic Carbon and Total Nitrogen in Sediments and Soils. In: Patras, Greece: Agriculture and Agricultural Science Procedia, p. 425–430.

PCBS, 2009. *Statistical Atlas of Palestine.* [Online]
Available at: http://www.pcbs.gov.ps/Downloads/book1624/index-e.htm
[Accessed 2017].

PEnA, 1999. National Biodiversity Strategy and Action Plan for Palestine. In: Hebron: Palestinian Environmental Authority - PEnA.

Ruth E. Wolf, USGS/CR/CICT, March, 2005. What is ICP-MS? … and more importantly, what can it do?. In: s.l.:U.S. Geological Survey / Central Region / Crustal Imaging and Characterization Team.

S. L. Yang, Z. L. Ding, 2004. Comparison of particle size characteristics of the Tertiary 'red clay' and Pleistocene loess in the Chinese Loess Plateau: implications for origin and sources of the 'red clay'. In: Beijing: Chinese Academy of Science, p. 77–93.

S. O. Obaje, I. A. Akpoborie, F. C. Ugbe, A. Onugba, 2015. Rare Earth and Trace Elements Distribution in Sediments of River Gora, Minna Area, North-Central Nigeria: Implication for Provenance. In: Lokoja, Abraka: Canadian Center of Science and Education.

Siraj Center, Human Interest, Visit Palestine, 2015. *IMEMC News.* [Online]
Available at: http://imemc.org/article/74241/
[Accessed 2017].

Stefania Gaudino, Chiara Galas, Maria Belli, Sabrina Barbizzi, Paolo de Zorzi, Radojko Ja´cimovi´c, Zvonka Jeran, Alessandra Pati, Umberto Sansone, 2007. The role of different soil sample digestion methods on trace elements analysis: a comparison of ICP-MS and INAA measurement results. Volume 12, p. 84–93.

Tanner, L. H., 2010. Continental Carbonates as Indicators of Paleoclimate. In: *Developments in Sedimentology*. New York: Le Moyne College, pp. 179-214.

U. Zain Eldeen, D. Delvaux, P. Jacobs, 2002. Tectonic evolution in the Wadi Araba Segment of the Dead Sea Rift, South-West Jordan. In: Palestine, Belgium: EGU Stephan Mueller Special Publication Series, European Geosciences Union, p. 63–81.

United States Department of Agriculture, n.d. Sedimentation. In: U.S.A.: United States Department of Agriculture.

W. Nesbitt, G. M. Young, 1982. Early Proterozoic Climates and Plate Motions Inferred from Major Elements Chemistry of Lutites. In: Ontario: University of Western Ontario.

Walling, D. E., Owens, P. N. & Graham, J. L., 1999. Fingerprinting suspended sediment sources in the catchment of the River Ouse. In: Yorkshire, UK: University of Exeter.

Appendices

Appendix A

Table 2: Stratigraphic Section of the West Bank (Department of Earth & Environmental Sciences, 2017)

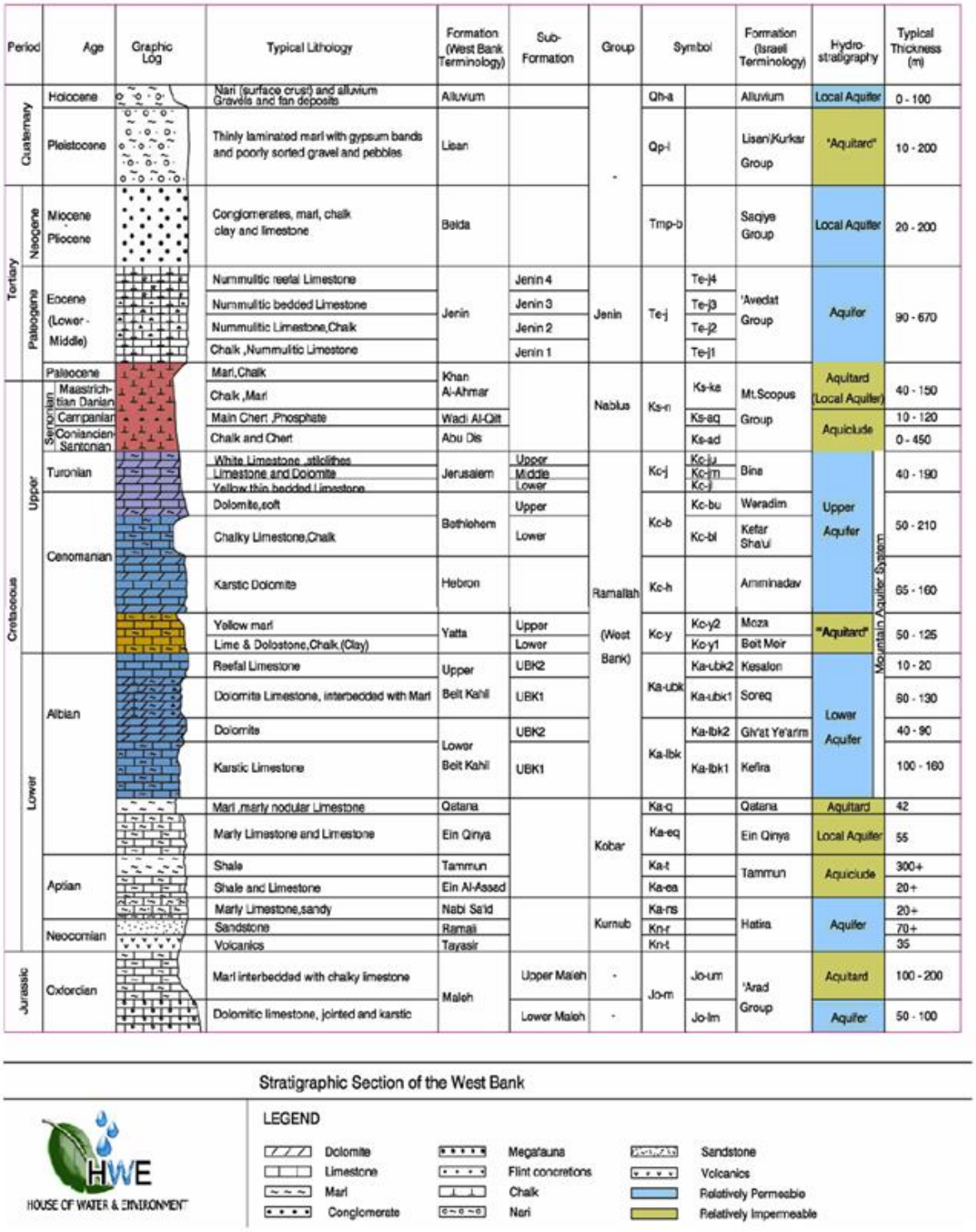

Period	Age	Graphic Log	Typical Lithology	Formation (West Bank Terminology)	Sub-Formation	Group	Symbol		Formation (Israeli Terminology)	Hydro-stratigraphy	Typical Thickness (m)
Quaternary	Holocene		Nari (surface crust) and alluvium Gravels and fan deposits	Alluvium		-	Qh-a		Alluvium	Local Aquifer	0 - 100
	Pleistocene		Thinly laminated marl with gypsum bands and poorly sorted gravel and pebbles	Lisan			Qp-l		Lisan/Kurkar Group	"Aquitard"	10 - 200
Tertiary	Neogene: Miocene - Pliocene		Conglomerates, marl, chalk clay and limestone	Belda			Tmp-b		Saqiye Group	Local Aquifer	20 - 200
	Paleogene: Eocene (Lower - Middle)		Nummulitic reefal Limestone	Jenin	Jenin 4	Jenin	Te-j	Te-j4	'Avedat Group	Aquifer	90 - 670
			Nummulitic bedded Limestone		Jenin 3			Te-j3			
			Nummulitic Limestone,Chalk		Jenin 2			Te-j2			
			Chalk ,Nummulitic Limestone		Jenin 1			Te-j1			
	Paleocene		Marl,Chalk	Khan Al-Ahmar		Nablus	Ks-n	Ks-ka	Mt.Scopus Group	Aquitard (Local Aquifer)	40 - 150
Cretaceous: Upper	Maastrichtian Danian		Chalk ,Marl								
	Campanian		Main Chert /Phosphate	Wadi Al-Qilt				Ks-aq		Aquiclude	10 - 120
	Coniancien-Santonian		Chalk and Chert	Abu Dis				Ks-ad			0 - 450
	Turonian		White Limestone ,stilolithes Limestone and Dolomite Yellow thin bedded Limestone	Jerusalem	Upper Middle Lower	Ramallah (West Bank)	Kc-j	Kc-ju Kc-jm Kc-j	Bina	Upper Aquifer	40 - 190
	Cenomanian		Dolomite,soft	Bethlehem	Upper		Kc-b	Kc-bu	Weradim		50 - 210
			Chalky Limestone,Chalk		Lower			Kc-bl	Kefar Sha'ul		
			Karstic Dolomite	Hebron			Kc-h		Amminadav		65 - 160
			Yellow marl	Yatta	Upper		Kc-y	Kc-y2	Moza	"Aquitard"	50 - 125
			Lime & Dolostone,Chalk,(Clay)		Lower			Kc-y1	Beit Meir		
Lower	Albian		Reefal Limestone	Upper Beit Kahil	UBK2		Ka-ubk	Ka-ubk2	Kesalon	Lower Aquifer	10 - 20
			Dolomite Limestone, interbedded with Marl		UBK1			Ka-ubk1	Soreq		80 - 130
			Dolomite	Lower Beit Kahil	UBK2		Ka-lbk	Ka-lbk2	Giv'at Ye'arim		40 - 90
			Karstic Limestone		UBK1			Ka-lbk1	Kefira		100 - 160
	Aptian		Marl ,marly nodular Limestone	Qatana		Kobar	Ka-q		Qatana	Aquitard	42
			Marly Limestone and Limestone	Ein Qinya			Ka-eq		Ein Qinya	Local Aquifer	55
			Shale	Tammun			Ka-t		Tammun	Aquiclude	300+
			Shale and Limestone	Ein Al-Assad			Ka-ea				20+
	Neocomian		Marly Limestone,sandy	Nabi Sa'id		Kurnub	Ka-ns		Hatira	Aquifer	20+
			Sandstone	Ramali			Kn-r				70+
			Volcanics	Tayasir			Kn-t				35
Jurassic	Oxfordian		Marl interbedded with chalky limestone	Maleh	Upper Maleh	-	Jo-m	Jo-um	'Arad Group	Aquitard	100 - 200
			Dolomitic limestone, jointed and karstic		Lower Maleh	-		Jo-lm		Aquifer	50 - 100

Mountain Aquifer System

Appendix B

Table 3: Element symbols and names

Trace Elements:

23 Na	Sodium
24 Mg	Magnesium
27 Al	Aluminum
31 P	Phosphorus
43 Ca	Calcium
51 V	Vanadium
53 Cr	Chromium
55 Mn	Manganese
56 Fe	Iron
59 Co	Cobalt
60 Ni	Nickel
66 Zn	Zinc
88 Sr	Strontium
208 Pb	Lead

Rare Earth Elements “REE”:

139 La	Lanthanum
140 Ce	Cerium
141 Pr	Praseodymium
146 Nd	Neodymium
147 Sm	Samarium
153 Eu	Europium
157 Gd	Gadolinium
159 Tb	Terbium
163 Dy	Dysprosium
165 Ho	Holmium
166 Er	Erbium
169 Tm	Thulium
172 Yb	Ytterbium
175 Lu	Lutetium

Appendix C

Table 4: Trace Element Concentrations (mg/kg)

	23 Na	24 Mg	27 Al	31 P	51 V	53 Cr	55 Mn	56 Fe	59 Co	60 Ni	66 Zn	88 Sr	208 Pb
Surface Sediment:													
R7	81.195	491.481	451.288	192.309	3.749	3.004	23.697	617.288	0.491	2.662	8.537	4.856	0.429
R4	86.083	364.647	180.132	264.859	3.410	3.223	19.365	540.268	0.409	4.639	8.443	4.060	0.240
R19	487.237	162.797	172.666	1012.570	11.760	8.702	47.861	28.613	0.957	149.480	102.825	86.748	2.390
R10	62.575	133.792	111.954	31.488	3.069	1.684	14.031	377.470	0.368	3.380	4.026	0.537	0.161
R13	670.363	613.297	1233.858	1658.395	19.150	14.485	104.246	976.842	2.559	81.442	84.637	69.612	4.844
R20	519.398	453.003	914.728	1581.096	20.820	16.847	79.935	685.851	2.276	45.076	104.377	71.522	3.487
R18	507.638	449.565	363.016	1108.723	15.352	27.667	59.570	684.240	0.572	48.555	101.999	178.950	2.907
R16	663.686	613.833	666.480	1561.276	24.881	24.430	83.253	1548.366	2.321	34.971	99.583	172.478	3.545
R14	592.613	309.649	429.887	1165.766	19.273	15.385	85.970	315.668	3.072	30.959	49.533	86.340	3.809
Quarries:													
R12	29.037	27.738	9.634	2.642	0.861	0.348	2.560	40.736	0.106	0.660	1.788	1.285	0.146
Al-Ma'zzeh Profile:													
R6	339.581	474.033	1318.488	187.370	17.182	12.791	10.822	77.906	3644.123	1.923	7.704	15.411	16.341
R2	793.099	423.279	1260.237	228.557	18.895	11.626	9.106	66.543	3421.035	1.813	6.060	15.320	21.396
R1	658.535	412.766	987.293	327.075	15.442	7.629	7.838	37.205	1504.542	1.003	5.742	15.092	10.173
R3	720.612	404.558	1054.021	247.830	15.428	9.338	8.988	54.060	2691.069	1.403	5.614	15.713	14.148
R4	86.083	364.647	180.132	264.859	5.211	3.410	3.223	19.365	540.268	0.409	4.639	8.443	4.060
R5	76.244	364.241	277.333	251.050	3.930	3.516	3.941	20.746	638.556	0.449	2.578	8.380	2.849
Masyadeh Profile:													
R9	335.933	398.101	879.782	66.514	7.980	7.331	6.353	55.189	2064.732	1.232	3.560	7.664	8.159
R8	1053.524	309.907	1115.619	75.142	21.232	11.179	8.599	68.814	3499.636	1.874	4.711	8.812	14.732
R10	62.575	133.792	111.954	31.488	1.780	3.069	1.684	14.031	377.470	0.368	3.380	4.026	0.537
R11	252.902	466.172	902.544	63.312	12.234	6.536	5.573	47.140	1614.653	1.012	2.848	6.956	6.434

Table 5: Trace Element Concentrations (ppb)

	23 Na	24 Mg	27 Al	31 P	51 V	53 Cr	55 Mn	56 Fe	59 Co	60 Ni	66 Zn	88 Sr	208 Pb
Surface Sediment:													
R7	4067.849	24623.220	22609.534	9634.668	187.839	150.487	1187.218	30926.109	24.605	133.345	427.696	243.295	21.473
R4	4321.375	18305.266	9042.628	13295.939	171.193	161.809	972.141	27121.464	20.524	232.885	423.820	203.793	12.056
R19	24556.761	8204.954	8702.344	2551676.113	592.702	438.599	2412.216	1442.100	48.228	7533.788	5182.390	4372.086	120.463
R10	3141.243	6716.361	5620.072	1580.720	154.048	84.516	704.375	18949.017	18.467	169.675	202.112	26.938	8.107
R13	34034.317	31137.096	62642.950	4209834.471	972.238	735.391	5292.563	49594.285	129.903	4134.822	4297.010	3534.208	245.946
R20	26047.796	22718.088	45873.623	3964597.132	1044.105	844.875	4008.758	34395.430	114.124	2260.541	5234.526	3586.839	174.885
R18	25838.769	22882.874	18477.500	2821700.678	781.437	1408.250	3032.089	34827.804	29.098	2471.472	5191.751	9108.574	147.968
R16	33602.424	31078.387	33743.889	3952371.192	1259.700	1236.871	4215.076	78393.751	117.519	1770.559	5041.904	8732.566	179.477
R14	30009.915	15680.625	21769.471	2951720.484	975.966	779.087	4353.519	15985.412	155.544	1567.750	2508.367	4372.242	192.883
Quarries:													
R12	1457.676	1392.447	483.636	132.611	43.219	17.477	128.533	2044.963	5.338	33.136	89.756	64.526	7.314
Al-Ma'zzeh Profile:													
R6	17080.908	23843.883	66319.922	9424.716	643.373	544.365	3918.672	183299.372	96.727	387.509	775.198	821.934	69.515
R2	39892.881	21290.914	63389.919	11496.396	584.769	458.037	3347.097	172078.074	91.169	304.806	770.598	1076.229	56.531
R1	33058.461	20720.831	49562.106	16419.175	382.959	393.462	1867.704	75528.000	50.346	288.257	757.601	510.665	31.265
R3	36102.651	20268.360	52806.459	12416.265	467.824	450.308	2708.402	134822.554	70.314	281.263	787.236	708.838	50.455
R4	4321.375	18305.266	9042.628	13295.939	171.193	161.809	972.141	27121.464	20.524	232.885	423.820	203.793	12.056
R5	3835.080	18321.299	13949.834	12627.835	176.852	198.253	1043.508	32119.376	22.586	129.657	421.538	143.322	12.817
Masyadeh Profile:													
R9	16830.236	19944.867	44077.067	3332.352	367.305	318.263	2764.990	103443.084	61.732	178.365	383.957	408.746	36.950
R8	52886.886	15557.313	56004.071	3772.138	561.188	431.658	3454.472	175681.730	94.085	236.512	442.352	739.521	58.864
R10	3141.243	6716.361	5620.072	1580.720	154.048	84.516	704.375	18949.017	18.467	169.675	202.112	26.938	8.107
R11	12695.685	23401.844	45307.694	3178.256	328.116	279.788	2366.412	81055.571	50.778	142.963	349.213	322.970	38.823

mg/kg = ((ppb / 1000) * volume) / weight

Table 6: Rare Earth Element (REE) Chondrite-Normalized

	139 La	140 Ce	141 Pr	146 Nd	147 Sm	153 Eu	157 Gd	159 Tb	163 Dy	165 Ho	166 Er	169 Tm	172 Yb	175 Lu
Chondrite	**0.319**	**0.820**	**0.121**	**0.615**	**0.200**	**0.076**	**0.267**	**0.049**	**0.330**	**0.076**	**0.216**	**0.033**	**0.221**	**0.033**
Surface Sediment:														
R7	0.124	0.075	0.081	0.067	0.041	0.035	0.034	0.028	0.024	0.021	0.022	0.020	0.018	0.020
R4	0.143	0.081	0.089	0.072	0.045	0.038	0.040	0.032	0.028	0.025	0.026	0.024	0.023	0.023
R19	0.026	0.014	0.015	0.012	0.007	0.006	0.006	0.005	0.005	0.005	0.005	0.005	0.005	0.004
R10	0.058	0.045	0.039	0.031	0.020	0.014	0.015	0.012	0.010	0.009	0.010	0.010	0.008	0.009
R13	0.029	0.019	0.019	0.015	0.010	0.009	0.007	0.006	0.005	0.005	0.005	0.004	0.004	0.004
R20	0.019	0.012	0.012	0.009	0.006	0.005	0.005	0.004	0.004	0.003	0.003	0.003	0.003	0.003
R18	0.052	0.026	0.031	0.024	0.015	0.018	0.013	0.010	0.010	0.009	0.010	0.009	0.008	0.009
R16	0.096	0.048	0.057	0.047	0.029	0.026	0.025	0.020	0.019	0.017	0.018	0.017	0.016	0.016
R14	0.025	0.016	0.016	0.013	0.008	0.008	0.007	0.006	0.005	0.005	0.005	0.005	0.004	0.005
Quarries:														
R12	0.004	0.003	0.003	0.002	0.001	0.001	0.001	0.001	0.001	0.001	0.001	0.001	0.001	0.001
Al-Ma'zzeh Profile:														
R6	0.002	0.002	0.001	0.001	0.001	0.004	0.001	0.000	0.000	0.000	0.000	0.000	0.000	0.000
R2	0.004	0.004	0.003	0.002	0.001	0.005	0.001	0.001	0.001	0.001	0.001	0.000	0.001	0.001
R1	0.001	0.001	0.001	0.000	0.000	0.001	0.000	0.000	0.000	0.000	0.000	0.000	0.000	0.000
R3	0.016	0.012	0.011	0.008	0.005	0.005	0.004	0.003	0.003	0.002	0.003	0.002	0.002	0.003
R4	0.143	0.081	0.089	0.072	0.045	0.038	0.040	0.032	0.028	0.025	0.026	0.024	0.023	0.023
R5	0.118	0.063	0.073	0.059	0.038	0.035	0.031	0.025	0.022	0.020	0.019	0.019	0.018	0.018
Masyadeh Profile:														
R9	0.222	0.172	0.152	0.120	0.076	0.055	0.059	0.050	0.042	0.036	0.038	0.034	0.033	0.035
R8	0.009	0.009	0.006	0.004	0.004	0.007	0.003	0.002	0.002	0.002	0.001	0.001	0.001	0.001
R10	0.058	0.045	0.039	0.031	0.020	0.014	0.015	0.012	0.010	0.009	0.010	0.010	0.008	0.009
R11	0.037	0.027	0.026	0.021	0.014	0.011	0.010	0.009	0.008	0.007	0.007	0.007	0.007	0.007

Table 7: Rare Earth Element (REE) Concentrations (ppb)

	139 La	140 Ce	141 Pr	146 Nd	147	153 Eu	157 Gd	159 Tb	163 Dy	165 Ho	166 Er	169 Tm	172 Yb	175 Lu
Surface Sediment:														
R7	39.585	61.868	9.810	40.998	8.256	2.638	9.122	1.348	7.921	1.634	4.781	0.669	4.033	0.652
R4	45.774	66.063	10.741	44.030	9.081	2.915	10.621	1.560	9.319	1.921	5.535	0.786	5.038	0.757
R19	8.448	11.870	1.755	7.177	1.431	0.468	1.672	0.255	1.635	0.353	1.003	0.154	1.025	0.145
R10	18.652	36.899	4.747	19.242	3.915	1.081	4.016	0.572	3.286	0.696	2.054	0.314	1.766	0.284
R13	9.344	15.910	2.249	9.412	1.949	0.709	1.979	0.285	1.780	0.347	1.008	0.140	0.899	0.131
R20	6.008	10.233	1.406	5.748	1.175	0.415	1.241	0.173	1.159	0.207	0.653	0.083	0.565	0.085
R18	16.733	20.917	3.693	14.838	3.049	1.340	3.390	0.511	3.166	0.707	2.076	0.283	1.828	0.308
R16	30.511	39.179	6.844	28.690	5.788	1.985	6.582	0.992	6.157	1.283	3.831	0.545	3.520	0.533
R14	8.123	12.713	1.931	7.881	1.610	0.643	1.908	0.279	1.718	0.366	1.080	0.156	0.960	0.176
Quarries:														
R12	1.221	2.217	0.304	1.260	0.235	0.058	0.267	0.033	0.224	0.042	0.127	0.023	0.118	0.019
Al-Ma'zzeh Profile:														
R6	0.557	1.880	0.151	0.645	0.146	0.272	0.246	0.018	0.142	0.019	0.076	0.010	0.054	0.011
R2	1.270	3.203	0.329	1.300	0.256	0.384	0.356	0.042	0.272	0.044	0.125	0.012	0.134	0.019
R1	0.301	0.711	0.069	0.241	0.063	0.043	0.090	0.009	0.067	0.019	0.040	0.007	0.036	0.007
R3	4.971	9.966	1.316	5.103	1.055	0.375	1.168	0.158	0.934	0.188	0.592	0.074	0.532	0.083
R4	45.774	66.063	10.741	44.030	9.081	2.915	10.621	1.560	9.319	1.921	5.535	0.786	5.038	0.757
R5	37.629	51.595	8.839	36.579	7.556	2.673	8.228	1.240	7.124	1.555	4.151	0.643	3.960	0.587
Masyadeh Profile:														
R9	70.703	141.219	18.393	73.806	15.159	4.143	15.784	2.438	14.009	2.759	8.109	1.136	7.356	1.163
R8	2.866	7.641	0.782	2.766	0.729	0.505	0.767	0.093	0.549	0.116	0.280	0.041	0.303	0.049
R10	18.652	36.899	4.747	19.242	3.915	1.081	4.016	0.572	3.286	0.696	2.054	0.314	1.766	0.284
R11	11.823	22.316	3.182	12.647	2.702	0.820	2.752	0.429	2.680	0.551	1.582	0.229	1.632	0.225

Chondrite-normalized = (ppb / 1000) / chondrite

Table 8: Total Carbon and Total Nitrogen Percentages (%)

	TC%	TOC%	TN%	C/N	IOC%	$CaCO_3$%
Surface Sediment:						
R7	9.939	0.268	0.017	15.772	9.671	80.562
R4	9.477	0.361	0.035	10.326	9.115	75.929
R19	9.570	0.206	0.009	22.861	9.365	78.007
R10	10.531	0.386	0.031	12.665	10.145	84.507
R13	11.161	0.274	0.017	16.106	10.887	90.691
R20	9.713	0.335	0.023	14.879	9.378	78.119
R18	9.067	0.171	0.008	21.426	8.896	74.102
R16	9.631	0.199	0.013	15.319	9.432	78.571
R14	9.636	0.175	0.010	17.491	9.461	78.813
Quarries:						
R12	12.088	0.131	n.d.	n.d.	11.956	99.597
Min	9.067	0.131	8.896	0.008	10.326	74.102
Max	12.088	0.386	11.956	0.035	22.861	99.597
Mean	10.081	0.251	9.831	0.018	16.316	81.890
SEM	0.291	0.028	0.296	0.003	1.240	2.462
Al-Ma'zzeh Profile:						
R6	6.815	0.491	0.047	10.440	6.324	52.682
R2	3.692	0.255	0.029	8.794	3.437	28.633
R1	6.086	0.160	0.009	17.729	5.926	49.365
R3	4.294	0.252	0.014	18.024	4.041	33.663
R4	9.477	0.361	0.035	10.326	9.115	75.929
R5	9.796	0.271	0.022	12.612	9.525	79.339
Min	3.692	0.160	0.009	8.794	3.437	28.633
Max	9.796	0.491	0.047	18.024	9.525	79.339
Mean	6.693	0.298	0.026	12.988	6.395	53.269
SEM	1.041	0.047	0.006	1.624	1.028	8.564
Masyadeh Profile:						
R9	4.533	0.116	0.007	16.630	4.416	36.787
R8	3.054	0.136	0.023	5.919	2.918	24.308
R10	10.531	0.386	0.031	12.665	10.145	84.507
R11	6.035	0.386	0.029	13.319	5.649	47.053
Min	3.054	0.116	0.007	5.919	2.918	24.308
Max	10.531	0.386	0.031	16.630	10.145	84.507
Mean	6.038	0.256	0.022	12.133	5.782	48.164
SEM	1.617	0.075	0.005	2.246	1.558	12.976

n.d.: not delectable

Table 9: Isotope Concentrations (per mille)

	δ^{13}Corg‰	δ^{13}Ccarb‰	δ^{18}Ocarb‰
Surface Sediment:			
R7	-25.113	-5.591	-4.274
R4	-24.306	-4.384	-3.909
R19	-23.919	-3.684	-3.372
R10	-26.312	-2.637	-7.433
R13	-24.576	-3.458	-4.933
R20	-23.418	-2.880	-4.564
R18	-24.131	-3.721	-3.882
R16	-23.172	-3.451	-4.064
R14	-23.940	-4.353	-3.643
Quarries:			
R12	-26.763	-1.156	-7.883
Min	-26.763	-5.591	-7.883
Max	-23.172	-1.156	-3.372
Mean	-24.565	-3.532	-4.796
SEM	0.373	0.374	0.498
Al-Ma'zzeh Profile:			
R6	-24.212	-4.287	-2.200
R2	-24.612	-3.998	-3.649
R1	-24.336	-3.444	-3.871
R3	-24.208	-3.647	-2.930
R4	-24.306	-4.384	-3.909
R5	-23.849	-5.579	-4.052
Min	-24.612	-5.579	-4.052
Max	-23.849	-3.444	-2.200
Mean	-24.253	-4.223	-3.435
SEM	0.101	0.309	0.296
Masyadeh Profile:			
R9	-22.973	-1.628	-4.002
R8	-22.852	-3.506	-3.479
R10	-26.312	-2.637	-7.433
R11	-25.190	-5.150	-4.624
Min	-26.312	-5.150	-7.433
Max	-22.852	-1.628	-3.479
Mean	-24.332	-3.230	-4.885
SEM	0.851	0.746	0.881

n.d.: not delectable

Table 10: Grain Size

Sample	Initial Weight (gram)	Sieve Size (mm)							
		7.5	9	38	125	180	300	600	2000
		Weight (gram)							
R7	500	1.756	0.404	0.146	8.718	3.970	11.186	21.972	52.010
R4	500	0.016	0.024	0.006	1.358	0.890	10.326	26.952	60.410
R19	353.2	7.327	0.402	0.461	16.617	6.271	13.344	16.891	38.916
R10	500	20.436	2.184	0.726	40.958	15.970	10.106	4.272	5.270
R13	291.6	2.840	0.144	6.972	4.798	5.607	13.453	18.676	48.028
R20	477.7	1.336	0.151	4.067	2.908	3.883	11.541	19.627	56.824
R18	500	2.116	0.184	0.146	5.518	2.930	8.806	16.112	64.690
R16	500	1.856	0.164	0.126	8.598	4.570	13.086	22.892	48.730
R14	500	10.216	0.604	0.446	30.958	9.050	21.466	16.072	11.210
Quarries:									
R12	500	5.856	2.484	0.306	36.598	13.730	13.286	8.452	19.250

Sand		Clay		Silt		USDA Texture
% Sand 1	97.00%	%Clay 1	3.00%	% Silt 1	0.00%	COARSE SAND
% Sand 2	97.00%	%Clay 2	3.00%	% Silt 2	0.00%	COARSE SAND
% Sand 3	97.00%	%Clay 3	3.00%	% Silt 3	0.00%	COARSE SAND
% Sand 4	77.00%	%Clay 4	23.00%	% Silt 4	0.00%	SANDY CLAY LOAM

Al-Ma'zzeh	
% Very Coarse	0.00%
% Coarse	88.60%
% Medium	0.00%
% Fine	8.40%
% Very Fine	0.00%

Masyadeh	
% Very Coarse	0.00%
% Coarse	72.60%
% Medium	0.00%
% Fine	24.40%
% Very Fine	0.00%

Al-Ghar	
% Very Coarse	0.00%
% Coarse	86.00%
% Medium	0.00%
% Fine	11.00%
% Very Fine	0.00%

Quarries	
% Very Coarse	0.00%
% Coarse	41.70%
% Medium	0.00%
% Fine	35.30%
% Very Fine	0.00%

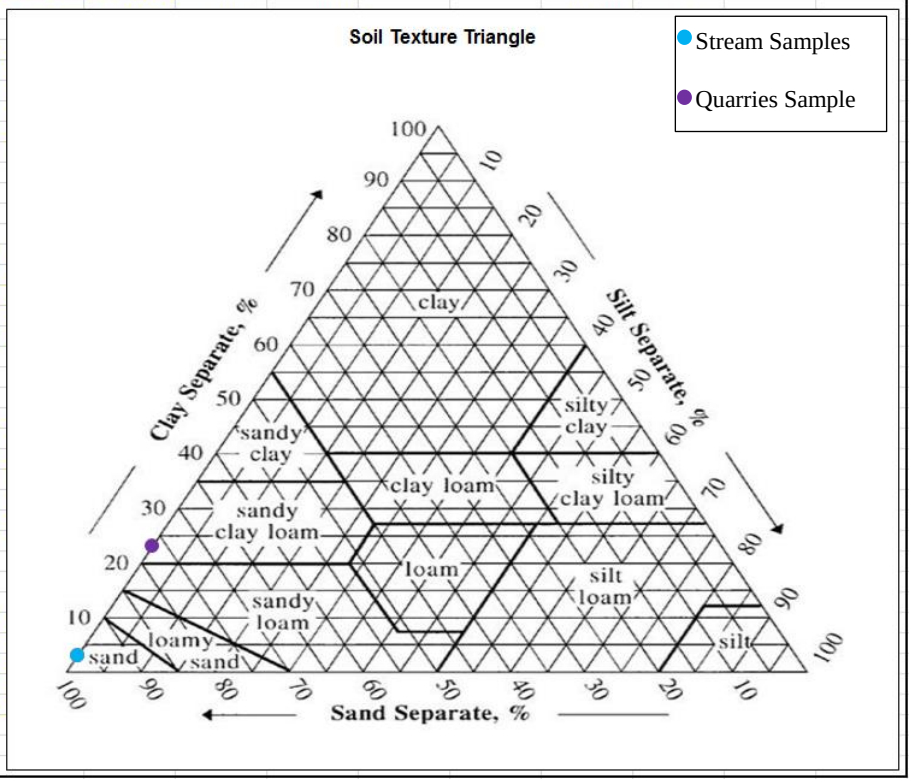

Figure 47: Grain Size Texture Groups (GRANISTAT, Adli, 2017)

Table 11: Chondrite-Normalized Total REEs and Some REE Ratios

	∑LREE	∑HREE	∑REE	∑LREE / ∑HREE	Ce / Ce*	Eu / Eu*	La / Yb
Surface Sediment:							
R7	0.457	0.153	0.611	2.982	0.752	0.924	6.801
R4	0.508	0.181	0.688	2.814	0.714	0.903	6.295
R19	0.087	0.033	0.120	2.614	0.739	0.921	5.711
R10	0.223	0.066	0.289	3.356	0.940	0.829	7.318
R13	0.109	0.033	0.142	3.333	0.832	1.098	7.201
R20	0.068	0.020	0.089	3.337	0.844	1.046	7.369
R18	0.178	0.065	0.243	2.737	0.638	1.267	6.342
R16	0.326	0.122	0.448	2.672	0.650	0.978	6.004
R14	0.093	0.035	0.128	2.661	0.769	1.115	5.862
Quarries:							
R12	0.014	0.004	0.018	3.266	0.871	0.703	7.151
Min	0.014	0.004	0.018	2.614	0.638	0.703	5.711
Max	0.508	0.181	0.688	3.356	0.940	1.267	7.369
Mean	0.206	0.071	0.278	2.977	0.775	0.979	6.605
SEM	0.054	0.019	0.073	0.100	0.031	0.051	0.202
Al-Ma'zzeh Profile:							
R6	0.012	0.002	0.014	5.078	1.555	4.362	7.149
R2	0.020	0.004	0.025	4.623	1.188	3.867	6.590
R1	0.004	0.001	0.005	2.875	1.187	1.727	5.859
R3	0.061	0.018	0.080	3.339	0.934	1.027	6.468
R4	0.508	0.181	0.688	2.814	0.714	0.903	6.295
R5	0.417	0.142	0.559	2.943	0.678	1.031	6.584
Min	0.004	0.001	0.005	2.814	0.678	0.903	5.859
Max	0.508	0.181	0.688	5.078	1.555	4.362	7.149
Mean	0.170	0.058	0.229	3.612	1.042	2.153	6.491
SEM	0.093	0.033	0.127	0.403	0.136	0.635	0.172
Masyadeh Profile:							
R9	0.855	0.269	1.124	3.180	0.938	0.814	6.659
R8	0.042	0.010	0.053	4.062	1.223	2.053	6.555
R10	0.223	0.066	0.289	3.356	0.940	0.829	7.318
R11	0.146	0.053	0.198	2.771	0.872	0.915	5.018
Min	0.042	0.010	0.053	2.771	0.872	0.814	5.018
Max	0.855	0.269	1.124	4.062	1.223	2.053	7.318
Mean	0.317	0.100	0.416	3.342	0.993	1.153	6.387
SEM	0.183	0.058	0.241	0.269	0.078	0.301	0.487

Table 12: Statistical Summary of Trace Element Concentrations (mg/kg)

	Minimum	**Maximum**	**Mean**	**SEM**
Na	29.037	670.363	369.982	85.363
Mg	27.738	613.833	361.980	63.729
Al	9.634	1233.858	453.364	122.160
P	2.642	1658.395	857.912	212.113
V	0.861	24.881	12.232	2.797
Cr	0.348	27.667	11.577	3.074
Mn	2.560	104.246	52.049	11.288
Fe	28.613	1548.366	581.534	142.437
Co	0.106	3.072	1.313	0.351
Ni	0.660	149.480	40.182	14.698
Zn	1.788	104.377	56.575	14.743
Sr	0.537	178.950	67.639	21.345
Pb	0.146	4.844	2.196	0.567

Table 13: Correlation Coefficient R-squared Statistics

	R^2			R^2
Na vs. Al	0.692		**TC% vs. $CaCO_3$%**	0.996
Mg vs. Al	0.808		**TOC% vs. $CaCO_3$%**	-0.221
P vs. Al	0.798		**IOC% vs. $CaCO_3$%**	1.000
V vs. Al	0.727		**TN% vs. $CaCO_3$%**	0.160
Cr vs. Al	0.514		**C/N vs. $CaCO_3$%**	-0.225
Mn vs. Al	0.837		**TN% vs. TOC%**	0.950
Fe vs. Al	0.661		**δ^{13}Corg‰ vs. δ^{13}Ccarb‰**	-0.455
Co vs. Al	0.741		**δ^{13}Corg‰ vs. δ^{18}Ocarb‰**	0.877
Ni vs. Al	0.260		**δ^{13}Ccarb‰ vs. δ^{18}Ocarb‰**	-0.755
Zn vs. Al	0.566		**δ^{13}Ccarb‰ vs. Al**	-0.162
Sr vs. Al	0.339		**δ^{18}Ocrab‰ vs. Al**	0.305
Pb vs. Al	0.792		**δ^{13}Ccarb‰ vs. TC%**	0.656
TC% vs. Al	-0.018		**δ^{18}Ocrab‰ vs. TC%**	-0.822
TOC% vs. Al	0.143			
IOC% vs. Al	-0.031		$0.0 < \mathbf{R^2} < 0.3$ → weak correlation	
TN% vs. Al	-0.176		$0.3 < \mathbf{R^2} < 0.7$ → moderate correlation	
C/N vs. Al	-0.041			
$CaCO_3$% vs. Al	-0.031		$0.7 < \mathbf{R^2} < 1.0$ → strong correlation	
TC% vs. Na	-0.345			
TC% vs. Mg	-0.379			
TC% vs. Al	-0.018			
TC% vs. Fe	-0.243			

Appendix D

Table 14: Sediment Quality Guideline based on effects to benthic-dwelling species (mg/kg dry weight)

	US EPA Toxicity classifications		
Element	Nonpolluted	Moderately Polluted	Heavily Polluted
Pb	<40	40–60	>60
Zn	<90	90–200	>200
Cu	<25	25–50	>50
Mn	<300	300–500	>500

Table 15: Sediment Particle Sizes and Class Names

Table 2.2.1-1. Sediment Particle Sizes and Class Names (modified Wentworth - Udden Scale)

Class Name	Millimeters	Micrometers
Boulders	>256	
Large Cobbles	256 - 128	
Small Cobbles	128 - 64	
V. Coarse Gravel	64 - 32	
Coarse Gravel	32 - 16	
Medium Gravel	16 - 8	
Fine Gravel	8 - 4	
V. Fine Gravel	4 - 2	
V. Coarse Sand		2000 - 1000
Coarse Sand		1000 - 500
Medium Sand		500 - 250
Fine Sand		250 - 125
V. Fine Sand		125 - 62.5
Coarse Silt		62.5 - 31
Medium Silt		31 - 16
Fine Silt		16 - 8
V. Fine Silt		8 - 4
Coarse Clay		4 - 2*
Medium Clay		2 - 1
Fine Clay		1 - 0.5
V. Fine Clay		0.5 - 0.25

2* - many sedimentologists consider that the silt/clay break occurs at 2μm rather than at 4μm.